

**EVALUATION OF PHOTOTHERMAL AND RB220 DYE  
DECOLORIZATION POTENTIAL OF BIOSYNTHESIZED  
COBALT OXIDE NANOPARTICLES FROM AN  
ENDOPHYTIC FUNGUS *ASPERGILLUS NIDULANS***

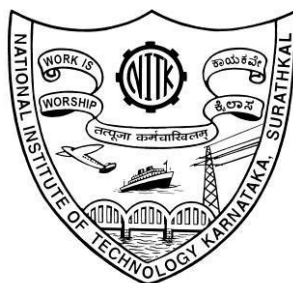
THESIS

Submitted in Partial Fulfillment of the requirements of the degree of

**DOCTOR OF PHILOSOPHY**

by

**Mr. AJUY SUNDAR. V. V**



**DEPARTMENT OF CHEMICAL ENGINEERING  
NATIONAL INSTITUTE OF TECHNOLOGY KARNATAKA,  
SURATHKAL, MANGALORE- 575 025**

**JUNE, 2020**

## DECLARATION

I, **Mr. Ajuy Sundar V. V**, *declare* that the Research Thesis entitled “Evaluation of photothermal and RB220 dye decolorization potential of biosynthesized cobalt oxide nanoparticles from an endophytic fungus *Aspergillus nidulans*” which is being submitted to the National Institute of Technology Karnataka, Surathkal in partial fulfillment of requirements for the award of the Degree of Doctor of Philosophy in Chemical Engineering is a *bonafide report of the research work carried out by me*. The material contained in this Research Thesis has not been submitted to any University or Institution for the award of any degree.

V V Ajuy Sundar

AJUY SUNDAR. V. V  
(145054CH14F01)

Department of Chemical Engineering  
National institute of technology Karnataka  
Surathkal-575025

Place: Surathkal

Date: 18-06-2020

## CERTIFICATE

This is to *certify* that the Research Thesis entitled “Evaluation of photothermal and RB220 dye decolorization potential of biosynthesized cobalt oxide nanoparticles from an endophytic fungus *Aspergillus nidulans*” submitted by Mr. Ajuy Sundar V. V. (Register Number: 145054CH14F01) as the record of the research work carried out by her, is *accepted as the Research Thesis submission* in partial fulfillment of the requirement of the award of degree of Doctor of Philosophy.

Research Supervisor

Prof. Raj Mohan B.

Chairman - DRPC

Dr. Prasanna B. D.

***Dedicated to my  
beloved parents and  
uncle***

## **ACKNOWLEDGEMENTS**

---

This thesis embodies the results of the last five and a half years' work whereby I have been accompanied and supported by many people. It is an honor and a very pleasant opportunity to be able to express my gratitude to all of them.

It has been a privilege to work under the dynamic leadership and guidance of my supervisor **Prof. Raj Mohan B**. His unerring support, coherence of scientific thoughts and remarkable presence of mind propelled me through my scholarly tenure to move forward during the finest days and darkest hours. I also thank my former supervisor **Dr. Noel Victoria** for choosing me to pursue research.

I am grateful to former HODs **Prof. Vidya Shetty K, Prof. Raj Mohan B, and Dr. Hari Mahalingam** and present HOD **Dr. Prasanna BD** for their support and help. I am also grateful to HOD in charges for their rapport.

I express my sincere gratitude to my RPAC members, **Prof. Gururaj Punekar**, Department of Electrical and Electronics Engineering and **Dr. Hari Mahalingam**, Department of Chemical Engineering for their unending encouragement and making me realize the importance of publication.

I thank my external examiners (**Prof. Meikap BC** and **Prof. Kannan Pakshirajan**) and DTAC members (**Prof. Lakshman Nandagiri** and **Dr. Jagadeesh Babu PE**) for their valuable inputs to increase the worth of the thesis.

I am grateful for the opportunity to study in the Department of Chemical Engineering, NITK, Surathkal for providing sophisticated instrument facilities like TGA, LCMS and DLS. I thank Physics and Metallurgy and Materials Engineering departments for providing SEM, PL and DC probe station facilities.

I am also obliged to Mr. Ananda, Mrs. Shashikala, Mr. Sadashiva, Mrs. Trithila, Mr. Sukesh, Mr. Mahadeva, Mr. Harish, Mr. Suresh, Mr. Ramesh, Mrs. Sasikala, Mrs. Bhavya, Mrs. Sandhya, Mrs. Vijetha and all technical and non-technical staff of the Department of Chemical Engineering for their wholehearted help during my work.

I thank former Directors, current Director and administration of the NITK, Surathkal for permitting me to pursue my research work at the institute.

I specially thank Dr. Vivekanandan S. for giving his time to evolve out the better results in my research work. I render my deepest gratitude to my mother **Mrs. Narmatha Lakshmi V.**, my father **Mr. Vijayanandan V.**, my uncle **Dr. Ganesh Kumar P. J.** and dear friends for the love, affection, and support.

I feel extremely grateful and thank all my Mass Transfer Lab mates and co-guide lab students for their continuous support in sharing knowledge, fruitful discussions to carry out my research successfully. I thank Mrs. Riya Sidhikku for working and helping me delivering contents for publishing.

I am thankful to all those who have been sticking to me in the campus during my hardships. I have been supported well by them during my crest and trough time, when I was let down. I specially thank you to everyone who is true, loyal to me, respected me and spent time with me amidst the fake ones.

Finally, I thank all those inside the department, outside the department, outside NITK, who directly/ indirectly helped me to complete the research work.

Praise to the **God** who bestows success and guides our destiny.

**AJUY SUNDAR V. V.**

## ABSTRACT

---

Endophytes are well known for producing biochemical molecules and bioactive metabolites. In addition, they have the capability to synthesize nanoparticles, whose properties are better than the chemical synthesized counterparts. Their potential of synthesizing nanoparticles in a greener way is relatively untapped. *Nothapodytes foetida* is a medicinal plant, which houses innumerable tolerant endophytic organisms. Various nanoparticles have been used for various applications. Metallic oxide nanoparticles have profound applications in electrochemical devices, supercapacitors, biosensors, and batteries. Though four fungi were isolated from *Nothapodytes foetida*, *Aspergillus nidulans* were found to be suitable for the synthesis of cobalt oxide nanoparticles, as it has proficient tolerance towards metal under study. The broth containing precursor solution and organism *Aspergillus nidulans* had changed from pink to orange indicating the formation of nanoparticles. Characterization by x-ray diffraction analysis (XRD), transmission electron microscopy (TEM), Fourier transform infrared spectroscopy (FTIR) and energy dispersive x-ray analysis (EDX) confirmed the formation of spinel cobalt oxide nanoparticles at an average size of 34 nm in spherical shape with sulfur-bearing proteins acting as a capping agent for the synthesized nanoparticles. The study was a greener attempt to synthesize cobalt oxide nanoparticles using endophytic fungus. The extracellular synthesis makes the process simple. Dielectric constant and dielectric loss values of  $\text{Co}_3\text{O}_4$  nanoparticles were measured at room temperature and frequency up to 1 MHz. They are plotted against frequency and these plots show dispersion at frequencies. Frequency dependence of the dielectric constant is found to increase with an increase in the frequency. Through Liquid Chromatography-Mass Spectrometry (LC-MS) analysis, phytochelatins are identified to be involved in the biosynthesis of  $\text{Co}_3\text{O}_4$  nanoparticles. Solar energy absorption is a process of capturing solar energy radiated from natural sunlight and converted to some other useful forms by appropriate methods.

In this way, a nanofluid based absorption system can provide a substitute for traditional solar collectors for the confinement of solar energy. This work proposes and validates a novel idea of using cobalt oxide nanofluids ( $\text{Co}_3\text{O}_4$ ) to enhance solar thermal conversion efficiency. Experimental results reveal that  $\text{Co}_3\text{O}_4$  nanofluids have a good specific absorption rate (SAR) and better photo-thermal conversion efficiency than water. Nanofluid exhibited a greater temperature gradient than pure water, which is desired. Thus the good absorption capability of  $\text{Co}_3\text{O}_4$  nanofluids for solar energy indicated that it is suitable for direct absorption solar thermal energy systems. The photocatalytic activity of the biosynthesized cobalt oxide ( $\text{Co}_3\text{O}_4$ ) nanoparticle is investigated using a textile dye Reactive Blue 220 (RB220) and decolorization (%) was monitored using UV-Vis spectrophotometer. The photocatalytic activity has been observed maximum at alkaline pH of 9, nanoparticle dosage of 250 mg/L, and reaction time of 270 min. In the presence of UV light irradiation, a maximum dye concentration of 10 mg/L was treated effectively using 150 mg/L nanoparticle, and 67% decolorization was achieved. Reaction kinetics has been analyzed and the reaction followed the pseudo kinetics model.

**Keywords:** Cobalt oxide nanoparticles; decolorization efficiency; endophytes; phytochelatins; RB220; specific absorption rate; surface plasmon resonance; temperature rise.

---



## CONTENTS

S. NO.	TITLE	PAGE NO.
	LIST OF FIGURES	i
	LIST OF TABLES	v
	NOMENCLATURE	vi
1	INTRODUCTION	1
1.1	ENDOPHYTES	1
1.2	<i>NOTHAPODYTES FOETIDA</i>	1
1.3	NEED FOR BIOSYNTHESIS	2
1.4	PREFERENCE FOR FUNGUS	3
1.5	NANOMATERIALS	3
1.6	TRANSITION ELEMENTS	4
1.7	COBALT OXIDE NANOPARTICLES	4
1.8	ENERGY UTILIZATION	5
1.9	PHOTOCATALYSIS	6
2	REVIEW OF LITERATURE	8
2.1	SYNTHESIS OF $C_{03}O_4$ NANOPARTICLES	8
2.2	<i>ASPERGILLUS NIDULANS</i> IN SYNTHESIS OF NANOPARTICLES	14
2.3	PHOTOTHERMAL CONVERSION	14

2.4	<b>Co<sub>3</sub>O<sub>4</sub> NANOPARTICLES AND RB220 DECOLORIZATION</b>	16
2.5	<b>BACKGROUND, MOTIVATION AND SCOPE FOR PRESENT INVESTIGATION</b>	18
2.5.1	<b>Background and research gaps</b>	18
2.6	<b>OBJECTIVES</b>	19
3	<b>MATERIALS AND METHODS</b>	20
3.1	<b>SAMPLE COLLECTION OF PLANTS</b>	20
3.2	<b>ISOLATION OF ENDOPHYTIC FUNGI</b>	20
3.3	<b>GROWTH RESPONSE STUDIES OF ISOLATED FUNGI</b>	21
3.4	<b>UPTAKE OF COBALT SALT BY TOLERANT FUNGAL ISOLATE FROM LIQUID MEDIUM</b>	21
3.5	<b>GROWTH STUDIES</b>	22
3.6	<b>INOCULATION INTO PDB MEDIUM</b>	22
3.7	<b>CHARACTERISATION OF NANOPARTICLES</b>	22
3.7.1	<b>UV-Visible spectroscopy</b>	22
3.7.2	<b>Photoluminescence spectroscopy</b>	23
3.7.3	<b>Fourier transform infrared spectroscopy</b>	23
3.7.4	<b>X-ray diffraction analysis</b>	24
3.7.5	<b>Scanning electron microscope</b>	24
3.7.6	<b>Field emission gun scanning electron microscope</b>	24

3.7.7	<b>Transmission electron microscope and selected area electron diffraction</b>	25
3.7.8	<b>Dynamic light scattering (DLS)</b>	25
3.7.9	<b>Electrochemical studies</b>	25
3.7.10	<b>Atomic force microscopy</b>	26
3.7.11	<b>Thermal characterization</b>	26
3.7.12	<b>Raman spectroscopy</b>	26
3.7.13	<b>Diffuse reflectance spectroscopy</b>	26
3.8	<b>PHOTOSTABILITY OF NANOPARTICLES</b>	27
3.9	<b>VIABILITY TEST</b>	27
3.10	<b>ELECTRICAL CHARACTERISATION OF NANOPARTICLES</b>	27
3.11	<b>MECHANISM BEHIND BIOSYNTHESIS OF <math>\text{Co}_3\text{O}_4</math> NANOPARTICLES THROUGH ENDOPHYTIC FUNGUS</b>	28
3.11.1	<b>Analysis of stress factors using LC-MS</b>	28
3.12	<b>MEASUREMENT OF PHOTOTHERMAL CONVERSION</b>	29
3.13	<b>FEASIBILITY STUDY OF ENERGY STORAGE FOR AN ELECTRICAL APPLICATION</b>	31
3.14	<b>DECOLORIZATION OF RB220</b>	34
3.14.1	<b>Materials</b>	34

3.14.2	<b>Method for photocatalytic decolorization of Reactive Blue 220 (RB220)</b>	34
3.14.3	<b>Effect of parameters and measurement of chemical oxygen demand (COD)</b>	36
3.14.4	<b>Kinetics</b>	37
4	<b>RESULTS AND DISCUSSION</b>	38
4.1	<b>ISOLATION OF ENDOPHYTIC FUNGI</b>	38
4.2	<b>RESPONSE STUDIES OF ISOLATED FUNGI</b>	39
4.3	<b>UPTAKE OF COBALT SALT BY TOLERANT FUNGAL ISOLATE FROM LIQUID MEDIUM</b>	42
4.4	<b>GROWTH STUDIES</b>	43
4.5	<b>COLOR CHANGE</b>	43
4.6	<b>UV-VISIBLE SPECTROSCOPY</b>	44
4.7	<b>FOURIER TRANSFORM INFRARED SPECTROSCOPY</b>	46
4.8	<b>X-RAY POWDER DIFFRACTION ANALYSIS</b>	48
4.9	<b>DYNAMIC LIGHT SCATTERING</b>	49
4.10	<b>SCANNING ELECTRON MICROSCOPE AND FIELD EMISSION GUN SCANNING ELECTRON MICROSCOPE</b>	51
4.11	<b>TRANSMISSION ELECTRON MICROSCOPE AND SELECTED AREA ELECTRON</b>	53

	<b>DIFFRACTION</b>	
4.12	<b>ATOMIC FORCE MICROSCOPY</b>	56
4.13	<b>ELECTROCHEMICAL STUDIES</b>	57
4.14	<b>THERMAL ANALYSIS</b>	58
4.15	<b>PHOTOLUMINESCENCE STUDIES AND QUANTUM YIELD</b>	61
4.16	<b>RAMAN SPECTROSCOPY</b>	62
4.17	<b>DIFFUSE REFLECTANCE SPECTROSCOPY</b>	62
4.18	<b>PHOTOSTABILITY OF NANOPARTICLES</b>	63
4.19	<b>VIABILITY TEST</b>	69
4.20	<b>EXPLORING THE MECHANISM BEHIND BIOSYNTHESIS OF <math>\text{Co}_3\text{O}_4</math> NANOPARTICLES THROUGH ENDOPHYTIC FUNGUS</b>	70
4.20.1	<b>Mechanism governing the biosynthesis of <math>\text{Co}_3\text{O}_4</math> nanoparticles by <i>Aspergillus nidulans</i></b>	71
4.21	<b>VIBRATING SAMPLE MAGNETOMETRY (VSM) ANALYSIS</b>	74
4.22	<b>ELECTRICAL CHARACTERIZATION</b>	76
4.23	<b>PHOTOTHERMAL CONVERSION</b>	80
4.24	<b>FEASIBILITY STUDY OF ENERGY STORAGE FOR AN ELECTRICAL APPLICATION</b>	86
4.25	<b>DYE DECOLORIZATION</b>	88

4.25.1	<b>Effect of time</b>	88
4.25.2	<b>Effect of pH</b>	89
4.25.3	<b>Effect of dye concentration</b>	90
4.25.4	<b>Effect of Co<sub>3</sub>O<sub>4</sub> nanoparticle dosage</b>	92
4.25.5	<b>COD Analysis</b>	93
4.25.6	<b>Kinetics</b>	94
4.25.7	<b>Mechanism of RB220 decolorization</b>	96
4.25.8	<b>Cost analysis of the method followed in the study for biological synthesis of Co<sub>3</sub>O<sub>4</sub> nanoparticles</b>	98
5	<b>CONCLUSION</b>	99
5.1	<b>Significant findings</b>	99
5.2	<b>Scope for future work</b>	101
	<b>REFERENCES</b>	102
	<b>APPENDIX</b>	135
	<b>LIST OF PUBLICATIONS and CONFERENCE/SYMPOSIUM PRESENTATIONS</b>	137
	<b>BIODATA</b>	139

## LIST OF FIGURES

Figure No.	Title	Page No.
1.1	<i>Nothapodytes foetida</i> plant sample	2
3.1	Beaker containing $\text{Co}_3\text{O}_4$ nanofluid in thermo cool	29
3.2	Schematic representation of the energy storage circuit	32
3.3	Types of loads used (1 - LED bulb, 2 - CFL bulb, 3 - 1 M $\Omega$ resistor, 4 - 220 k $\Omega$ resistor, 5 - 380 k $\Omega$ , resistor and 6 - motor)	33
3.4	Multimeter and beaker with electrodes and $\text{Co}_3\text{O}_4$ nanofluid	33
3.5	Structure of RB220 dye (Bodurođlu et al. 2014)	34
3.6	RB220 dye decolorization – (a) Experimental set up (b) Schematic set up	36
4.1	Fungi isolated from <i>Nothapodytes foetida</i> (a) Fungus 1 (b) Fungus 2 (c) Fungus 3 (d) Fungus 4	38
4.2	Colony diameter of fungal isolates against salt concentrations (a) 500 ppm (b) 1000 ppm	39
4.3	Tolerance index of fungal isolates against salt concentrations (a) 500 ppm (b) 1000 ppm	40
4.4	Growth of fungal isolates in presence of 500 ppm salt concentration (a) Fungus 1 (b) Fungus 2 (c) Fungus 3 (d) Fungus 4	41
4.5	Effect of higher concentrations of cobalt salt on the growth of <i>Aspergillus nidulans</i>	42
4.6	Quantity of biomass obtained	43

4.7	Change of color of flasks	44
4.8	UV-Vis analysis of biosynthesized nanoparticle (a) UV-Vis spectrum (b) tauc plot	45
4.9	FTIR profile of (a) nanoparticle solution (b) precursor solution	47
4.10	X-ray diffraction pattern of nanoparticles	48
4.11	DLS analysis of nanoparticles (a) particle size distribution (b) zeta potential measurement	50
4.12	Electron microscope images of $\text{Co}_3\text{O}_4$ nanoparticles (a) FEGSEM image (b) SEM image of nanoparticles (c) EDAX pattern	51
4.13	Electron microscope images of $\text{Co}_3\text{O}_4$ nanoparticles (a) TEM image of cobalt oxide nanoparticles (b) TEM image of nanoparticles (c) single nanoparticle in higher TEM magnification (d) particle size histogram obtained from TEM (e) selected area electron diffraction pattern of nanoparticles	53
4.14	AFM image of synthesized nanoparticles (a) 2D profile (b) 3D profile	56
4.15	Cyclic voltammetry curve of cobalt oxide nanoparticles	57
4.16	Thermal analysis of nanoparticles (a) TGA Thermogram (b) DSC Thermogram (c) DTA Thermogram (d) DTG Thermogram	58
4.17	Photoluminescence spectrum of nanoparticles	61
4.18	Raman spectrum of nanoparticles	62
4.19	Diffuse reflectance spectrum	63
4.20	Photostability curve of nanoparticles (a) intensity of absorbance with respect to time in 2 mM salt concentration (at room temperature) (b) intensity of absorbance with respect to time in 2 mM salt concentration (at 17 °C) (c) wavelength maxima with respect to time in 2 mM salt concentration (at room temperature) (d) wavelength maxima	63



with respect to time in 2 mM salt concentration (at 17 °C) (e) intensity of absorbance with respect to time in 10 mM salt concentration (at room temperature) (f) intensity of absorbance with respect to time in 10 mM salt concentration (at 17 °C) (g) wavelength maxima with respect to time in 10 mM salt concentration (at room temperature) (h) wavelength maxima with respect to time in 10 mM salt concentration (at 17 °C).

4.21	Viable fungal mycelium after exposure to salt solution	69
4.22	LC profile of Co <sub>3</sub> O <sub>4</sub> nanoparticles	70
4.23	Mass spectrum of nanoparticles at retention time 3 min, revealing m/z ratio peaks at 308.65, 537.3, and 676.15.	71
4.24	Probable mechanism for the biosynthesis of Co <sub>3</sub> O <sub>4</sub> nanoparticles in <i>Aspergillus nidulans</i>	73
4.25	VSM profile of Co <sub>3</sub> O <sub>4</sub> nanoparticles at room temperature (2 mM concentration)	74
4.26	VSM profile of Co <sub>3</sub> O <sub>4</sub> nanoparticles at room temperature (10 mM concentration)	75
4.27	Dielectric constant of Co <sub>3</sub> O <sub>4</sub> nanoparticles as a function of log frequency	77
4.28	Dielectric loss of cobalt oxide nanoparticles as a function of log frequency	77
4.29	AC conductivity of cobalt oxide nanoparticles as a function of log frequency	78
4.30	Loss tangent of cobalt oxide nanoparticles as a function of log frequency	79
4.31	Loss tangent of cobalt oxide nanoparticles as a function of frequency	79
4.32	Transient temperature and electrical conductivity profile of Co <sub>3</sub> O <sub>4</sub> nanofluids synthesized by 10 mM precursor concentration with respect to time	84
4.33	Values of voltage and current obtained in nanofluids synthesized by 10 mM precursor concentrations with	87

different loads

4.34	Decolorization efficiency of dye with respect to time (Dye conc. = 20 mg/L, nanoparticle dosage = 150 mg/L, pH = 7)	88
4.35	Decolorization efficiency of nanoparticles with respect to pH (Dye concentration = 20 mg/L, nanoparticle dosage = 150 mg/L, time = 270 min)	90
4.36	Decolorization efficiency of nanoparticles with respect to dye concentration (Nanoparticle dosage = 150 mg/L, pH = 9, time = 270 min)	91
4.37	Decolorization efficiency of nanoparticles with respect to nanoparticles' concentration (Dye concentration = 10 mg/L, pH = 9, time = 270 min)	92
4.38	COD analysis with respect to time (Dye conc. = 10 mg/L, nanoparticle dosage = 150 mg/L, pH = 9)	94
4.39	Pseudo-first order decay curve	95
4.40	(a) RB220 dye before the reaction (b) RB220 dye after the reaction	96
4.41	Mechanism of RB220 decolorization	97

## LIST OF TABLES

<b>Table No.</b>	<b>Title</b>	<b>Page No.</b>
2.1	Chemical and physical methods of synthesis of cobalt oxide nanoparticles	9
2.2	Biological methods of synthesis of cobalt oxide nanoparticles	13
2.3	Types of nanofluids used for photothermal studies	16
4.1	Planar spacing of synthesized nanoparticles	48
4.2	Intensity of sunlight throughout the day	81
4.3	Temperature rise achieved for different nanofluids ((He at al. (2013); Hashim et al. (2013); Xuan et al. (2014); Filho et al. (2014); Zhang et al. (2014); Liu et al. (2015); Chen et al. (2015); Khasan et al. (2017); Bhalla and Tyagi (2017); Beicker et al. (2018))	81
4.4	Temperature of the fluid within the beaker (under natural sunlight)	82
4.5	Temperature of the fluid within the beaker (under solar simulator)	83
4.6	Value of electrical conductivity obtained in $\text{Co}_3\text{O}_4$ nanofluids synthesized by different precursor concentrations	85
4.7	Value of electrical conductivity obtained in $\text{Co}_3\text{O}_4$ nanofluids before and after keeping in sunlight for 1 h	85
4.8	Values of voltage obtained in nanofluids synthesized by precursor concentrations (10 mM) after keeping in sunlight for 1 h	87

## NOMENCLATURE

<b>Symbol</b>	<b>Description</b>
$\eta, \kappa$	Optical constants
$\varepsilon'$	Real part of dielectric constant
$\varepsilon''$	Imaginary part of dielectric constant
A	Absorption
A	Band tailing parameter (constant)
A	Illumination area of the beaker
AO	Acridine orange
BCB	Brilliant cresyl blue
$c_n$	Specific heat of nanofluid
$\text{Co}_3\text{O}_4$	Cobalt oxide
COD	Chemical oxygen demand
$c_p$	Specific capacity of fluid
CV	Cyclic voltammetry
$c_w$	Specific heat of water
D	Particle diameter
Dia.	Diameter
DLS	Dynamic light scattering
DR	Direct red
EDAX	Energy dispersive analysis using x-rays
$E_g$	Bandgap

$E_{\text{total}}$	Total energy stored by the fluid
$E_U$	Urbach energy
$f$	Nano-colloidal volume fraction
FEGSEM	Field emission gun scanning electron microscope
FTIR	Fourier transform infrared spectroscopy
$f_v$	Fraction volume
GCE	Glassy carbon electrode
h	Hour
$h\nu$	Photon energy
I	Amount of light entering the fluid
I	Intensity of irradiance
$I_0$	Amount of light passing through the fluid
ICDD	International centre for diffraction data
k	Molar extinction coefficient
$K_\alpha$	Spectral absorption coefficient
l	Cuvette length
L	Optical thickness
LAF	Laminar air flow
LED	Light-emitting diode
lx	Lux
$m$	Mass of fluid
MB	Methylene blue
min	Minute

mM	Millimolar
$m_n$	Mass of nanofluid
$m_w$	Mass of water
MWCNT	Multiwalled carbon nanotubes
n	Refractive index
n	Exponent depends on the type of transition
$\eta$	Photothermal conversion efficiency
NF	Nanofluid
$\eta_n$	Photothermal conversion efficiency of nanoparticle
NP	Nanoparticles
$\eta_w$	Photothermal conversion efficiency of water
PDA	Potato dextrose agar
PDB	Potato dextrose broth
$Q_{abs}$	Absorption efficiency
$Q_{ext}$	Extinction efficiency
$Q_{scat}$	Scattering efficiency
R	Reflectance
RB 220	Reactive blue 220
RBO	Remazol brilliant orange
RTD	Resistance temperature detector
SAED	Selected area electron diffraction
SAR	Specific absorption rate
SCE	Saturated calomel electrode

SEM	Scanning electron microscope
SER	Storage energy ratio
T	Transmittance
TEM	Transmission electron microscope
TI	Tolerance index
$T_{\max}$	Maximum temperature attained
$T_{\min}$	Initial temperature of the study
$T_{\text{nf}}(0)$	Initial temperature of nanofluid
$T_{\text{nf}}(t)$	Temperature of nanofluid at time t
$T_{\text{w}}(0)$	Initial temperature of water
$T_{\text{w}}(t)$	Temperature of water at time t
UV	Ultraviolet
UV-VIS	Ultraviolet-visible
VSAR	Volumetric specific absorption rate
$\alpha$	Absorption coefficient
$\beta$	Size parameter
$\Delta T$	Temperature rise in $\Delta t$ time interval (exposure time)
$\lambda$	Wavelength
$\rho_{\text{np}}$	Density of $\text{Co}_3\text{O}_4$ nanoparticles
$\sigma$	Cross-sectional area
$\Omega$	Ohm





# CHAPTER 1

## INTRODUCTION

### 1.1 ENDOPHYTES

The term 'Endophyte' was coined by de Bary in 1866. In Greek, 'Endon' means within and 'phyte' means plant. They are defined as "microbes that colonize living, internal tissues of plants without causing any immediate, overt negative effects." (Staneik et al. 2008). Endophytes find applications in agriculture, medicine, and industry. As endophytes are very diverse and a lesser number of scientists working in that field, a greater number of endophytic species is still unexplored. Some endophytes became extinct due to deforestation and loss of biodiversity. With larger usage of endophytes comes from an increase of crop resistance and synthesizing drugs, their utilization in the greener synthesis of nanoparticles is relatively new.

### 1.2 *NOTHAPODYTES FOETIDA*

*Nothapodytes foetida* is a plant having medicinal properties distributed over Western Ghats (Fig. 1.1). It is a producer of camptothecin, which is an alkaloid inhibiting topoisomerase I-DNA inhibitor (Namdeo and Sharma 2012). It is reported to house more than 170 species of endophytes and the dominant ones are highly tolerant to toxic metals even at high concentrations and harsh conditions (Musavi and Balakrishnan 2013). Moreover, their adaptability is one of the major reasons to be used to produce metal-oxide nanoparticles. Though *Nothapodytes foetida* is widely known for synthesizing biochemical metabolites, they have the potential to synthesize nanoparticles, whose properties are superior to the chemical synthesized nanoparticles (Fathima and Balakrishnan 2014; Jacob et al. 2014; Uddandarao and Balakrishnan 2016; Kadam et al. 2019). *Aspergillus nidulans* is a fungus coming under division Ascomycota. It contains phytochrome FphA stimulating asexual reproduction (Blumenstein et al. 2005) and its

synthesis of nitrate reductase enzyme is induced by nitrate and repressed by ammonium (Cove 1965).



**Fig. 1.1 *Nothapodytes foetida* plant sample**

### **1.3 NEED FOR BIOSYNTHESIS**

Chemical methods are expensive as they use costly equipment, need harsh reaction conditions; undergo decomposition and combustion, thereby affecting the ecosystem and economy. Physical methods involve more than one step, high energy requirement and low material conversion (Loo et al. 2012). In chemical methods, the usage of solvent has led to contamination in the land, air, and water, which in turn pressing the need for a solvent-free approach (DeSimone 2002). Also, separate capping and stabilization agents are needed to stabilize and control the growth of nanoparticles to get rid of agglomeration. Extraction and purification problems too exist (Seabra and Duran 2015). Chemical methods use stringent protocol. Although chemical methods provide large yield in relatively short times, they are energy-intensive and employ toxic chemicals (Yadav et al. 2015). Due to these detriments, there is a shift towards biological methods of nanoparticle synthesis. The biological methods are cheap, clean, non-toxic and pollution-free. They do not require harsh treatments and costly equipment, although the yield is

less. There is no provision to add capping and stabilizing agents distinctly as proteins secreted by microorganisms can act as both capping and stabilizing agent to control the size distribution of nanoparticles. Moreover, they yield biocompatible particles of less toxicity.

#### **1.4 PREFERENCE FOR FUNGUS**

Chemical and physical synthesis methods are mainly used to prepare  $\text{Co}_3\text{O}_4$  nanoparticles by the reduction of cobalt salt. In this framework, synthesis can be attempted with the assistance of endophytic fungi. Using endophytic fungi in synthesizing nanomaterials is relatively new compared to the chemical and physical methods as it forms a field of bio-nanotechnology. 'Nano bio interface' can provide stability and activity to nanomaterial due to dynamic physicochemical interactions, kinetics and thermodynamic exchanges (Nel et al. 2009). For synthesis, the fungus is preferred over bacterium as it has economically viability, uncomplicated downstream processing, biomass management and optimum growth of mycelia with extensive surface area (Tomar 2015). Also, it is effectively visible; it provides high yield, a high amount of proteins and a large amount of biomass to be handled. The method involving is environmentally friendly and commercially economic (Ingale and Chaudhari 2013).

#### **1.5 NANOMATERIALS**

Nanomaterials are materials having dimensions on the nanoscale. They are the materials in the dimension of  $10^{-9}$  m. The main types of nanomaterials are carbon-based nanomaterials, metal-based nanomaterials, dendrimers, and composites. They are synthesized by both top-down and bottom-up methods. In top-down methods, macroscopic initial structures are reduced to nano-scale structures. Lithography, photolithography, micromachining, laser machining, etching and ball milling are some of the top-down methods. While in bottom-up methods, self-assembly of miniature compounds are performed. Few of the methods include atomic layer deposition, inert-gas expansion, inert-gas condensation, ultrasonic dispersion, sol-gel methods, plasma-based

synthesis, vapor condensation, molecular beam epitaxy, and electrodeposition. Nanoparticles exhibit unique and different physical and chemical properties due to their small size when compared to their macro scaled viz. bulk material counterparts (Ullah et al. 2014). In addition, they have better electric, mechanical, thermal, catalytic and magnetic properties than macrostructures as they are holding better surface area to volume ratio. They exhibit quantum confinement effect, which is an increase in bandgap with a decrease in particle size (Manzoor et al. 2009). They have potential applications in imaging, drug delivery, antimicrobials, solar energy harvesting, catalysis, environmental cleaning, fuel cells and fuel additives, optoelectronics, and information storage.

## **1.6 TRANSITION ELEMENTS**

Transition metals are 'd' block elements and they occupy the center position in the periodic table. They possess variable valencies due to more than one oxidation state and have been mainly useful in applications such as alloys and catalysts. They are highly air-sensitive and can form oxides easily. Owing to these, their oxides have attained significance. Transition metal oxide nanoparticles have been emerging as a significant tool in the nanotechnology industry because of its tendency to form transition metal ion complexes and ligands. Among transition metals, ferromagnetic materials gain attraction due to their tendency of being magnetized. Nowadays, ferromagnetic materials are indispensable in electrical and electromechanical devices. The prevailing ones in the list are iron, nickel, and cobalt.

## **1.7 COBALT OXIDE NANOPARTICLES**

Metal oxides like cobalt, copper, by unique structures, physical and chemical properties have found better applications in optoelectronics. Their nanomaterial counterparts encompass applications in sensing, lithium batteries and electrochemical devices (Salavati-Niasari et al. 2009). Cobalt oxide nanoparticles are one of the metallic oxide nanoparticles, being cobalt as one of the transition metals. They are synthesized by reducing cobalt salts and are used in an array of applications namely biosensing,

bioimaging and color additives to ceramics. Further, they have found usefulness in energy storage systems, electrochromic thin films, heterogeneous catalysis and magneto-resistive devices (Athawale et al. 2010).

## **1.8 ENERGY UTILIZATION**

The term ‘nanofluid’ was coined by Stephen Choi in 1995 (Subramanian et al. 2015). Nanofluids are dispersed nanoparticles in a basic fluid like water and ethylene glycol, having greater solar absorption capability, thermal conductivity and excellent stability (Khullar and Tyagi 2012). When nanoparticles that absorb incident radiation of visible wavelengths, is present in base fluids, the absorption property is expected to increase gradually (Kameya and Hanamura 2011). Besides, nanofluids have high absorption in the solar range and low emission in the infrared region (Taylor et al. 2011). Moreover, they are not transparent to solar radiation as they absorb and scatter solar irradiance passing through them (Khullar et al. 2012). Nanoparticles present a high opportunity in quantum efficiency enhancement by increasing light trapping and photocarrier collection without additional cost in solar cell fabrication. It has also been shown that the light trapping efficiency of the nanoparticle is mainly due to the increase of photon path inside the nanostructures (Dhineshababu et al. 2016) which increases the electron-hole creation probability. Nanoparticles have a very high heat transfer coefficient in the order of  $10^8 \text{ Wm}^{-2}\text{K}$ , leading to the efficient transfer of heat to the fluid in immediate contact (Bhalla and Tyagi 2017; Khullar et al. 2014). Though several types of solar collectors have been used to harness solar energy, they exhibit several shortcomings, such as limitations on incident flux density, relatively high heat losses, and corrosion effects (Tyagi et al. 2009). Replacing nanofluids for water as the working fluid can minimize heat transfer losses and increase the efficiency of the collectors. Nanofluids, due to their unique optical and thermal properties also enhance the thermal conductivity, mass diffusivity, and light absorption efficiency of the working fluid (Tyagi et al. 2009).

## 1.9 PHOTOCATALYSIS

A way of utilizing sunlight is by the conversion of light energy into chemical energy by photocatalysts, which can be used for the treatment of wastewater from textile, paper and some other industries that contain residual dyes that are non-biodegradable (Khanna and Shetty 2014; Sharma et al. 2012). Semiconductor nanoparticles have peculiar optical properties and small size that make them interesting candidates for applications in optoelectronics, catalysts and fluorescence spectroscopy (Sharma et al. 2012). Very little research has been accomplished on the potential of  $\text{Co}_3\text{O}_4$  nanoparticles for energy capturing and photocatalysis of RB220 dye. Photocatalysis in the presence of nanoparticles offers a great solution for the elimination of pollutants from the environment. ZnS nanoparticle obtained from endophytic fungus *Aspergillus flavus* has been employed for degradation of organic pollutants like methyl violet, 2,4 dichlorophenoxy acetic acid and paracetamol (Uddandarao et al. 2019). RB220 is vinyl sulfone azo dye mainly used in textile industries and more than 50% of cotton is dyed with reactive dyes only (Niebisch *et al.* 2010). In this work, the efficiency of Tricobalt tetroxide or cobalt oxide ( $\text{Co}_3\text{O}_4$ ) nanoparticle (NP) synthesized through endophytic fungus has been utilized for the photocatalytic decolorization of RB220 dye through electron transfer process.

The research study is presented and explained in five chapters as given below:

- ❖ **Chapter 1** introduces the significance of endophytic fungus in the synthesis of biological nanoparticles. Further, it explains the scenario of energy utilization and highlights the utility of nanomaterials for the harvesting of energy.
- ❖ **Chapter 2** throws light on a comprehensive literature review that includes an overview of the synthesis of nanoparticles through *Aspergillus nidulans*. The importance of the biological synthesis of  $\text{Co}_3\text{O}_4$  nanoparticles was discussed. Moreover, the application of nanoparticles on photosensitivity has been discussed.

- ❖ **Chapter 3** includes the materials and methods required to achieve the biosynthesis and characterization of nanoparticles. This includes the collection of samples, isolation, screening, identification of metal tolerant species. Also, it involves studies of properties and applications of nanoparticles like dye decolorization and solar energy harvesting.
- ❖ **Chapter 4** presents the results of the optical, structural, dielectric and thermal properties of  $\text{Co}_3\text{O}_4$  nanoparticles and illustrates the potential photo-thermal capacity the nanoparticles and decolorization efficiency of reactive blue 220 (RB220) dye. Further, the nanofluid system is added to electrical circuits to evaluate its electrical potential.
- ❖ **Chapter 5** gives a summary of this dissertation by bringing out the significant findings and possible future scope of the work. It accesses an outlook for novel nanobiotechnological miniature in photosensitivity applications like solar energy harvesting and dye decolorization.

## CHAPTER 2

### REVIEW OF LITERATURE

#### 2.1 SYNTHESIS OF $\text{Co}_3\text{O}_4$ NANOPARTICLES

Diverse methods have been in use for the synthesis of  $\text{Co}_3\text{O}_4$  nanomaterials with most of them covered under chemical technique. Srinivasan and Weidner (2002) used the electrochemical precipitation method at room temperature to synthesize  $\text{Co}_3\text{O}_4$  nanoparticles involving sodium nitrate and cobalt nitrate. Xu et al. (2010) attempted to synthesize  $\text{Co}_3\text{O}_4$  nanotubes for the first time by chemical deposition of cobalt hydroxide and thermal annealing at 500 °C. Gao et al. (2010) synthesized  $\text{Co}_3\text{O}_4$  nanoarrays supported on nickel foam and thermal treatment at 300 °C in air. Solution combustion synthesis (SCS) at 400 °C involving sodium fluoride with cobalt nitrate was reported by Wen et al. (2012). Venkatachalam et al. (2014) synthesized  $\text{Co}_3\text{O}_4$  nanomaterial through ultra-sonication, precipitation, and calcination at 400 °C. Cobalt nitrate was dissolved in ethanol and pH was adjusted with ammonia and the calcined product was found to be spherical. Zhou et al. (2016) reported NaOH concentration played an important role in the formation of  $\text{Co}_3\text{O}_4$  nanomaterials. Table 2.1 gives a list of papers involving the method of synthesis, the precursor used and particle size obtained. The biological methods adopted are given in Table 2.2.



**Table 2.1 Chemical and physical methods of synthesis of Co<sub>3</sub>O<sub>4</sub> nanoparticles**

S.No	Author(s)	Precursor	Method	NP size/dia.
1	Li et al. (2004)	Cobalt nanowires	Calcination	30 nm
2	Yang et al. (2004)	Cobalt nitrate, ammonium bicarbonate	Milling, chemical reaction.	13 nm
3	Liu et al. (2005)	Cobalt chloride	Hydrothermal	40 nm
4	Shinde et al. (2005)	Cobalt chloride	Spray pyrolysis	80 nm
5	Grass and Stark (2006)	Cobalt 2- ethylhexanoate	Flame synthesis	20-60 nm
6	Ahmed et al. (2008)	Cobalt oxalate	Reverse micellar, thermal decomposition	35 nm
7	Vidal-Abarca et al. (2008)	Cobalt chloride	Reverse micellar extraction	
8	Yuanchun et al. (2008)	Cobalt(II) acetate tetrahydrate, cobalt(II) nitrate hexahydrate	Solvothermal	70 nm
9	Fernandez-Osorio et al. (2009)	Cobalt chloride hexahydrate	Facile synthesis	20.5 nm
10	Ji et al. (2009)	Cobalt nitrate hexahydrate	Solvent-free thermal	85 nm
11	Salavati-Niasari et al. (2009)	Cobalt(II) acetate, N-N'- bis(salicylaldehyde	Precipitation, thermal treatment	30-50 nm

		)-1,2-phenylenediimino cobalt(II), cobalt (II) acetate tetrahydrate		
12	Salavati-Niasari et al. (2009)	Cobalt oxalate	Thermal decomposition	20 nm
13	Wang et al. (2009)	Cobalt chloride	Hydrothermal method	16-75 nm
14	Xu et al. (2009)	Quaternary microemulsion, CTAB/water/cyclohexane/n-pentanol, dicarboxylic acid	Microemulsion, calcination	200 nm
15	Athawale et al. (2010)	Alcohols, aniline	Gamma radiolysis	29 nm
16	Barreca et al. (2010)	Co(II) adduct	CVD	150 nm
17	Yang et al.(2010)	Cobalt nitrate	Simple soft chemistry	20 nm
18	Zheng et al. (2010)	Cobalt nitrate hexahydrate	Solvothermal, calcination	100 nm
19	Bhatt et al. (2011)	Cobalt nitrate hexahydrate	Microwave irradiation	3 - 12 nm
20	Gupta et al. (2011)	Cobalt nitrate	Thermal decomposition	10-75 nm
21	Kodge et al. (2011)	Cobalt chloride	Thermal decomposition,	

			microwave oven treatment	
22	Shim et al. (2011)	Cobalt chloride	Electrostatic interaction with bacteria, heat treatment	2-5 nm
23	Shim et al. (2011)	Cobalt ions	Chemical	2 – 5 nm
24	Sinko et al. (2011)	Cobalt nitrate and cobalt chloride	Co-precipitation, sol-gel	85 nm
25	Athar et al. (2012)	Cobalt acetate	Soft chemical	50 nm
26	Manimekalai et al. (2012)	Metal phenoxyacetate trihydrazinate, metal 2,4 dichlorophenoxy acetate dihydrazinate, metal crotonate dihydrazinate	Thermal decomposition	18-28 nm
27	Nassar and Ahmed (2012)	Cobalt carbonate	Hydrothermal	30.5- 47.35 nm
28	Allen et al. (2013)	Co(II) with H <sub>2</sub> O <sub>2</sub>	Constrained synthesis in protein cage	5 nm
29	Farhadi et al. (2013)	[Co <sup>II</sup> (NH <sub>3</sub> ) <sub>6</sub> ](NO <sub>3</sub> ) <sub>2</sub>	Thermal dissociation	13 nm
30	Farhadi et al.	Carbonatotetra(am	Thermal	6-16 nm

	(2013)	mine)cobalt(III) nitrate complex	decomposition	
31	Farhadi et al. (2013)	<i>mer</i> - Co(NH <sub>3</sub> ) <sub>3</sub> (NO <sub>2</sub> ) <sub>3</sub> complex	Thermal decomposition	19 nm
32	George and Anandhan (2013)	Cobalt(II) acetate	Sol-gel, electrospinning	200 nm
33	Makhlouf et al. (2013)	Sucrose	Combustion	13-32 nm
34	Manteghi and Peyvandipour (2013)	Cobalt nitrate and ammonium oxalate	Co-precipitation	38 nm
35	Sinduja et al. (2013)	Cobalt nitrate hexahydrate	Thermal decomposition	13 nm
36	Agilandeswari and Kumar (2014)	Cobalt nitrate	Precipitation	50-100 nm
37	Kimura et al. (2014)	Cobalt(III) acetylacetonate	Precipitation with oleylamine	80 nm
38	Yarestani et al. (2014)	Cobalt(II) chloride	Hydrothermal method	26.6 nm
39	Liu et al. (2015)	Cobalt carbonate hydroxide	Solvothermal synthesis, calcination	150-250 nm
40	Shadrokh et al. (2016)	Cobalt nitrate	Co-precipitation	25 nm
41	Raman et al. (2016)	Cobalt chloride	Chemical synthesis	40-60 nm
42	Rahimi-Nasrabadi	Cobalt nitrate	Chemical,	41 nm

	et al. (2017)		calcination	
43	Singh et al. (2018)		Green chemical route	
44	Wolf et al. (2018)	Cobalt(II) acetate tetrahydrate	Sol-gel	3-10 nm
45	Pritchard et al. (2018)	Cobalt nitrate	Modified surfactant-free	11-22 nm

**Table 2 Biological methods of synthesis of Co<sub>3</sub>O<sub>4</sub> nanoparticles**

S.No.	Authors	Precursor	Method	Nanoparticle size/diameter
1	Kumar et al. (2008)	Cobalt acetate	Bacterial ( <i>Brevibacterium casei</i> )	5-7 nm
2	Shim et al. (2011)	Cobalt chloride hexahydrate	Bacterial ( <i>Bacillus subtilis</i> ) and chemical	2-5 nm
3	Diallo et al. (2015)	Cobalt nitrate hexahydrate	Plant extract ( <i>Aspalathus linearis</i> )	3.5 nm
4	Khalil et al. (2017)	Cobalt acetate	Plant extract ( <i>Sageritia thea</i> )	20 nm
5	Bibi et al. (2017)	Cobalt nitrate hexahydrate	Plant extract ( <i>Punica granatum</i> )	40-80 nm
6	Saeed et al. (2019)	Cobalt nitrate and silver nitrate	Plant extract ( <i>Helianthus annuus</i> )	

## **2.2 ASPERGILLUS NIDULANS IN SYNTHESIS OF NANOPARTICLES**

Initially, Naveen et al. (2011) synthesized silver nanoparticles using *Aspergillus nidulans* in the particle size ranging from 73-108 nm. The activity of nitrate reductase, which was responsible for the synthesis, had been found out as 15 nmol/h/ml. Prusinkiewicz et al. (2012) used the wild-type strain of *Aspergillus nidulans* for the synthesis of gold nanoparticles. Initial pH of 6.5 was determined as optimal for fungal culture and the synthesis process was due to defense or detoxification mechanism. Khalil (2013) reported the synthesis of silver nanoparticles using *Aspergillus niger*, *Aspergillus terreus*, *Aspergillus fumigatus*, and *Aspergillus nidulans* using cell-free enzymes by autolyzing biomass. The synthesized nanoparticles displayed good antifungal activity against the human parasitic fungus *Aspergillus fumigatus*. Ravindra and Rajasab (2014) made a comparative report on the size of silver nanoparticles synthesized using culture filtrate of four different fungal species, *Rhizopus nigricans*, *Fusarium semitectum*, *Colletotrichum gloeosporioides*, and *Aspergillus nidulans*. The crystallite size was measured as 35-38 nm and the average size of particles varied between 23-74 nm. Vardhana et al. in the year 2015 isolated *Aspergillus japonicus*, *Aspergillus terreus*, *Aspergillus nidulans*, *Aspergillus flavus*, *Bortyodiplodia*, *Aspergillus niger*, *Trichoderma* and *Monilia* from the soil samples for the synthesis of silver nanoparticles, but opted to go for *Aspergillus niger* for synthesis, as it exhibited maximum growth, compared to other species. In 2017, Rajeswari et al. synthesized silver nanoparticles extracellularly using *Aspergillus* consortium of marine fungi, which also included *Aspergillus nidulans*, obtained from soil samples in the south-west coast of Tamil Nadu. The synthesized nanoparticles were tested for anticancer activity against human breast adenocarcinoma cell line (MCF7).

## **2.3 PHOTOTHERMAL CONVERSION**

Photosensitivity is a responsivity of an object, the amount to which it reacts upon receiving photons, especially visible light. It is the sensitivity to the action of radiant energy, mainly sunlight. In the photochemical context, it is a process of initiating a reaction through a substance capable of absorbing light and transferring the energy to the

desired reactants. In another context, it is about producing electric currents on reaction to light.

On account of global warming and to lessen CO<sub>2</sub> emission, solar energy utilization is significant and it can be better explored through solar thermal utilization (Han et al. 2011). Since solar energy is free and unlimited and it can meet the world's future energy needs (Faizal et al. 2015), the use of sunlight as a thermal energy source for the generation of electricity is one of the viable options to replace fossil fuels (Lenert and Wang 2012) and the cost for the process should be reduced to make the market competitive and affordable (Chieruzzi et al. 2017). Nanofluids are dispersed nanoparticles in a basic fluid like water and ethylene glycol, having better solar absorption capability, thermal conductivity and excellent stability (Khullar and Tyagi 2012). Under irradiation, temperature increases with time, while radiation weakens, temperature decreases automatically. This is attributed to the absorption of nanoparticles, leading to an increase in the temperature of nanofluids when compared to water. When nanoparticles that absorb incident radiation of visible wavelengths, are dispersed in base fluids, the absorption property is expected to increase gradually (Kameya and Hanamura 2011). Besides, solar irradiation is stronger in the visible region (Xuan et al. 2014). Moreover, nanofluids are not transparent to solar radiation as they absorb and scatter solar irradiance passing through them (Khullar et al. 2012). The incident radiation is absorbed over the entire volume of nanofluid instead of a thin layer on the surface, thus limiting heat losses to the surrounding (Hordy et al. 2014). There is a concept of volumetric absorption which is direct absorbance of solar radiation by heat transfer fluid (Hewakuruppu et al. 2015).

Table 2.3 represents the authors who have done studies with different types of nanofluids. For any application, temperature rise decides the efficiency. Plasmonic nanoparticles can be valuable candidates in direct photothermal energy conversion to raise the solar thermal efficiency, notably in the visible light spectrum.

**Table 2.3 Types of nanofluids used for photothermal studies**

S.No.	Author	Year	Type of nanofluid
1	He et al.	2013	Copper
2	Hashim et al.	2013	Aluminium oxide
3	Ladjewardi et al.	2013	Graphite
4	Zhang et al.	2014	Gold
5	Xuan et al.	2014	Silver and titanium dioxide
6	Filho et al.	2014	Silver
7	Liu et al.	2015	Graphene
8	Said et al.	2015	TiO <sub>2</sub>
9	Chen et al.	2015	Silver
10	Chen et al.	2016	Gold
11	Khashan et al.	2017	Fe <sub>3</sub> O <sub>4</sub> @ SiO <sub>2</sub>
12	Beicker et al.	2018	Gold and MWCNT

#### 2.4 Co<sub>3</sub>O<sub>4</sub> NANOPARTICLES AND RB220 DECOLORIZATION

A way of employing light is by the conversion of light energy into chemical energy via photocatalyst and employed for the treatment of industrial wastewaters like textiles, paper, etc., which contain non-biodegradable dyes in trace quantities (Sharma et al. 2012). Synthetic dyes are used in textile and paper industries due to the broad color spectrum (Kushwaha et al. 2018). Textile industries generate deep-colored effluents encompassing carcinogenic dye materials, causing allergic dermatitis, skin irritation, and mutation in humans, plants, and animals (Moon et al. 2018; Karthikeyan et al. 2019). These compounds also avert the sunlight to enter plants and animals in water, thereby annihilating photo-synthetically active radiation (PSA) in the ecosystem (Saleh 2018). To provide a clean aquatic environment, photocatalytic degradation has been used to remove harmful recalcitrant compounds by mineralization (Manimozhi et al. 2018). Though methods to remove dye include coagulation, membrane separation, flocculation, chemical oxidation, photochemical degradation, anaerobic biological degradation and



electrochemical oxidation have been employed, they exhibit low removal efficiency, require stern operating conditions and high energy demand (Moon et al. 2018; Xu et al. 2018). Due to the chemical stability of most of the dyes, advanced oxidation processes (AOPs) have been employed for degradation of dyes into environmentally benign products, which is based on the formation of hydroxyl radicals in the solution for mineralization of dyes through the usage of nanoparticles (Kushwaha et al. 2018). For azo dyes, biological decolorization is not a quite useful technique (Saleh 2018). Peculiar optical properties and minuscule size render semiconductor nanoparticles as interesting candidates for applications in optoelectronics, catalysts and fluorescence spectroscopy (Sharma et al. 2012). Metal oxides are impressive to detoxify organic pollutants (Manimozhi et al. 2018) and metal oxide photocatalysis has the potential to transform organic dyes into CO<sub>2</sub>, H<sub>2</sub>O and other non-toxic compounds (Saleh 2018). Also, photocatalysis in the presence of nanoparticles offers a great solution for the elimination of pollutants from the environment. The advantage of the process is that only nanoparticles and dye are the two components added to the reaction mixture without the involvement of harsh chemicals and conditions.

RB220 has been degraded in only two cases when nanomaterials are used (Mahmoodi et al. 2006; Khanna and Shetty 2014). Most of the studies revolving around Co<sub>3</sub>O<sub>4</sub> nanoparticles for dye degradation were observed for the treatment of methylene blue (MB) dye (Farhadi et al. 2016; Bazgir and Farhadi 2017; Mathew and Shetty 2017; Nassar et al. 2017; Vennela et al. 2019). Very few literature is available on potential of Co<sub>3</sub>O<sub>4</sub> nanoparticles to be photocatalyst for other dyes viz., rhodamine B (32% decolorization) and direct red 80 (78% decolorization) (Dhas et al. 2015), methyl orange and rhodamine B (Abbasi et al. 2018), eosine blue (Koli et al. 2018) and methyl orange (Saeed et al. 2019).

## **2.5 BACKGROUND, MOTIVATION AND SCOPE FOR PRESENT INVESTIGATION**

From the literature it has been grasped that most of the  $\text{Co}_3\text{O}_4$  nanoparticle synthesis process has been achieved with the chemical method. Though some processes are executed through physical means, adopting biological methods for synthesis is a rarity. From the literature, it is perceived that *Aspergillus nidulans* has been utilized in synthesizing primarily silver and gold nanoparticles. Since the above-mentioned fungus has the potential to synthesize various nanoparticles, it can be adopted for synthesizing  $\text{Co}_3\text{O}_4$  nanoparticles too. Though  $\text{Co}_3\text{O}_4$  nanoparticles are synthesized by various methods, they are primarily obtained by acidic treatment of chemical cobalt precursor sources in a solvent environment. Their production costs are higher, energy-consuming, often involve post-treatment and need harsh conditions. Literature available is scanty for the biological route of  $\text{Co}_3\text{O}_4$  synthesis. Hence synthesis can be bidden using potential microorganisms possibly endophytes that are relatively tolerant of these metals and quick in response to metal toxicity. Rather than bacteria, fungi provide a large amount of biomass that can be easily handled with high recovery yields. Hence, the study can be regarded as an attempt to exploit biologically synthesized  $\text{Co}_3\text{O}_4$  nanoparticles in photosensitivity studies. The synthesized ( $\text{Co}_3\text{O}_4$ ) nanoparticles are expected to be responsive to natural light and can store energy. Hence, investigating the photosensitivity of biologically synthesized  $\text{Co}_3\text{O}_4$  nanoparticles will be the fundamental requirement and heart of the proposed work since the need for solar energy utilization looms large. Thus, the present study can be regarded as an attempt to exploit biologically synthesized  $\text{Co}_3\text{O}_4$  nanoparticles in photosensitivity studies.

### **2.5.1 Background and research gaps**

- ❖ Most of the  $\text{Co}_3\text{O}_4$  nanoparticle synthesis process has been achieved with the chemical method by acidic treatment of precursor sources in the solvent environment.

- ❖ Their production costs are higher, energy-consuming, often involve post-treatment and need harsh conditions.
- ❖ Though some synthesis processes are executed through physical means, there is scantiness of available literature for the biological route of  $\text{Co}_3\text{O}_4$  nanoparticles synthesis.
- ❖ From reports, it is perceived that *Aspergillus nidulans* has been utilized for primarily synthesizing silver and gold nanoparticles.
- ❖ Biosynthesized nanoparticles have not been exploited for energy storage.
- ❖ Biosynthesized nanoparticles have not been utilized for RB220 decolorization.

## 2.6 OBJECTIVES

The overall aim of the study is to synthesize  $\text{Co}_3\text{O}_4$  biocompatible nanoparticles using endophytic fungus isolated from plant *Nothapodytes foetida* and to design a strategy to utilize the synthesized nanoparticles for harnessing solar energy and dye decolorization.

The following objectives have been carried out in the study.

- ❖ To isolate endophytic fungi from a medicinal plant *Nothapodytes foetida*
- ❖ To screen the best fungal species that is tolerant to cobalt precursor salt solution.
- ❖ To biologically synthesize  $\text{Co}_3\text{O}_4$  nanoparticles and analyze their physical, chemical, optical and electrochemical properties.
- ❖ To evaluate  $\text{Co}_3\text{O}_4$  nanofluids for solar energy harvest via photothermal conversion.
- ❖ To assess the feasibility of the energy storage in an electrical application.
- ❖ To evaluate the decolorization potential of  $\text{Co}_3\text{O}_4$  nanoparticles using RB220 dye.

## CHAPTER 3

### MATERIALS AND METHODS

#### 3.1 SAMPLE COLLECTION OF PLANTS

Samples of plant *Nothapodytes foetida* were collected from Agumbe forest located in the Western Ghats (13° 30' N, 75° 02' E), Shimoga district, Thirthahalli taluk in the Malnad region of Karnataka, India. Fresh and healthy parts of the plant like stem, seed, and leaves were cut with a sterile knife and stored in a polythene bag inside the refrigerator for further use.

#### 3.2 ISOLATION OF ENDOPHYTIC FUNGI

The laminar air flow (LAF) chamber and the cell culture room were put into fumigation. Fumigation was done using placing three beakers containing potassium permanganate, into which formaldehyde solution is added. The room was closed and left undisturbed for one day. Isolation was carried out by the method described as in Wang et al. (2007) with little modification in process time. Plant samples were surface sterilized in a tray with 75% ethanol for 1 min and 2.5% sodium hypochlorite solution for 3 min followed by repeated rinsing and washing with sterile distilled water for 2 min. The tray containing plant samples were kept for drying.

Two conical flasks of 250 ml were taken and 3.9 g of Potato Dextrose Agar (PDA) (Sisco Research Laboratories, Mumbai, India) (composition given in Appendix) was weighed and dissolved in 100 ml of distilled water. Flasks were heated in a microwave oven until the compound dissolved in water. Then the flasks were kept in an autoclave for sterilization.

Seven plastic petri dishes are kept under UV illumination in the laminar air flow chamber. Then the flasks are taken out. 20 ml of PDA with a pinch of chloramphenicol (Himedia Chemicals Pvt. Ltd., Mumbai) was poured in each of the petri dishes and

allowed to cool to room temperature in LAF. Plant samples were cut and the infected side (black color) was exposed to the side of the medium. The closed dishes were pasted with parafilm wax and properly labeled with the date. Then they were kept for incubation at room temperature in the cell culture room. These plates were used for the subculturing of individual fungi.

### **3.3 GROWTH RESPONSE STUDIES OF ISOLATED FUNGI**

The tolerance study was conducted in PDA based on Anahid et al. (2011). The isolates were screened for growth response towards salt at concentrations 500 ppm, 1000 ppm on PDA. Fungal isolates without salt solution served as control. Observations on the growth of isolates were taken by measuring the colony diameter every day. The tolerance index was estimated by measuring the diameter of the colony extension in the presence of a salt solution against the control (medium without metallic salt). The index is the ratio of the extension diameter of the treated colony to that of the untreated colony. The strain with the maximum tolerance index was chosen for further studies. Also, the strain was identified by physical examination and 23S rRNA sequencing (Yaazh Genomics, Coimbatore).

### **3.4 UPTAKE OF COBALT SALT BY TOLERANT FUNGAL ISOLATE FROM LIQUID MEDIUM**

The more tolerant strain was subjected to tolerance study in potato dextrose broth (PDB) (Himedia Chemicals Pvt. Ltd., Mumbai) (composition given in Appendix) containing metal salt in a concentration range of 1 mM – 5 mM, 10 mM, 20 mM, 25 mM, 30 mM, and 50 mM. 250 ml flasks with 100 ml PDB containing respective concentrations of salt were sterilized and inoculated with 1 ml of fresh spore suspension of strain prepared by dispersing mycelial agar disc taken from an actively growing colony on PDA plate in a solution containing Tween 80 (0.1% v/v) (Merck India) . It was then put on a shaker at 150 rpm for 5 days at room temperature. Then they were filtered and biomass was harvested. Biomass was dried in a hot air oven. The dry weight of the biomass was calculated.

### **3.5 GROWTH STUDIES**

Mycelial discs of fungi were taken from PDA plates and inoculated into 5 flasks of each containing 100 ml PDB solution. They were kept at incubator shaker at 28 °C at 150 rpm. Each day, biomass was harvested from one flask. It was dried at 45 °C for 7 hours and weighed periodically at regular intervals. The same was repeated for remaining flasks harvested on different days.

### **3.6 INOCULATION INTO PDB MEDIUM**

The protocol for the synthesis of these  $\text{Co}_3\text{O}_4$  quantum particles was adopted (Vahabi et al. 2011; Uddandarao and Balakrishnan 2016) with changes in precursor concentration and rpm. 5 mycelial discs from agar plates (PDA) was taken out (using cork borer) and poured into 100 ml PDB (The composition of PDA and PDB is given in the appendix). It was kept at 115 rpm in a rotary shaker at room temperature for three days. The solution was filtered by Whatman paper no.1 to remove medium components from the biomass. The mycelial biomass was washed with distilled water three times. The washed biomass was spilled into 100 ml 10 mM cobalt acetylacetonate solution (Sigma Aldrich, Mumbai) and was kept for stirring at room temperature for 5 days. Positive control containing only biomass and negative control containing only 10 mM cobalt acetylacetonate solution was kept simultaneously to verify the reaction. After 5 days, the reaction mixture was filtered by Whatman filter paper grade no.1 and the supernatant was taken for further analysis.

### **3.7 CHARACTERISATION OF NANOPARTICLES**

#### **3.7.1 UV-visible spectroscopy**

Spectral studies were done on the reaction mixture to monitor the formation of nanoparticles, confirm the bioreduction of salt solution and find absorption maximum. Aliquots of samples were taken out from the reaction mixture at various time intervals.

The samples were subjected to spectral analysis from 200 nm to 900 nm using a dual-beam UV-Vis spectrophotometer (Shimadzu UV-1800, Labomed USA). The optical band gap of the sample was calculated using Tauc's relation Eq. (3.1),

$$(\alpha h\nu)^n = A(h\nu - E_g), \quad (3.1)$$

Where  $\alpha$  denoted the absorption coefficient, A was constant,  $E_g$  was band gap,  $h\nu$  was photon energy and exponent n depended on the type of transition. The optical band gap was calculated by plotting  $(\alpha h\nu)^2$  against  $h\nu$  extrapolating the curve to X-axis.

### 3.7.2 Photoluminescence spectroscopy

Photoluminescence (PL) study was performed to check the fluorescence ability of nanoparticles. The solution containing nanoparticles was conducted to luminescence study by spectrofluorometer (Fluoromax-4, Horiba Scientific, Japan) to obtain photoluminescent spectra. The fluorescence spectrum was accomplished on a 1×1 cm quartz cell. Emission peak in photoluminescent spectrum was determined. To evaluate quantum yield, reference was used (Rhodamine 6G) (Loba Chemie, Mumbai). The quantum yield can be computed by the following equation Eq. (3.2),

$$QY = QY_{ref} * (\eta^2 / \eta_{ref}^2) * (I/I_{ref}) * (A_{ref}/A) \quad (3.2)$$

Where QY was quantum yield of sample, ref was reference dye used (Rhodamine-6G),  $\eta$  was the refractive index of solvent used, I was the integrated intensity of fluorescence and A was the absorbance at the excited wavelength.

### 3.7.3 Fourier transform infrared spectroscopy

Functional groups would be detected and the presence of protein capping on biosynthesized nanoparticles would be confirmed by FTIR spectroscopic studies. FTIR analyses of samples were recorded using a spectrophotometer in the range of 4000-600  $\text{cm}^{-1}$  to determine the chemical functional groups present on the surface of nanoparticles. Attenuated total reflectance (ATR) method was used to record the infrared spectrum (Perkin Elmer Spectrum 100, USA).

### 3.7.4 X-ray diffraction analysis

To examine diffraction peaks and determine crystallite size and structure, the dried reaction mixture with nanoparticles was used for x-ray diffractometry analysis. It was operated at a current of 20 mA and a voltage of 30 kV with CuK $\alpha$  radiation having a wavelength,  $\lambda=1.5405 \text{ \AA}$ . The diffracted intensities were recorded as  $2\theta$  angle ranging  $5^\circ$  to  $110^\circ$  at a scan speed of  $2^\circ$  per min (Rigaku miniflex 600 diffractometer, Japan). The average crystallite size was estimated using Scherrer equation Eq. (3.3),

$$D = (0.9 * \lambda) / (\beta * \cos\theta) \quad (3.3)$$

Where 0.9 is Scherrer's constant,  $D$  is the mean crystalline diameter,  $\lambda$  is the X-ray wavelength,  $\beta$  is the full width half maximum (FWHM) of metal oxide diffraction peak and  $\theta$  is the diffraction angle.

The lattice constant was calculated using the following equation Eq. (3.4),

$$\frac{1}{d^2} = (h^2 + k^2 + l^2) / a^2 \quad (3.4)$$

Where  $h$ ,  $k$ , and  $l$  are miller indices,  $a$  is lattice parameter,  $d$  is interplanar spacing.

### 3.7.5 Scanning electron microscope

The surface morphology of nanoparticles was observed by an analytical scanning electron microscope. The lyophilized particles were dissolved in ethanol and then dried in aluminum foil in a hot air oven. Gold sputtering was done before the analysis to prevent the charging of specimens with an electron beam (JEOL-JSM-6380-LA, Japan). SEM analysis would be followed by EDAX analysis to know the elemental composition of the nanoparticles.

### 3.7.6 Field emission gun scanning electron microscope

The morphology of nanostructures was observed further and analyzed by field emission gun scanning electron microscope (Field Emission Gun Nano Nova Scanning Electron



Microscope 450, Thermofisher Scientific, USA). The liquid solution was used directly for analysis which prevented agglomeration of particles.

### **3.7.7 Transmission electron microscope and selected area electron diffraction**

The size distribution, size and average diameter of  $\text{Co}_3\text{O}_4$  nanostructures were evaluated by transmission electron microscopy (JEOL/JEM 21000, USA). Nanoparticle solution was ultrasonicated for 15 min before analysis. Then 1  $\mu\text{l}$  of the solution was placed in a copper grid and kept it for drying. The dried grid was taken into observation. Selected area diffraction pattern was also performed to check the crystallinity of the sample.

### **3.7.8 Dynamic light scattering (DLS)**

Nanoparticles were subjected to DLS analysis (Horiba Scientific Nanopartica SZ-100) to determine mean hydrodynamic diameter and zeta potential to perceive the stability behavior of nanoparticles. The nanoparticles were characterized by nanoparticle analyzer. 3 ml of solution was taken in a cuvette and kept inside the instrument to measure the size distribution of particles and their mean diameter. For zeta potential measurement, the solution was taken in the syringe and filtered through a syringe filter to get rid of impurities (Horiba Scientific Nanopartica SZ-100, Japan).

### **3.7.9 Electrochemical studies**

To evaluate the electrochemical performance of nanoparticles, potentiostatic cyclic voltammetry for nanoparticle solution was performed at room temperature using electrochemical workstation (Autolab, Metrohm A G, Netherlands) in a three-electrode arrangement containing GCE modified  $\text{Co}_3\text{O}_4$  nanoparticle solution as working electrode, SCE as reference electrode and platinum wire as the counter electrode. The scan rate was fixed at 100 mV/s and the voltage was varied in the range -1.5 V to 1.5 V.

### **3.7.10 Atomic force microscopy**

To get information about the surface topography, the nanoparticle solution was mounted onto atomic force microscope (AFM) (Bruker Dimension Icon, USA) stub. It was analyzed in tapping mode for measuring height and thickness. Observations were carried out in the air. AFM scans were performed to measure the morphology of the sample's surface at room temperature.

### **3.7.11 Thermal characterization**

The thermal stability, moisture content and organic content of the samples were studied using thermogravimetric analysis (TGA), differential thermal analysis (DTA) and differential thermogravimetry (DTG) (Exstar TG/DTA 6300 from Hitachi high-technologies Corporation, Japan) and differential scanning calorimeter (DSC 404 F1 Pegasus Netzsch, Germany). 10 mg of samples were heated at the rate of 10 °C/min in the temperature range 40-860 °C in TG/DTA. For differential scanning calorimetry (DSC), samples were heated at a rate of 10 °C/min in an aluminium pan under a nitrogen atmosphere in the temperature range 30-950 °C while using an empty pan as the reference.

### **3.7.12 Raman spectroscopy**

The vibrational property of nanoparticle was analyzed by Raman spectroscopy (Horiba Jobin Yvon, Labram HR 800, Japan) with excitation of a laser beam at 532 nm. The dried nanoparticles were placed on a glass substrate and the spectra were collected in the wavenumber range 100-3000 cm<sup>-1</sup> at room temperature.

### **3.7.13 Diffuse reflectance spectroscopy**

The samples were analyzed for reflecting properties by diffuse reflectance spectroscopy (DRS) (Varian Cary 500 scan, South Africa) in the wavelength range of 190-3300 nm.

### **3.8 PHOTOSTABILITY OF NANOPARTICLES**

The nanoparticles were studied for photostability by performing a UV spectral scan every day to check consistency in the absorption maximum of nanoparticles. A part of the solution was stored at room temperature and the other part was stored at 17 °C in the refrigerator. Aliquots of samples were taken out from stored nanoparticles every day and the samples were subjected to spectral analysis from 200 nm to 900 nm using dual-beam UV-Vis spectrophotometer (Hitachi NCR III 40 Spectrophotometer, Japan).

### **3.9 VIABILITY TEST**

Fungal beads exposed to salt were checked for viability by randomly picking two beads and inoculated on fresh PDA plates under sterile conditions. These plates were incubated at room temperature and observed for fungal growth.

### **3.10 ELECTRICAL CHARACTERISATION OF NANOPARTICLES**

To confirm and endorse the electrical conductivity of nanoparticles, electrical characterization is ought to be performed. The dried nanoparticles were ground in mortar and pestle with polyvinylidene fluoride as binder dissolved in solvent N-methyl-2-pyrrolidone. The sample was deposited on a stainless steel substrate using vacuum-free spin coater (Navson NT 200) at 400 rpm with an acceleration time of 2 s and a steady state time of 15 s. The film was analyzed by SEM to obtain thickness. The dielectric properties of Co<sub>3</sub>O<sub>4</sub> nanoparticles have been investigated through DC probe station (E49990A Impedance analyzer, Keysight Technologies, USA) from frequency 50 Hz to 5,000,000 Hz with tungsten probe tip of diameter 20 μm. Dielectric constant, dielectric loss, loss tangent and AC conductivity were measured at room temperature at a constant voltage of 1 V with RMS amplitude of 0.5 V.

The dielectric constant was calculated by the following equation Eq. (3.5),

$$\epsilon' = C * d / (\epsilon_0 * A) \quad (3.5)$$

Where  $\epsilon'$  is dielectric constant,  $C$  is the capacitance of the sample,  $d$  is the thickness of the sample,  $A$  is the area of the sample,  $\epsilon_0$  is the permittivity of free space ( $8.85 \times 10^{-12}$  F/m).

Dielectric loss is calculated by the following equation Eq. (3.6),

$$\epsilon'' = \epsilon' * D \quad (3.6)$$

Where  $\epsilon''$  is the dielectric loss,  $\epsilon'$  is dielectric constant,  $D$  is the dissipation factor.

The AC conductivity was calculated using the equation Eq. (3.7),

$$\sigma_{ac} = \epsilon' * \epsilon_0 * \omega \tan(\delta) \quad (3.7)$$

Where,  $\omega = 2\pi f$ , angular frequency,  $\tan(\delta)$  is the dielectric loss tangent.

### **3.11 MECHANISM BEHIND BIOSYNTHESIS OF $\text{Co}_3\text{O}_4$ NANOPARTICLES THROUGH ENDOPHYTIC FUNGUS**

#### **3.11.1 Analysis of stress factors using LC-MS**

The  $\text{Co}_3\text{O}_4$  nanofluid obtained at the end of the biosynthesis process was characterized using a C18 reversed-phase liquid chromatography column and the system was operated using acetonitrile/water in binary mode with isopropanol and water in the ratio 20:80 in isocratic conditions to separate the components. These components were filtered through a 0.2  $\mu\text{m}$  membrane filter before use and were pumped from the solvent reservoir at a flow rate of 1 ml/min at ambient temperature. The sample injection volume was 20  $\mu\text{l}$  and the wavelength of the UV-Vis detector was set at 254 nm. The other conditions were oven temperature of 40  $^\circ\text{C}$ ,  $\text{N}_2$  as a carrier gas and pump pressure of 79 bars. Mass spectrometric analysis was performed using Liquid Chromatograph Mass Spectrometer (LCMS-2020, Shimadzu, USA), single quadrupole mass spectrometer coupled with Electron Spray Ionisation (ESI) operated in positive mode.

### 3.12 MEASUREMENT OF PHOTOTHERMAL CONVERSION

250 ml of biosynthesized  $\text{Co}_3\text{O}_4$  nanofluid and an equal amount of water (blank) were taken in a beaker ( $h = 7 \text{ cm}$ ,  $r = 7 \text{ cm}$ ) separately and were exposed to a LED solar simulator (Royal Enterprises, Chennai, India) and sunlight as light sources. Solar intensity was measured by lux meter (HTC instrument LX-101A light meter lux meter, Mumbai) throughout the day and peak intensity time of 90 min during the mid-day was selected for experiment and average intensity was utilized for further calculations. Increase in temperature of the solution was measured by RTD (Temperature Controller Heatron Industrial Heaters, Mangaluru) until the maximum temperature was observed. The experiments had also been conducted in triplicates for concordant values. The beaker used for the experiment has been shown in Fig. 3.1.

Using  $\text{Co}_3\text{O}_4$  nanoparticles, as an illustration, this study has interrogated the direct photothermal conversion capacity of plasmonic  $\text{Co}_3\text{O}_4$  nanofluids as the experiments were performed under both solar simulator and natural sunlight. Further, the enhancement of thermal conversion efficiency and the specific absorption rate of nanofluids would be estimated and correlated with other studies.



**Fig. 3.1 Beaker containing  $\text{Co}_3\text{O}_4$  nanofluid in thermo cool**

Considering the fluid as a medium of storing energy, the photothermal conversion efficiency is represented as the proportion of the increase in internal energy of the fluid to the total incoming radiation input (Jin et al. 2016), the photothermal conversion efficiency of nanofluid can be calculated from the equation Eq. (3.10) (Zhang et al. 2014),

$$\eta = [(c_w * m_w) + (c_n * m_n)\Delta T]/(I * A * \Delta t), \quad (3.10)$$

where  $\eta_n$  is photothermal conversion efficiency,  $c_w$  is specific heat of water,  $m_w$  is mass of water,  $c_n$  is specific heat of nanoparticle,  $m_n$  is mass of nanofluid,  $\Delta T$  is temperature rise in  $\Delta t$  time interval (exposure time) for nanofluid,  $I$  is the intensity of irradiance and  $A$  is illumination area of the beaker.

The photothermal conversion efficiency of water can be calculated from the equation Eq. (3.11) (Zhang et al. 2014),

$$\eta_w = [(c_w * m_w)\Delta T]/(I * A * \Delta t), \quad (3.11)$$

where  $\eta_w$  is photothermal conversion efficiency,  $c_w$  is specific heat of water,  $m_w$  is mass of water,  $\Delta T$  is temperature rise in  $\Delta t$  time interval (exposure time),  $I$  is the intensity of irradiance and  $A$  is illumination area of the beaker.

The enhancement of the photothermal conversion efficiency of the nanoparticles has been given in the equation Eq. (3.12) (Zhang et al. 2014),

$$\frac{(\eta_w - \eta_n)}{\eta_w} * 100\%, \quad (3.12)$$

where  $\eta_w$  is photothermal conversion efficiencies of water and nanofluid respectively.

Specific absorption rate, SAR of nanofluid is calculated from the equation Eq. (3.12) (Zhang et al. 2014),

$$SAR = c_w * \frac{m_w}{1000 * m_n} \left( \frac{\Delta T_n}{\Delta t} - \frac{\Delta T_w}{\Delta t} \right), \quad (3.13)$$

where  $SAR$  is specific absorption rate in W/g,  $c_w$  is specific heat of water,  $m_w$  is mass of water,  $m_n$  is mass of nanofluid,  $\Delta T_n$  is temperature rise of nanofluid in  $\Delta t$  time interval,  $\Delta T_w$  is temperature rise of water in  $\Delta t$  time interval.

Volumetric specific absorption rate (VSAR) is useful to figure out the impact of the volume of nanoparticles dispersed in water and is estimated by the following equation Eq. (3.14),

$$VSAR = SAR * \rho_{np}, \quad (3.14)$$

where  $VSAR$  is volumetric specific absorption rate,  $SAR$  is specific absorption rate obtained from Eq. (3.13) and  $\rho_{np}$  is the density of  $Co_3O_4$  nanoparticles, which is  $6.11 \text{ g/cm}^3$ .

Stored energy ratio (SER) is described as the ratio between energy stored by the nanofluid and water. It provides knowledge about the extra energy absorbed by the nanofluid due to the existence of nanoparticles and is determined using the following equation Eq. (3.15) (Beicker et al. 2018),

$$SER = [(T_{nf}(t) - T_{nf}(0))/(T_w(t) - T_w(0)]], \quad (3.15)$$

where  $SER$  is stored energy ratio,  $T_{nf}(t)$  is the temperature of nanofluid at time  $t$ ,  $T_{nf}(0)$  is the initial temperature of nanofluid,  $T_w(t)$  is the temperature of water at time  $t$  and  $T_w(0)$  is the initial temperature of water.

The total energy stored by the fluids ( $E_{total}$ ) during heating phase is directly proportional to maximum temperature variation experienced by fluid during the test period and it has been calculated by the equation Eq. (3.16) (Beicker et al. 2018),

$$E_{total} = m * c_p * (T_{max} - T_{min}), \quad (3.16)$$

where  $m$  is mass of fluid,  $c_p$  is specific capacity of fluid and  $T_{max}$  is maximum temperature attained and  $T_{min}$  is the initial temperature of the study.

### **3.13 FEASIBILITY STUDY OF ENERGY STORAGE FOR AN ELECTRICAL APPLICATION**

To assess the feasibility of the energy storage for an electrical application, voltage drop has been checked for different loads in an electrical circuit containing  $Co_3O_4$  nanofluid as

an electrolyte. A beaker containing 200 ml of the nanofluid was exposed to solar irradiation for the optimum time and further connected to an electrical circuit of different loads. The circuit scheme has been shown in Fig. 3.2. The electrical circuit was fabricated using ThinkTac Battery (DIY Science Kit) with copper strip as a cathode and zinc strip as an anode. The electrodes were wrapped with filter paper and inserted inside plastic straws and connected using copper wires to measure the voltage of the solution. The external circuit connecting electrodes facilitates the flow of electrons between electrodes through a variable load. The loads used in the study were red LED bulb (5 mm, 2.2 V, DC 20 mA), miniature screw base light bulb (1.5 V), DC motor (uxcell RF 300 FA, 5.9 V) and resistors of 1 M $\Omega$ , 380 k $\Omega$  and 220 k $\Omega$  (¼ W, Vishay Resistors) as shown in the Fig. 3.3. Digital multimeter (SEW DT830D, Shah Electronics, Chennai) had been used to measure the voltage (Fig. 3.4). Besides, electrical conductivity had also been checked for different concentrations of Co<sub>3</sub>O<sub>4</sub> nanofluids before and after keeping in sunlight for 1h, measured by a digital conductivity meter (EQ – 665, Equiptronics, Mumbai).

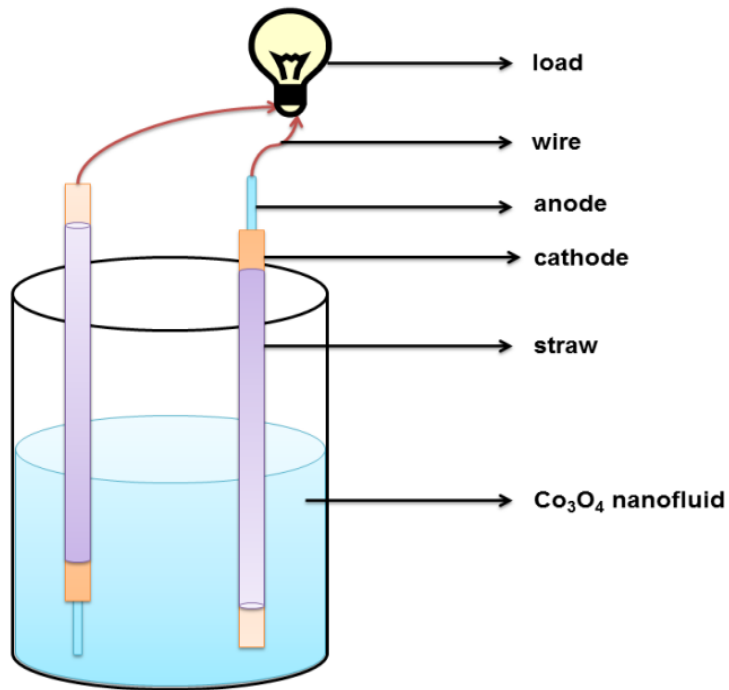


**Fig. 3.2 Schematic representation of the energy storage circuit**



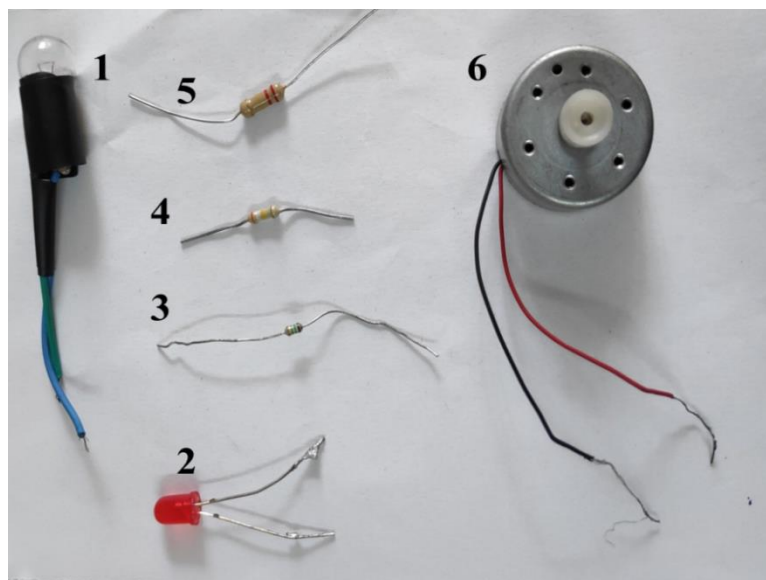


**Fig. 3.3 Types of loads used (1- Miniature screw base light bulb, 2 – LED bulb, 3- 1M $\Omega$  resistor, 4- 220 k $\Omega$  resistor, 5 – 380 k $\Omega$  resistor and 6 – motor)**



**Fig. 3.4 Multimeter and beaker with electrodes and Co<sub>3</sub>O<sub>4</sub> nanofluid**

### 3.14 DECOLORIZATION OF RB220

#### 3.14.1 Materials

To assess the decolorization by  $\text{Co}_3\text{O}_4$  nanoparticles and since textile effluent contains RB220 dye, RB220 (Indian Fine Chemicals Pvt. Ltd., Bengaluru, India) solution has been used in the present study. Structure of RB220 has been given in Figure 1 (b). Stock solutions of the dye were formulated by dissolving dyestuff powder in distilled water to a concentration of 0.005% (w/v). Different concentration of the dye was prepared by taking appropriate volumes of the stock solution and pH of the dye solution was adjusted to the desired value using 0.1 M NaOH or 0.1 M HCl. Structure of RB220 has been given in Fig. 3.5.

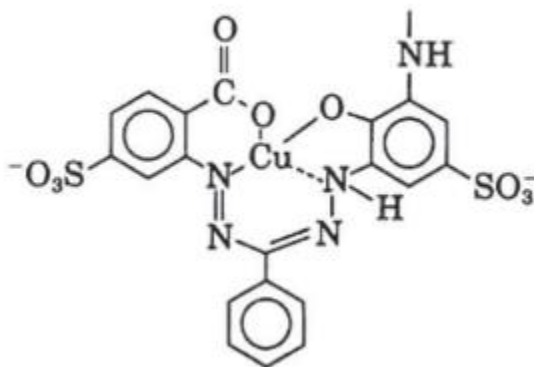


Fig. 3.5 Structure of RB220 dye (Bodurođlu et al. 2014)

#### 3.14.2 Method for photocatalytic decolorization of Reactive Blue 220 (RB220)

The synthesis of  $\text{Co}_3\text{O}_4$  nanoparticles using endophytic fungus, *Aspergillus nidulans* isolated from the plant *Nothapodytes foetida* as the reducing agent and cobalt (II) acetylacetonate as precursor compound was reported by Vijayanandan and Balakrishnan (2018). Photocatalytic activity of  $\text{Co}_3\text{O}_4$  nanoparticle was examined by degradation of

RB220 under UV light with respect to time (Deshmukh et al. 2018). 20 ml of RB220 dye was taken from the stock solution and 3 mg of  $\text{Co}_3\text{O}_4$  nanoparticle was added to the dye solution. Since the natural pH of the dye solution was 6.5-7 and to attain an adsorption-desorption equilibrium (Azeez et al. 2018), the reaction composite was stirred in the dark for half an hour on a magnetic stirrer before exposing to the UV light. Fig. 3.6 shows the scheme of the experimental set up which consists of a wooden chamber equipped with three UV lamps as an irradiation source (Philips TL-D 18W). A 250 ml borosilicate glass beaker was used as the reactor, which was placed inside the closed chamber and the reaction mixture was magnetically stirred constantly at room temperature (Fairuzi et al. 2018). The aliquots of the sample were periodically withdrawn, centrifuged at 5000 rpm for 10 min before measuring absorbance for removing nanocatalysts and progress of the reaction was tracked by measuring absorbance at 609 nm of clear supernatants using UV-Vis spectrophotometer (Shimadzu UV-1800, Labomed USA) (Khanna and Shetty 2014; Mahmoodi et al. 2006).

Dye decolorization efficiency of  $\text{Co}_3\text{O}_4$  nanoparticle was estimated using the following equation Eq. (3.17):

$$\text{Decolorization (\%)} = [(A_i - A_t)/A_i] \times 100 \quad (3.17)$$

where  $A_i$  is the initial absorbance of the dye and  $A_t$  is absorbance of the dye at any time interval (Forootanfar et al. 2012).

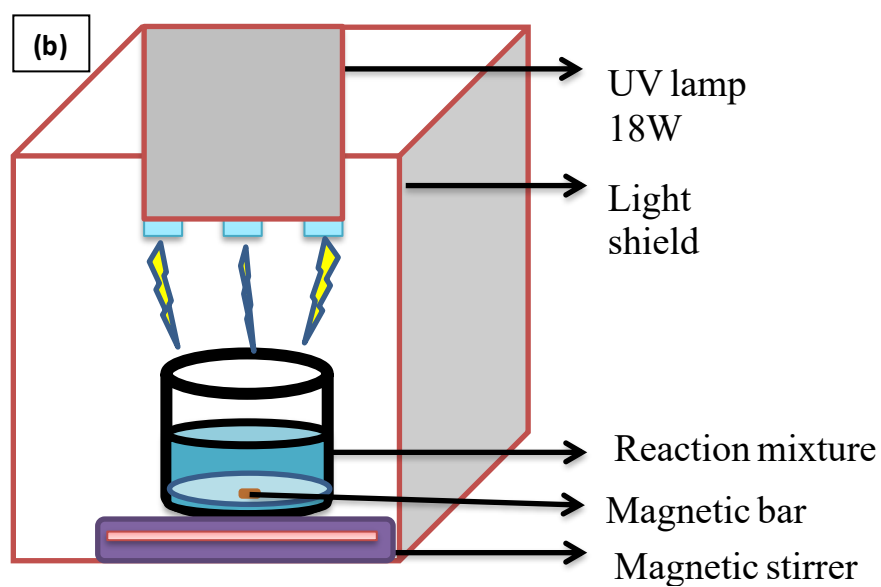


**Fig. 3.6 RB220 dye decolorization – (a) Experimental set up (b) Schematic set up**

### **3.14.3 Effect of parameters and measurement of chemical oxygen demand (COD)**

The optimum time for dye decolorization was determined by irradiating the samples with UV light and measuring their absorbances at 609 nm for every 15 min up to 5 h. The pH of the dye solution was adjusted to 7 by adding 0.1 M NaOH and 0.1 M HCl, keeping

both the concentration of the dye and nanoparticles constant at 20 mg/L and 150 mg/L respectively. The influence of dye concentration on photocatalytic decolorization was investigated for a range between 10 mg/L to 50 mg/L for the optimum pH, contact time and concentration of the nanoparticle obtained from the previous experiments. The impact of nanoparticle concentration was explored by adding 150 mg/L, 250 mg/L, 350 mg/L, 450 mg/L and 550 mg/L concentrations of nanoparticles to dye solution at optimized pH, concentration of dye and contact time. The COD of the samples under optimum conditions was determined at regular intervals using dichromatic oxidation method, which involves standard titration procedure taking distilled water as blank.

#### 3.14.4 Kinetics

The kinetics model of decolorization of dye is a pseudo-first-order rate equation represented by Equation (3.18)

$$\frac{dC_t}{dt} = -k_1 C \quad (3.18)$$

Where,  $k_1$  is first-order rate constant,  $C_t$  is concentration of dye at  $t$  min, and  $t$  is reactive time.

When  $t=0$ ,  $C_t$  is equal to  $C_0$  and the Equation (3.18) becomes Equation (3.19) as follows:

$$C_t = C_0 e^{-k_1 t} \quad (3.19)$$

## CHAPTER 4

### RESULTS AND DISCUSSION

#### 4.1 ISOLATION OF ENDOPHYTIC FUNGI

After 1 week of inoculation of plant parts in petri plates supplemented with PDA, colonies of fungi began to grow up. Plates were kept on routine monitoring every day to keep track of the growth. Different colors of fungi were observed as different varieties. Post another week, growth of colonies stopped. The colonies were subcultured during the emergence of hyphal tips from plant parts. After some time, there would be three or four fungi growing in each plate. Some fungi could be found difficult to subculture as they lose viability soon. The fungi were repeatedly subcultured until pure isolates were acquired. Negative control (without inoculation of explant) was also kept to check the contamination of fungi. In our study, four isolates were obtained from *Nothapodytes foetida* as displayed in Fig. 4.1 (a-d).

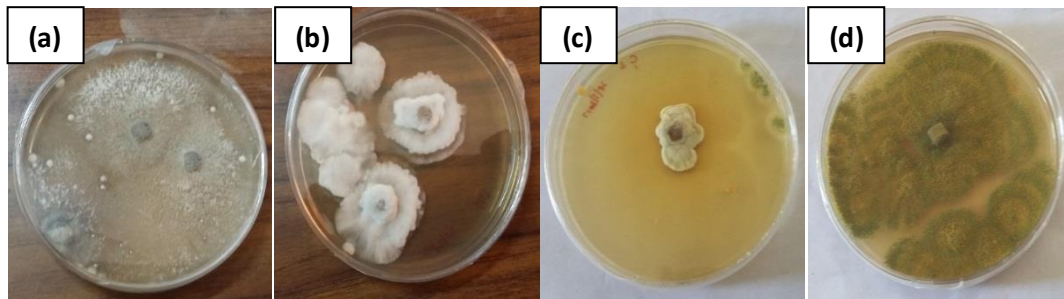


**Fig. 4.1 Fungi isolated from *Nothapodytes foetida* (a-d) (Fungus 1, Fungus 2, Fungus 3, Fungus 4)**

## 4.2 RESPONSE STUDIES OF ISOLATED FUNGI

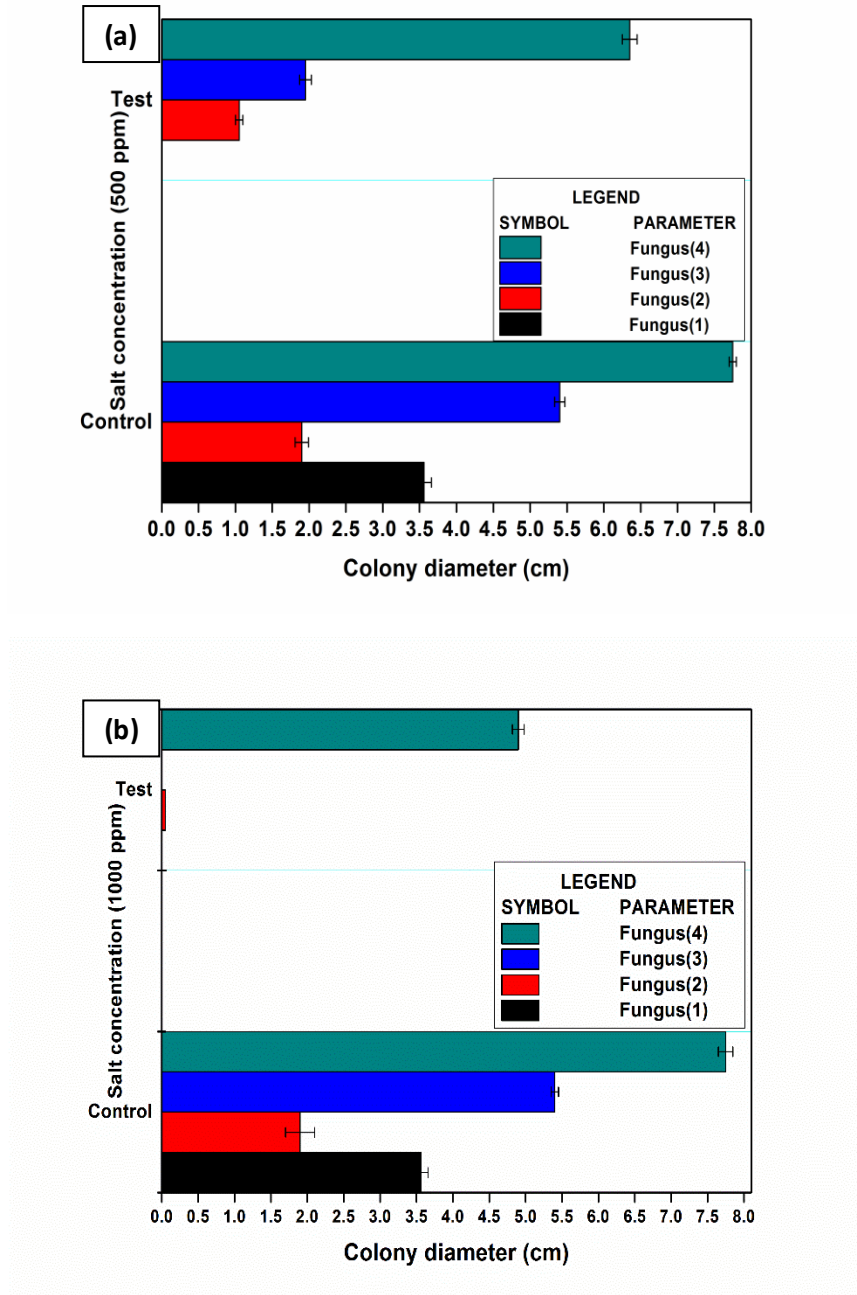


**Fig. 4.2 Colony diameter of fungal isolates against salt concentrations (a) 500 ppm  
(b) 1000 ppm**

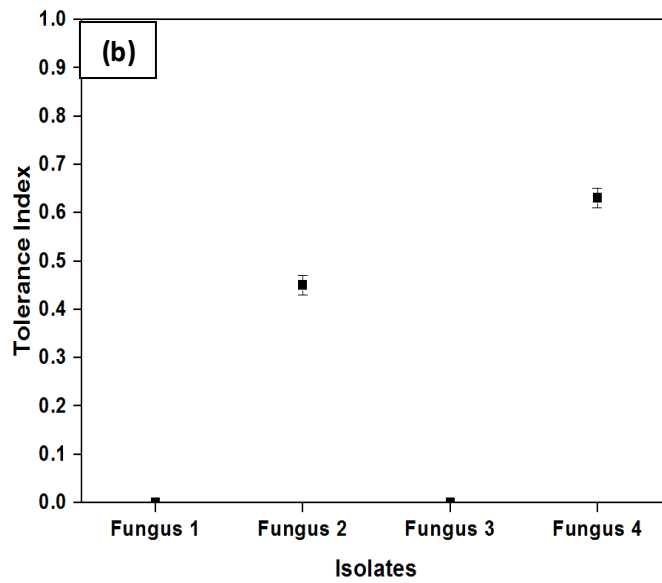
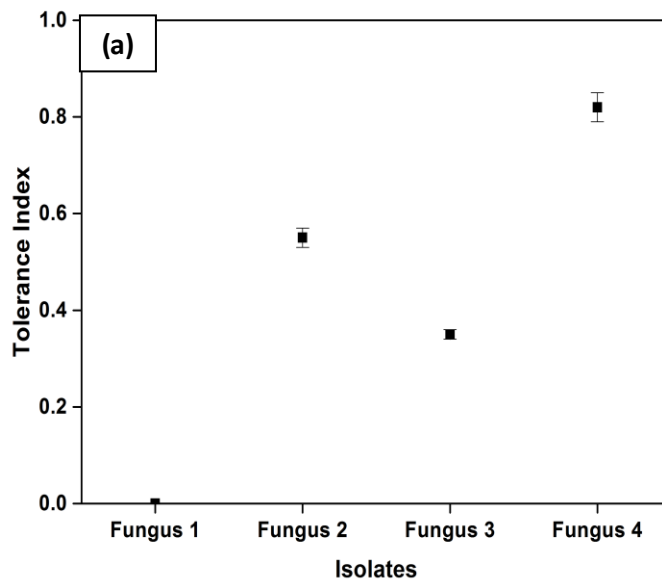


**Fig. 4.3 Tolerance index of fungal isolates against salt concentrations (a) 500 ppm  
(b) 1000 ppm**



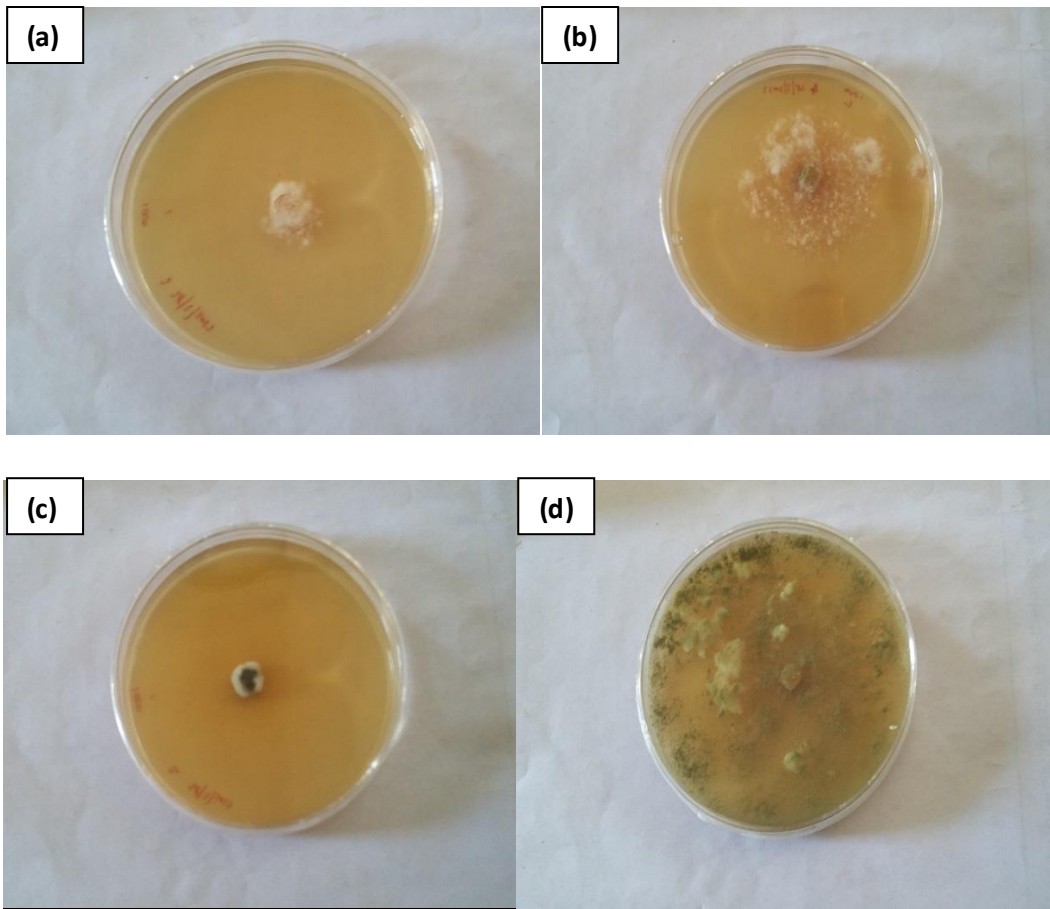


**Fig. 4.4 Growth of fungal isolates in presence of 500 ppm salt concentration (a-d)**

To find out the isolate which exhibited more salt tolerance, the fungi were subjected to growth response studies in agar plates. As displayed in Fig. 4.2 (a, b), Fungus 1 did not grow in the presence of salt and hence, it was not tolerant to 500 ppm and 1000 ppm salt concentration. In the case of fungus 2, the colony diameters were very less and the growth rate was slower. In Fig. 4.2 (b), fungus 3 was not tolerant against 1000 ppm concentration. Fungus 4 showed augmented tolerance towards salt in 500 and 1000 ppm concentration. Moreover, the rate of growth was faster and the colony diameter was more in the test than the other fungi. From Fig. 4.3 (a), the tolerance index (TI) of fungus 4 was the highest (0.81) as compared to other fungi. In Fig. 4.3 (b) also, fungus 4 exhibited the maximum TI (0.63). All four fungi in the presence of 500 ppm salt concentration had

been displayed in Fig. 4.4 (a-d). Hence fungus 4 was considered for further studies. It was identified as *Aspergillus nidulans* by physical examination and 23S rRNA sequencing (data given in Appendix)

### 4.3 UPTAKE OF COBALT SALT BY TOLERANT FUNGAL ISOLATE FROM LIQUID MEDIUM

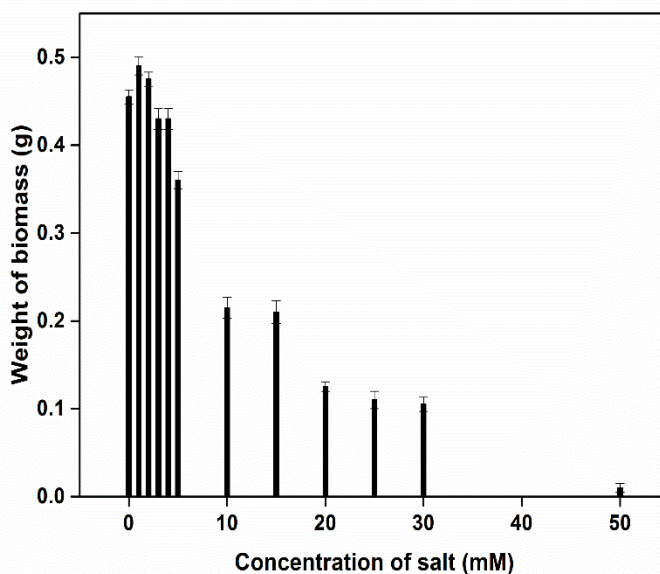


**Fig. 4.5 Effect of higher concentrations of cobalt salt on the growth of *Aspergillus nidulans***

As *Aspergillus nidulans* evinced greater TI, it was subjected to a higher concentration of metals in PDB. Axenic culture was used for inoculation into PDB. Compared to control, fungus formed more biomass in 1 mM concentration, but after that, biomass decreased gradually up to 5 mM. For 10 mM and 15 mM concentrations, still, some biomass had been produced by the fungus. But beyond 15 mM, the amount of biomass harvested was negligible as depicted in Fig. 4.5. It intimated audibly that fungus could not tolerate

concentration beyond 30 mM as scanty biomass was formed and 10 mM salt concentration was taken for synthesis.

#### 4.4 GROWTH STUDIES

Quantity of biomass kept increasing from 1<sup>st</sup> day up to 4<sup>th</sup> day. The highest biomass was obtained in 4<sup>th</sup> day. Then, it attained constant value in 5<sup>th</sup> day. So the stationary phase had been attained. Hence for biosynthesis, it was prudent to utilize the biomass harvested after 3<sup>rd</sup> day. Biomass on each day is given in Fig. 4.6.

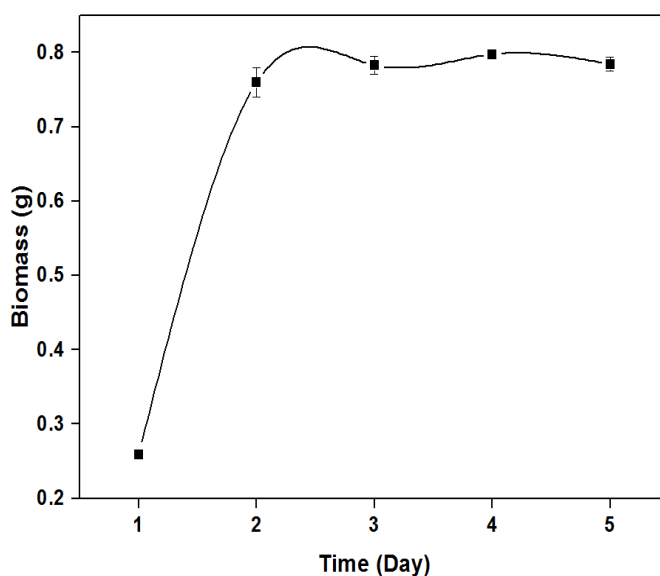


**Fig. 4.6** Quantity of biomass obtained from *Aspergillus nidulans*

#### 4.5 COLOR CHANGE

Change in color provided the first visual interference of nanoparticle synthesis. In Fig. 4.7, in the first flask, the orange color solution was our desired product (nanoparticle solution). Second flask contained 2 mM solution of cobalt (II) acetylacetonate (negative control – without biomass). Third flask contained biomass only without any salt solution (positive control – with biomass). Before the inoculation of *Aspergillus nidulans* into PDB, the color of the salt solution was pink.

After inoculation, color change in solution had been observed from pink to orange when nanoparticles were formed. The color change is an important phenomenon in the synthesis of nanoparticles, which indicates the formation of cobalt oxide nanoparticles by reduction of cobalt acetylacetonate ions (Ninganagouda et al. 2013). The color change was not observed in negative control, affirming that the nanoparticle synthesis is not a thermal process (Jain et al. 2010).



**Fig. 4.7 Change of color of flasks**

#### **4.6 UV-VISIBLE SPECTROSCOPY**

Fig. 4.8 (a) showed the UV-Vis spectra of synthesized  $\text{Co}_3\text{O}_4$  nanoparticles. The spectrum exhibits an absorption zone at the UV-region with an elevated intensity indicating absorption maximum at 315 nm, which was by cause of surface plasmon resonance band (Ghorbani et al. 2015) and the curve was narrow indicating the particles were monodisperse and were of limited size distribution. It could be assigned to ligand metal charge transfer  $\text{O}^{\text{II}} \rightarrow \text{Co}^{\text{III}}$  (Chen et al. 2007). In the literature, the blue shift had occurred due to the quantum size effect as the absorption maximum was reported as 339.60 nm (Kumar et al. 2014).

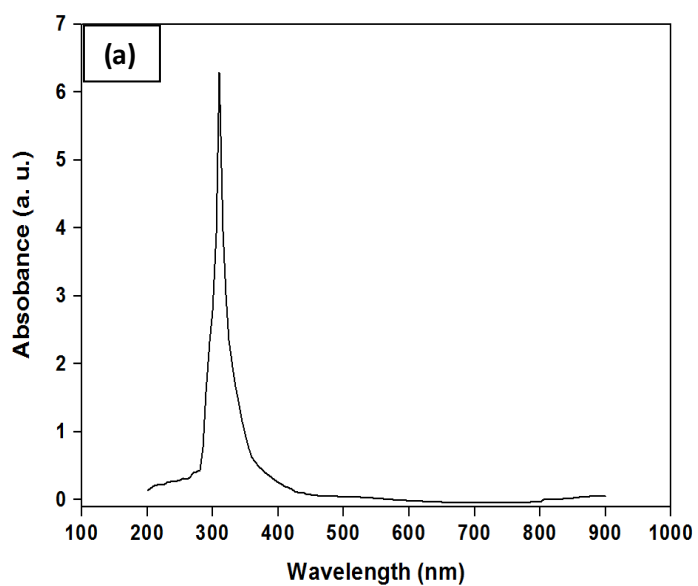


**Fig. 4.8 (a) UV-Vis spectrum of biosynthesized  $\text{Co}_3\text{O}_4$  nanoparticles**

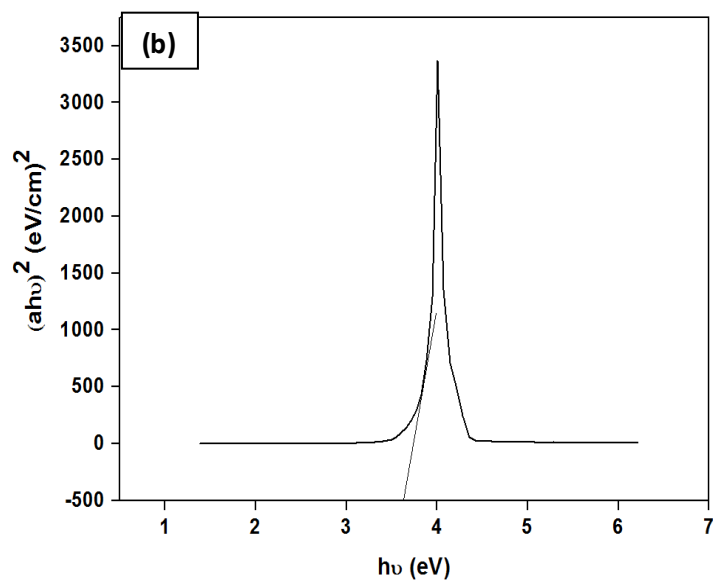


**Fig. 4.8 (b) Tauc plot of biosynthesized  $\text{Co}_3\text{O}_4$  nanoparticles**

The absorbance data were used for the calculation of bandgap and the band gap of  $\text{Co}_3\text{O}_4$  crystallite was estimated to be 3.63 eV as seen in Fig. 4.8 (b). This value was

greater than 2.58 eV-2.07 eV for Co<sub>3</sub>O<sub>4</sub> nanoparticles having a direct band gap (Patil et al. 2012). Other reported values in previous studies were 2.4 eV (Kandalkar et al. 2009), 1.4-1.5 eV and 2.18-2.23 eV (Drasovean and Condurache-Bota 2009), 2.1 eV (Koumoto and Yanagida 1981), 4.07 eV (Wadekar et al. 2017) and 3.5 eV (Agilandeswari and Rubankumar 2014).

#### **4.7 FOURIER TRANSFORM INFRARED SPECTROSCOPY**

Nanoparticle solution had been analyzed by FTIR spectroscopy to recognize the functional groups involved in the bonding of molecules and ligand capping on the surface of nanoparticles. FTIR spectrum was shown in Fig. 4.9 (a). The peak at 650.85 cm<sup>-1</sup> indicated the presence of C-S stretch. This could be because of sulfur-bearing protein residues like cysteine and methionine (Sanghi and Verma 2010). The peak at 1638.31 cm<sup>-1</sup> was due to amide I bond indicating the presence of carbonyl stretch. This was owing to the bending vibration of amines (Sundaramoorthi et al. 2009). The peak at 3367.89 cm<sup>-1</sup> could be by cause of secondary amide bonds indicating N-H stretch bond formation (Kitching et al. 2015). Therefore, FTIR data pointed towards absorption at wavenumbers that corresponded to amide and carboxylic bonds of proteins. Proteins attached to nanoparticles through amine and cysteine groups. They had been implicated in acting as a reducing agent of molecules to nanoparticles and capping agent to stabilize them, thereby preventing agglomeration (Kulkarni et al. 2014). Functional groups were acquired from heterocyclic compounds like protein, which were present in the fungal extract and are capping ligands of the nanoparticles (Saravanan 2010). Besides, protein capping augmented the biocompatibility of particles too (Jacob et al. 2014). Through FTIR, it was avowed that protein capping stabilized nanoparticles. FTIR spectrum of the salt solution alone was depicted in Fig. 4.9 (b). There was higher transmittance in C-S and amide bonds compared to nanoparticle solution. So, the nanoparticles increased the absorbance as the nanoparticle solution exhibited lesser transmittance than the salt solution. Secondary amide bond had been shifted from 3367 cm<sup>-1</sup> to 3295 cm<sup>-1</sup> owing

to the absence of fungal biomass. Shifting to lower wavenumbers proved salt solution had greater molecular mass compared that of nanoparticles.

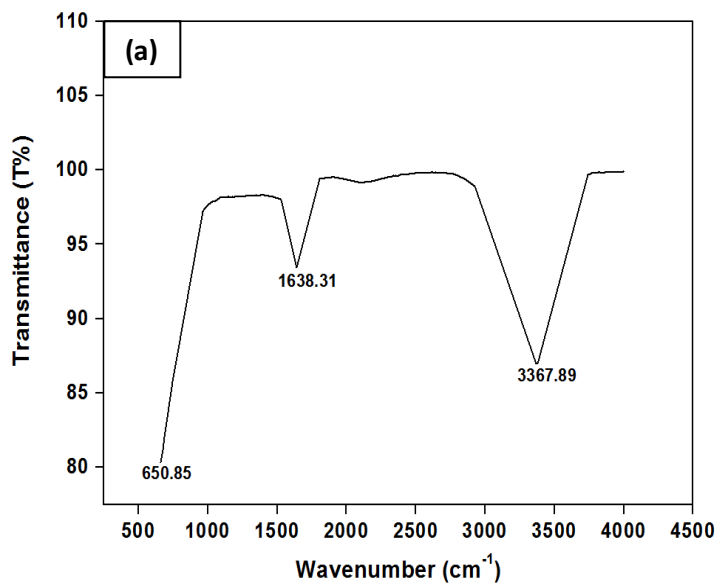


**Fig. 4.9 (a) FTIR profile of nanoparticle solution**

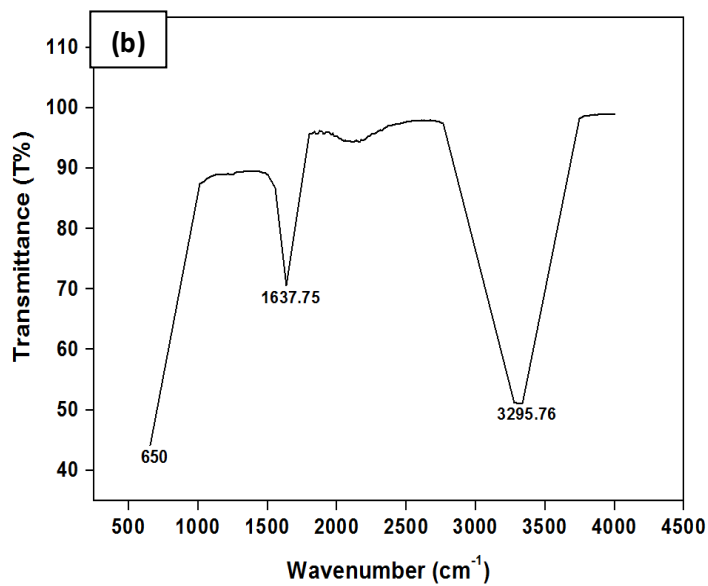


**Fig. 4.9 (b) FTIR profile of precursor solution**

## 4.8 X-RAY POWDER DIFFRACTION ANALYSIS

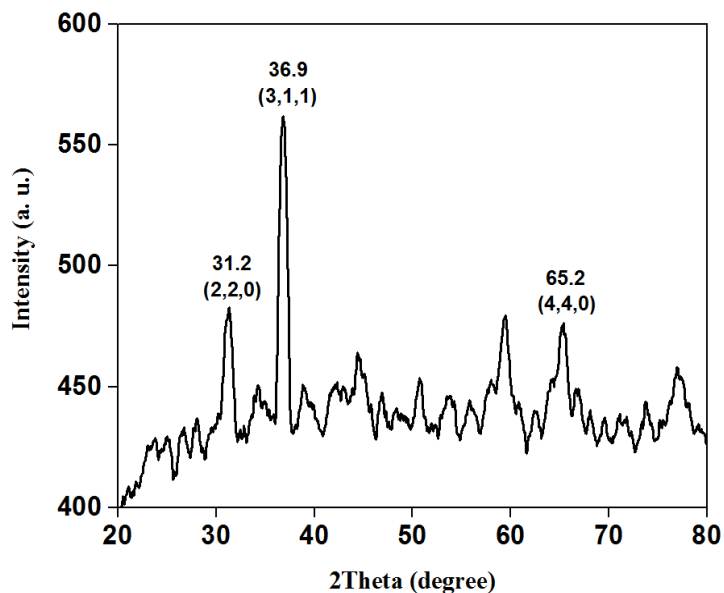


**Fig. 4.10 X-ray diffraction pattern of nanoparticles**

**Table 4.1 Planar spacing of synthesized nanoparticles**

S.N.	2 $\Theta$ (degree)	hkl	d(A $^{\circ}$ )	D(A $^{\circ}$ )
1	31.2	220	2.8	3.31
2	36.9	311	2.439	2.83
3	65.2	440	1.43	1.65

(2 $\Theta$ : XRD peak; *hkl*: indices of plane; d: calculated interplanar spacing; D: interplanar spacing according to ICDD datum (01-073-1704)).

There is a major peak formation at 36.9 $^{\circ}$  as exhibited in Fig. 4.10. Other significant peaks are figured at 31.2 $^{\circ}$ , 59.5 $^{\circ}$ , and 65.2 $^{\circ}$ . The peaks are in concordance with the data obtained in the International Centre for Diffraction Data (ICDD) card no. 01-073-1704,



which has been indicated in Table 4.2. Apart from this, the peaks are also in concurrence with Manigandan et al. (2013), having a cubic phase structure. Short insignificant impurity peaks observed could be attributed to organic substances in the culture supernatant (Kalishwaralal et al. 2008). The shift in some of the peaks could be by protein molecule from fungal biomass components. Other crystallographic impurities were observed at the XRD profile owing to the biomass residue (Gaikwad and Bhosale 2012). The structure of the crystallite was recognized to be a tetragonal spinel (Joshi et al. 1982). The size of the nanocrystallite size of computed using the Scherrer equation is 7.53 nm. The lattice constant was estimated to be 8.08 Å which is in equivalence with Latha et al. (2018) and the volume of the unit cell was determined as 527.5 Å<sup>3</sup>.

#### **4.9 DYNAMIC LIGHT SCATTERING**

The mean diameter was calculated as 30 nm. Thus, the diameter decreased on increasing the concentration and the distribution also became broad indicating various sizes of particles. The size distribution of particles has been shown in Fig. 4.11 (a). The discrepancy between DLS and TEM results could be attributed to the dependency of scattering angle on polydispersity in DLS as the nanoparticles were polydisperse (Babick et al. 2012). The hydrodynamic diameter was measured by DLS analysis, which was characterized by a ball model having the same diffusion coefficient as a measured nanoparticle. Hence the size of measured nanoparticles diverged from that of measured by TEM (Tomaszewska et al. 2013).

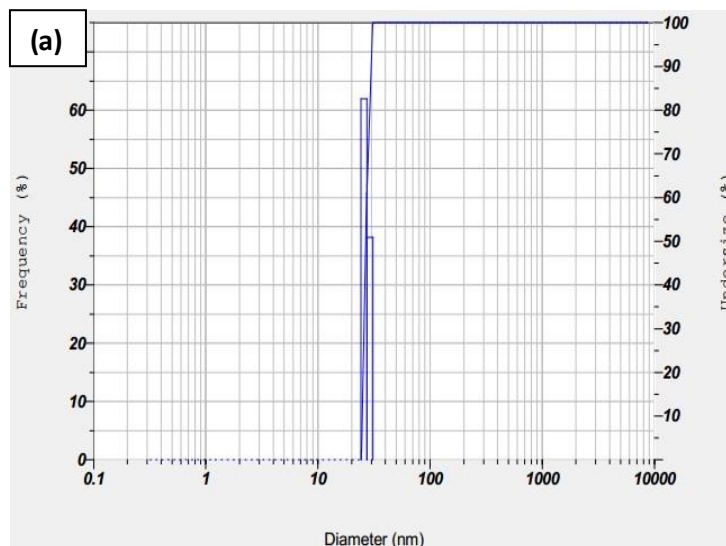


**Fig. 4.11 (a) DLS analysis of nanoparticles showing particle size distribution**

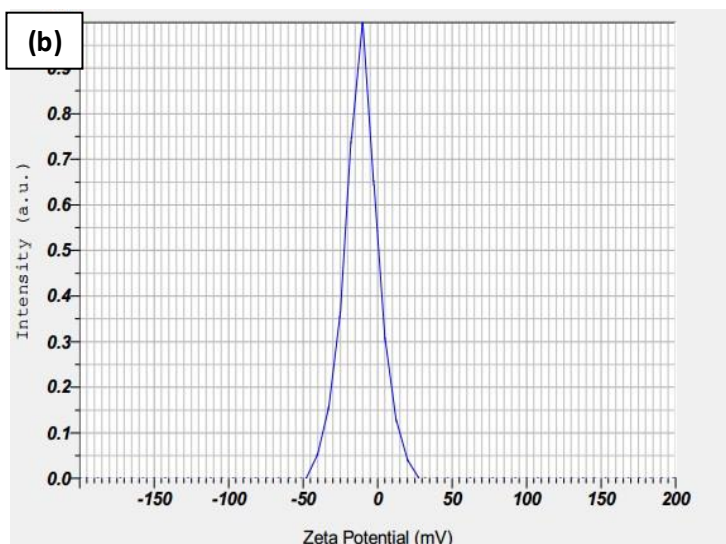
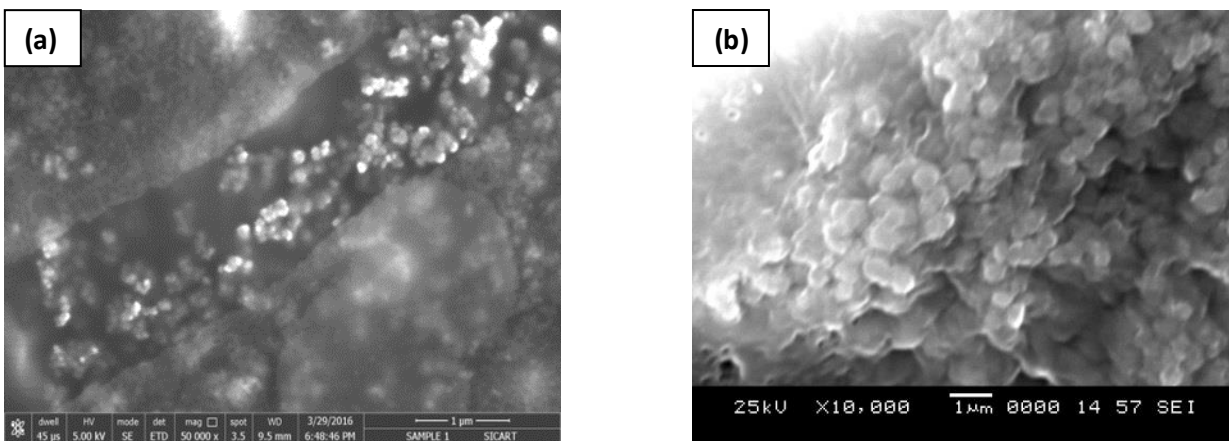


**Fig. 4.11 (b) DLS analysis of nanoparticles showing zeta potential**

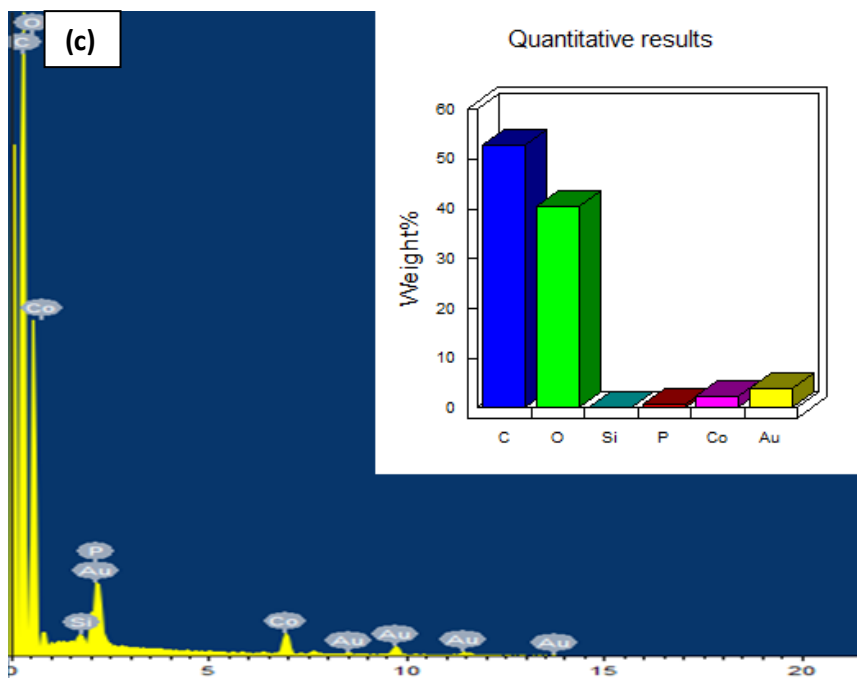
The zeta potential of nanoparticles was determined to be -10.8 mV from Fig. 4.11 (b), which revealed the surface of nanoparticles was negatively charged and a repulsive force among the particles establishing stability and preventing them from accumulation (Anandalakshmi 2016). The capping material provided the negative charge to nanoparticles and helped in stabilizing them (Haider and Mehdi 2014).

#### 4.10 SCANNING ELECTRON MICROSCOPE AND FIELD EMISSION GUN SCANNING ELECTRON MICROSCOPE

To comprehend the morphology of nanoparticles, the nanoparticles were characterized by FEGSEM and SEM. Biosynthesized nanoparticles were found to be spherical as envisioned in Fig. 4.12 (a, b). Assembled spheres indicated good connectivity, dispersibility, and homogeneity between spheres. The aggregated particles were adsorbed on the surface due to magnetic induction between the particles (Manigandan 2013). The EDAX analysis was performed to determine the composition of the product. Fig. 4.12 (c) showed the EDAX image of nanoparticles. Peaks of cobalt and oxygen were inspected corroborating the presence of  $\text{Co}_3\text{O}_4$  nanoparticles. The high concentration of carbon and oxygen was attributed to molecular formula  $\text{Co}(\text{C}_5\text{H}_7\text{O}_2)_2$  and their elemental signatures. Phosphorus and silicon could have arisen from organic substances in the cell wall of biomass content (Chin et al. 2014; Ishida et al. 2014).



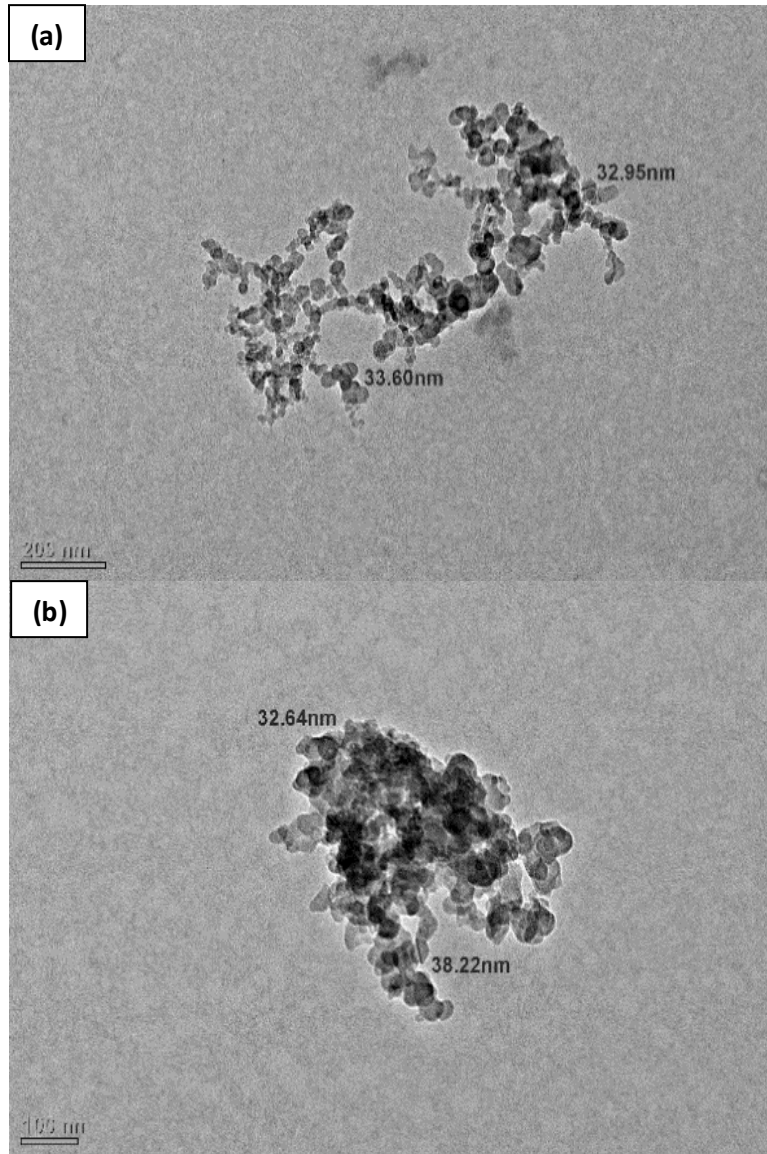
**Fig. 4.12** Electron microscope images of  $\text{Co}_3\text{O}_4$  nanoparticles (a) FEGSEM image  
(b) SEM image of nanoparticles

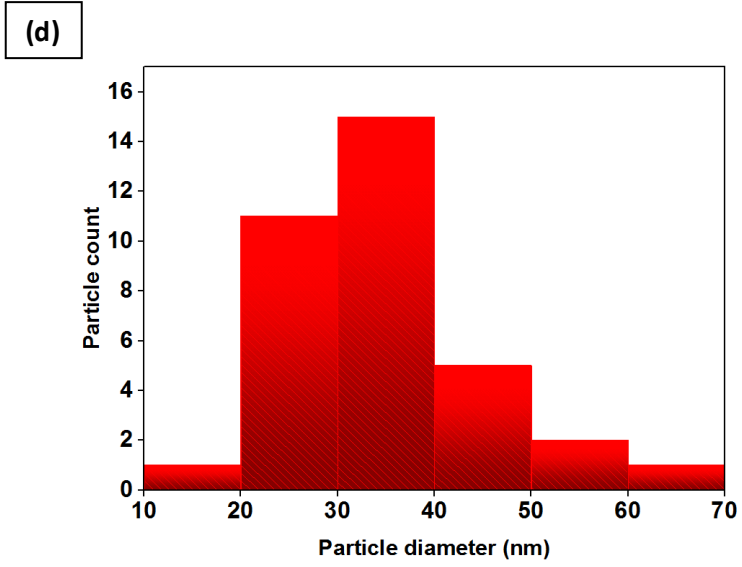
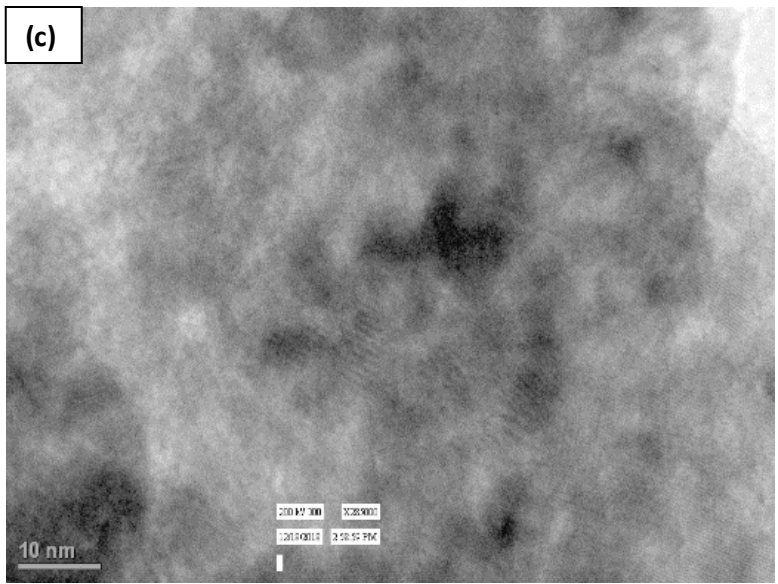


**Fig. 4.12 (c) EDAX pattern of  $\text{Co}_3\text{O}_4$  nanoparticles**

The presence of excess oxygen could be from enzymes or proteins of fungal extract (Vanaja et al. 2015). Abundant carbon could also have originated from the grid used (Sharma et al. 2010). The presence of both cobalt and oxygen indicated the formation of  $\text{Co}_3\text{O}_4$  in the synthesized samples (Athawale et al. 2010). Carbon and oxygen signals occurred due to the existence of proteins along with nanoparticles (Baskar et al. 2015). The peak for Au arose thanks to sputter coating performed before SEM analysis.

#### 4.11 TRANSMISSION ELECTRON MICROSCOPE AND SELECTED AREA ELECTRON DIFFRACTION





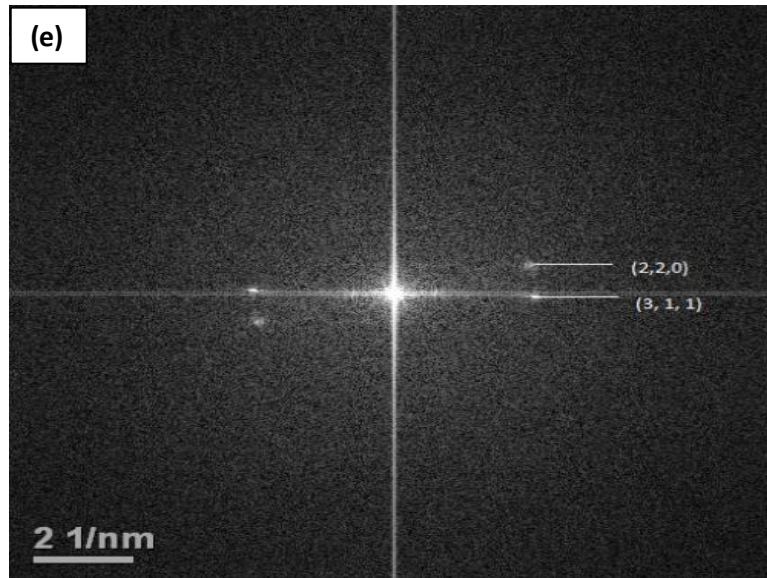


**Fig. 4.13 Electron microscope images of  $\text{Co}_3\text{O}_4$  nanoparticles (a) TEM image nanoparticles (b) TEM image (c) single nanoparticle in higher TEM magnification (d) particle size histogram obtained from TEM (e) selected area electron diffraction pattern**

To determine the size distribution of nanoparticles, homogeneity and examine the size distribution, the nanostructures had been further examined by TEM. Fig. 4.13 (a, b) depicted the shape of nanoparticles as predominantly spherical, with the particles showing dense bulk (Luisetto et al. 2008). Fig.4.13 (c) shows lattice fringes in different orientations, indicating polycrystallinity of nanoparticles (Vala 2014). The distance between fringes is 2.9 nm. Fig. 4.13 (d) shows the histogram for the particle size distribution. The size was determined to be in the range of 16 to 60 nm. Though the sizes were of variant diameter, it affirmed most of the nanoparticles fell in the size range from 30 to 40 nm and the average particle size was estimated to be 34 nm.

SAED pattern had exposed some concentric rings and dots which revealed the particles were polycrystalline nature (Fig. 4.13 (e)). The diffraction spots correspond to planes (2, 2, 0) and (3, 3, 1). The average diameter of nanoparticles is 34 nm, which is larger than the crystallite size, as particle often contains more crystals as acknowledged by Kayani et al. (2015).

#### 4.12 ATOMIC FORCE MICROSCOPY

AFM image collected on an area of  $100\ \mu\text{m}^2$ , in non-contact dynamic (tapping mode), of the sample, after deposition of the nanoparticles, is shown in Fig. 4.14 (a, b). The average roughness was found to be 3.16 nm and root mean square roughness was estimated to be 5.60 nm. It could be recognized that the nanoparticles looking like grains, were uniformly distributed and scattered over the substrate. The particles are nearly spherical and discrete as reported in Papis et al. (2009) and the grooves were not found to be homogenous (Bibi et al., 2017). The height difference between valleys and peaks were within an average range of 38 nm.

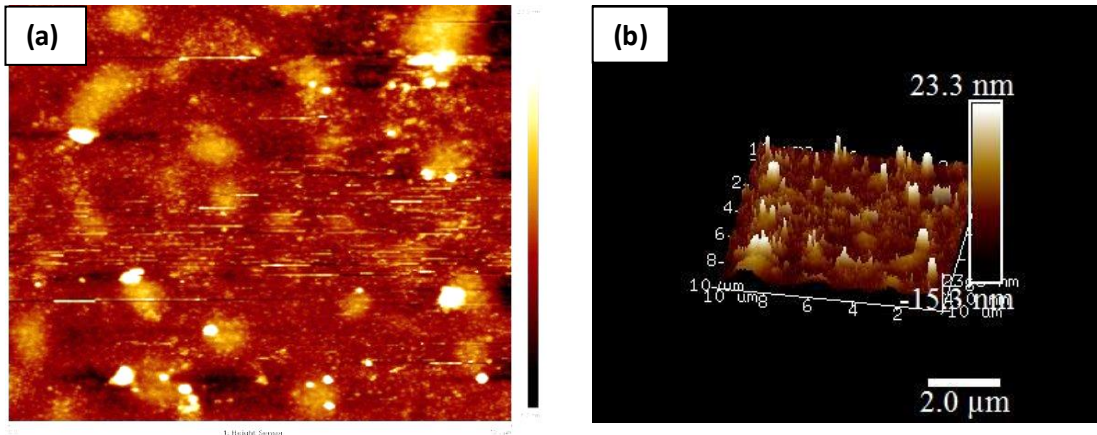
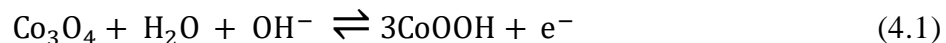


**Fig. 4.14** AFM image of synthesized nanoparticles (a) 2D profile (b) 3D profile

#### 4.13 ELECTROCHEMICAL STUDIES

The electrochemical activity of biologically synthesized nanoparticle solution was evaluated by Cyclic Voltammetry. CV was conducted to measure the specific capacitance of  $\text{Co}_3\text{O}_4$  nanoparticles. Fig. 4.15 displays the CV profile of nanoparticle solution.

The reaction involved in the process (Lichušina et al. 2008) was as follows:



Electrochemical charge transfer reaction had occurred and the change of oxidation state occurred as  $\text{Co (II)} \leftrightarrow \text{Co (III)}$ .



The anodic oxidation peak was observed at -0.983 V during the positive potential scan, whereas in the negative potential scan, the cathodic reduction peak has occurred at -0.34 V. The nanoparticles exhibited a greater current response in the positive potential region 0.5 - 0.6 V. The amount of current during the subsequent cycle has not decreased compared to the first cycle. The transport of electrons indicates a change in oxidation state, Co (II)  $\leftrightarrow$  Co (III) as depicted in Lichušina et al. (2008). The anode peak and cathode peak represent the following oxidation (Eq. 4.2) and reduction reactions (Eq. 4.3) respectively as proclaimed by Lima-Tenório et al. (2018):

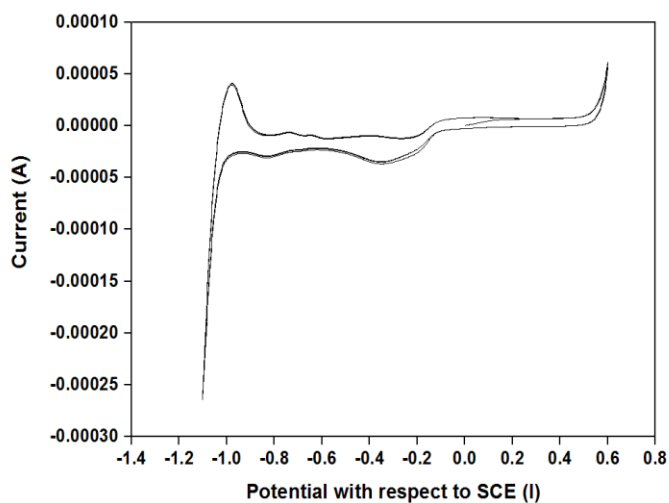


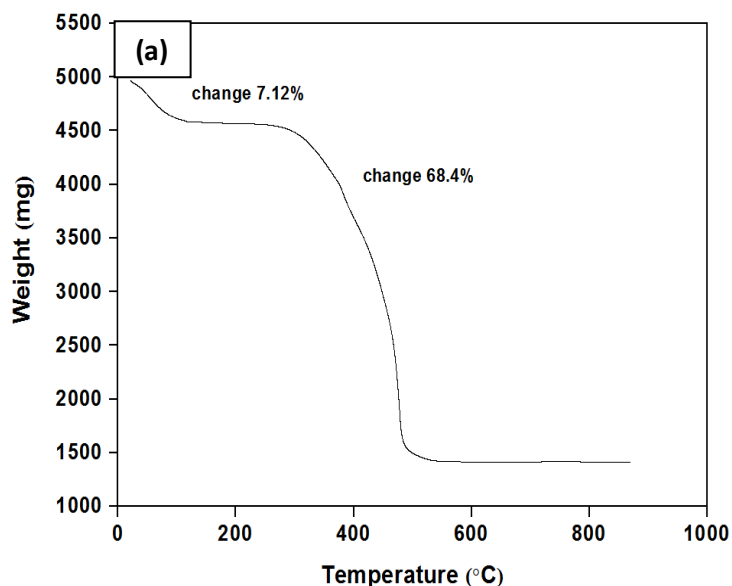
**Fig. 4.15 Cyclic voltammetric curve of Co<sub>3</sub>O<sub>4</sub> nanoparticles**

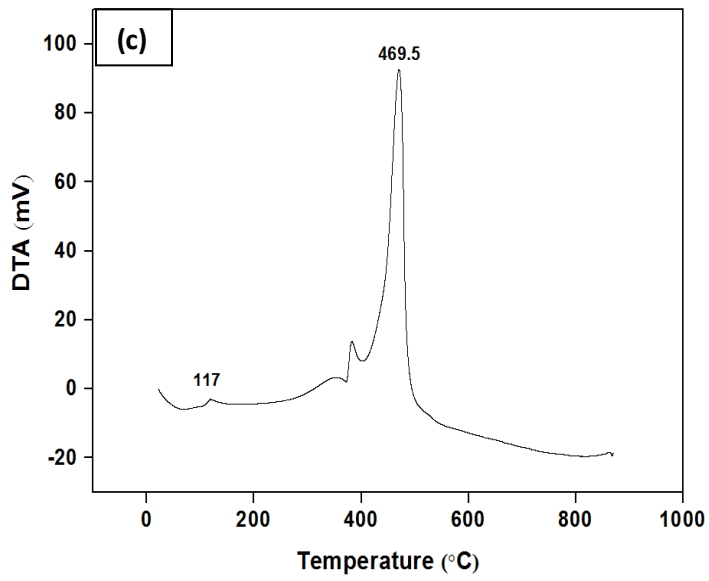
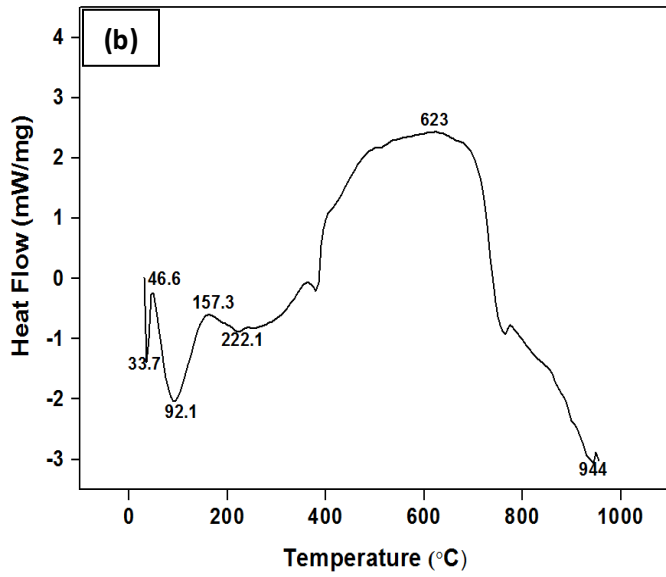


#### 4.14 THERMAL ANALYSIS

Upon increasing temperature, weight loss steps occurred. TGA Thermogram as seen in Fig. 4.16 (a) demonstrated two weight-loss behaviors from room temperature to 530 °C. The first decomposition started around 30 °C (4940 μg) and continued till 135 °C (4588 μg). The first weight loss was 7.12%. The first step was characterized by dehydration of residual moisture and loss of absorbed water. The second step could be because of desorption and subsequent evaporation of bio-organic compounds present in the sample (Mani et al. 2013). The second decomposition started at 280 °C (4526 μg) and ended at 530 °C (1430 μg). The second weight loss was intense such that it was 68.4%.

Fig. 4.16 (b) presented DSC curve of  $\text{Co}_3\text{O}_4$  nanoparticles. Low-temperature endothermic peaks at 33.7, 92.1, 222.1 °C and exothermic peaks at 46.6, 157.3 °C were all attributed to a gradual loss of residual moisture due to evaporation. A large high-temperature exothermic peak at 623 °C was observed pertaining to the desorption of bio-organic compounds present in the sample (Mani et al. 2013). An exothermic peak at 944 °C was related to the formation of crystalline particles (Athar et al. 2012).





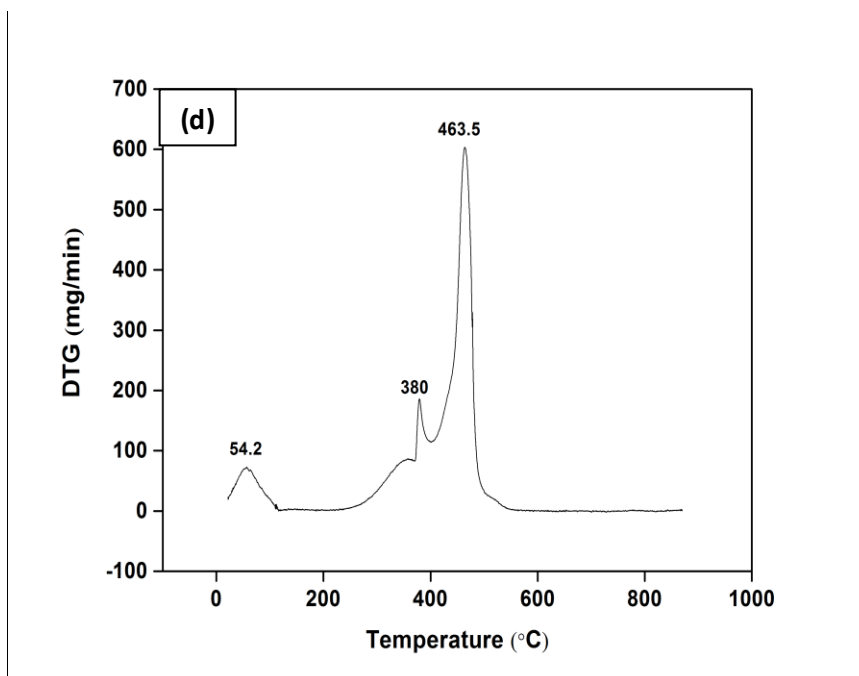


**Fig. 4.16 Thermal analysis of nanoparticles (a) TGA Thermogram (b) DSC Thermogram (c) DTA Thermogram (d) DTG Thermogram**

DTA Thermogram had been shown in Fig. 4.16 (c). The largest peak, exothermic at 469.5 °C was in the range of second weight loss peak in TGA and a large peak in DSC confirming desorption of bio-organic compounds present in the sample (Mani et al. 2013). The other peaks were related to the evaporation of residual moisture.

DTG Thermogram exhibited some peaks as displayed in Fig. 4.16 (d). An exothermic peak at 54.2 °C indicated thermal dehydration and evaporation of physically adsorbed impurities. An endothermic peak at 380 °C can be recognized as the vaporization of adsorbed water. The exothermic peak at 463.5 °C revealed the desorption of bio-organic compounds attached to nanoparticles present in the sample (Mani et al. 2013).

#### 4.15 PHOTOLUMINESCENCE STUDIES AND QUANTUM YIELD

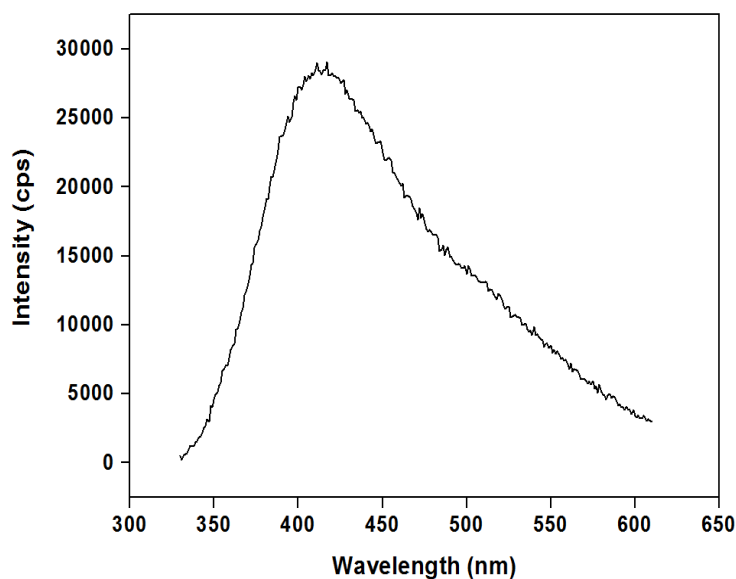


**Fig. 4.17 Photoluminescence spectrum of nanoparticles**

Photoluminescence studies could be used to evaluate the optical property of nanoparticles as photonic materials (Vigneshwaran et al. 2007). As in Fig. 4.17, the fluorescence spectrum of the nanoparticles was depicted under UV illumination. The fluorescence peak was observed related to relaxation from the motion of surface plasmon electrons and recombination of sp electrons with holes in the d band (Parang et al. 2012). The photoluminescence measurement of  $\text{Co}_3\text{O}_4$  nanoparticles was executed at an excitation wavelength of 315 nm. The emission peak was revealed at 417 nm, which fell in the visible region. The fluorescence quantum yield of nanoparticle was a probability of the occurrence of emitting a photon per photon absorbed by the system. Relied on our data, the quantum yield of nanoparticles was estimated as 4.5%. The quantum yield for undoped cobalt oxide nanoparticles has not been reported in literature so far. For CdSe quantum dots, quantum yield has been reported near to 5%. But, when ZnS shell coating

is provided to CdSe, quantum yield has increased up to 50% (Grabolle et al. 2008). Graphene quantum dots has exhibited better quantum yield (27.8%) (Zhu et al. 2015).

#### 4.16 RAMAN SPECTROSCOPY

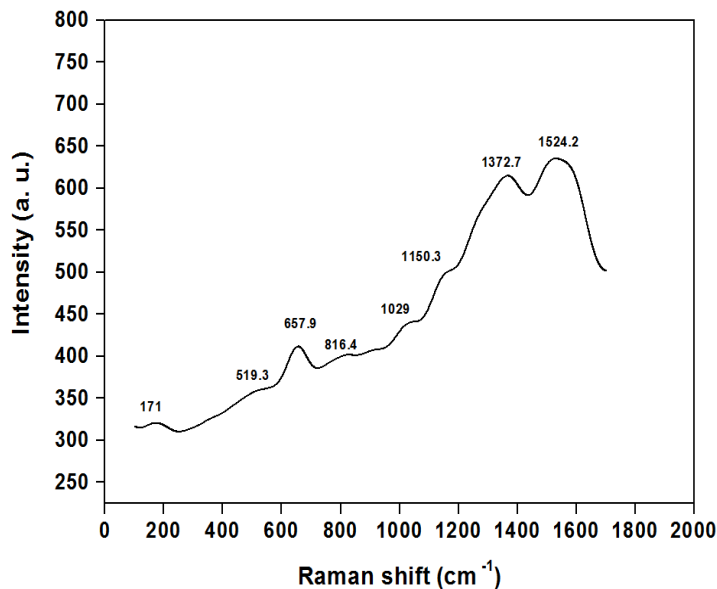


**Fig. 4.18 Raman spectrum of nanoparticles**

Raman bands at 171, 519.3, 657.9, 816.4, 1029, 1150.3, 1372.7 cm<sup>-1</sup>, 1524.2 cm<sup>-1</sup> were detected as seen in Fig. 4.18. 657.9 cm<sup>-1</sup> was attributed to the characteristic of the octahedral sites. 171 cm<sup>-1</sup> and 519.36 cm<sup>-1</sup> were signature modes of the Co<sub>3</sub>O<sub>4</sub> crystalline phase (Rashad et al 2013). 816.4 cm<sup>-1</sup> was related to the bending of the OH group. 1029 cm<sup>-1</sup> was comprehended to stretching of CH<sub>3</sub> group. 1150.3 cm<sup>-1</sup> and 1524.2 cm<sup>-1</sup> were linked to symmetric stretching of NH<sub>3</sub><sup>+</sup> group (Krishnan et al. 1973). 1372.7 cm<sup>-1</sup> related to symmetric bending of CH<sub>3</sub> group (Gunasekaran and Ponnusamy 2005). This illustrated that the surface of nanoparticles was well bonded with biomolecules, which aided in the stability of nanoparticles. The observed values were in accordance with the values of Co<sub>3</sub>O<sub>4</sub> spinel structure yet with an average shift in the order of  $\Delta\nu \sim 10$  cm<sup>-1</sup>. The shift could be attributed to size effects or surface stress/strain (Diallo et al. 2015).

#### 4.17 DIFFUSE REFLECTANCE SPECTROSCOPY

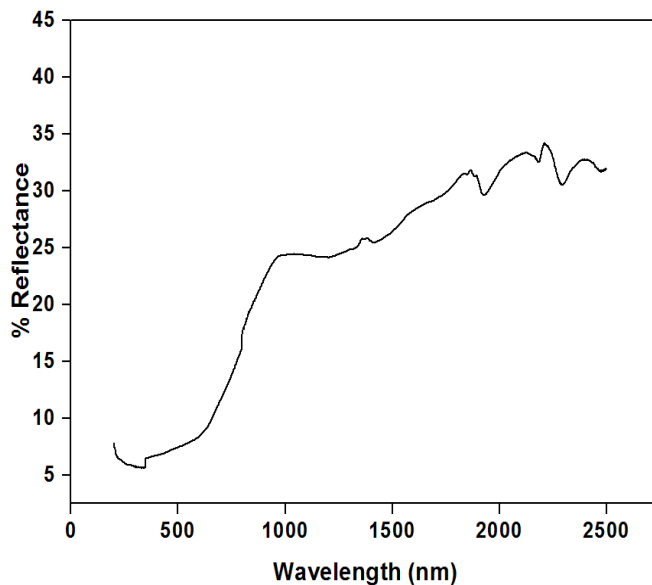


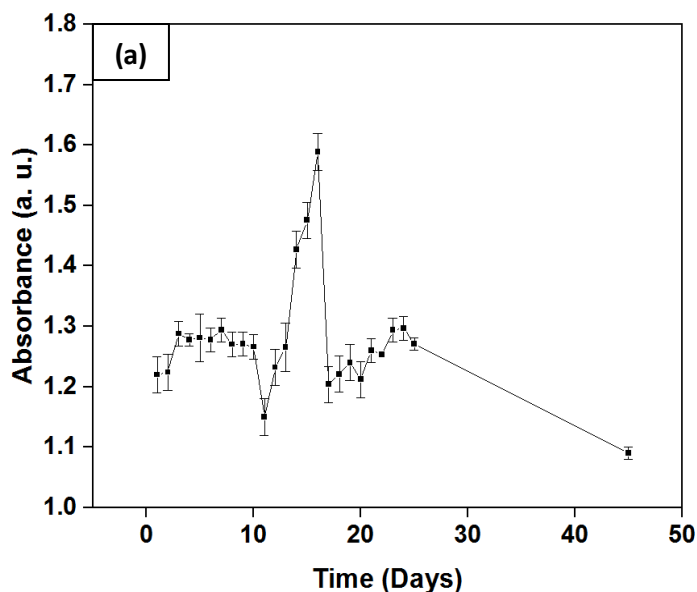
**Fig. 4.19 Diffuse reflectance spectrum**

Optical properties of nanoparticles were reviewed by diffuse reflectance spectroscopy (DRS) in Fig. 4.19. Up to 640 nm, the reflectance was lower than 10%. Then, there was a surge in reflectance from 640 nm to 970 nm thanks to the weak absorption of the material. Beyond this, there was an increase up to 35% with some dips at intervals from 1300 nm to 2500 nm.

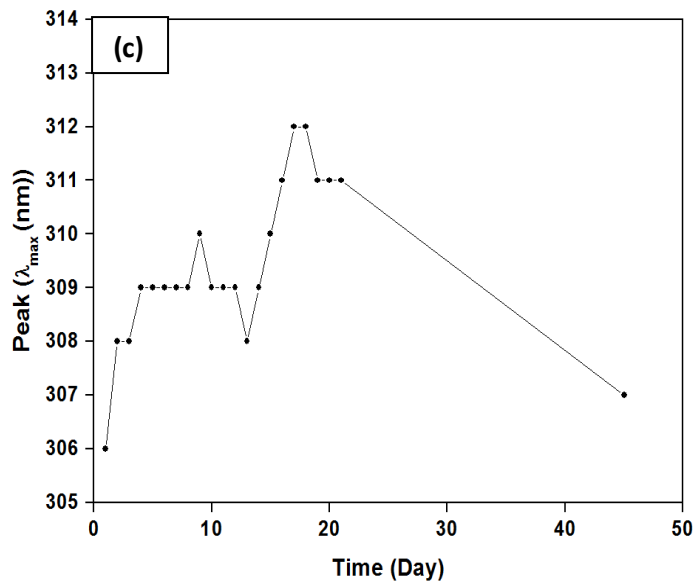
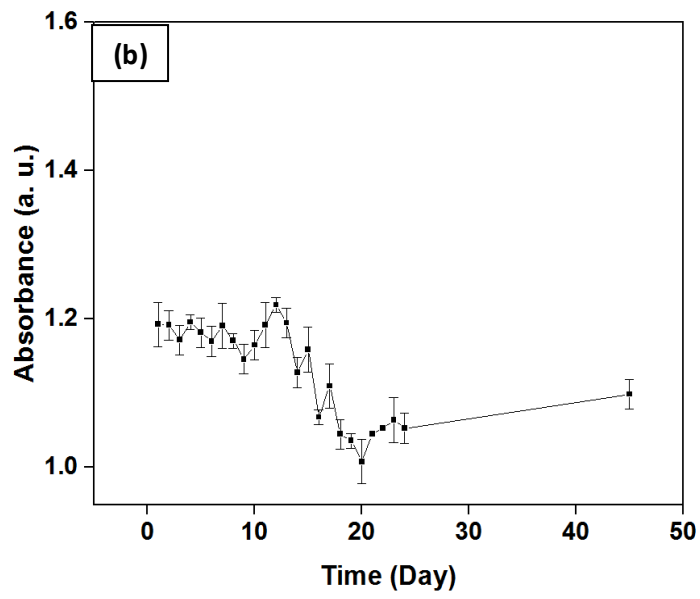
#### 4.18 PHOTOSTABILITY OF NANOPARTICLES

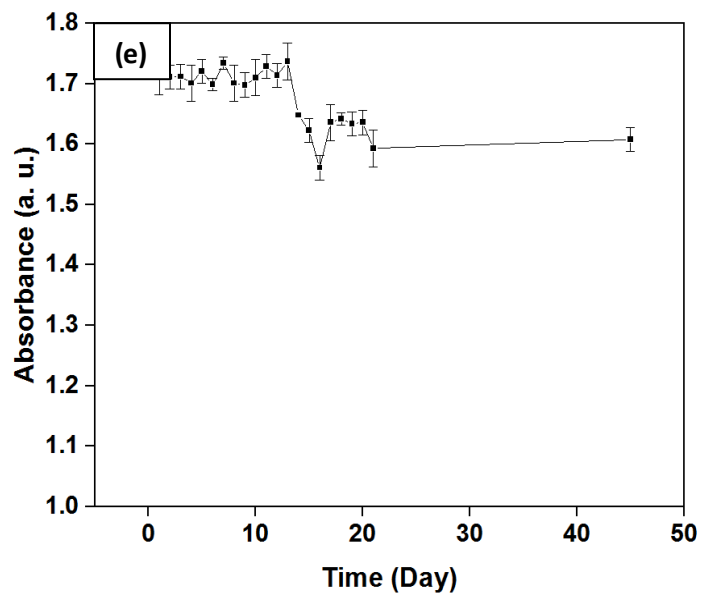
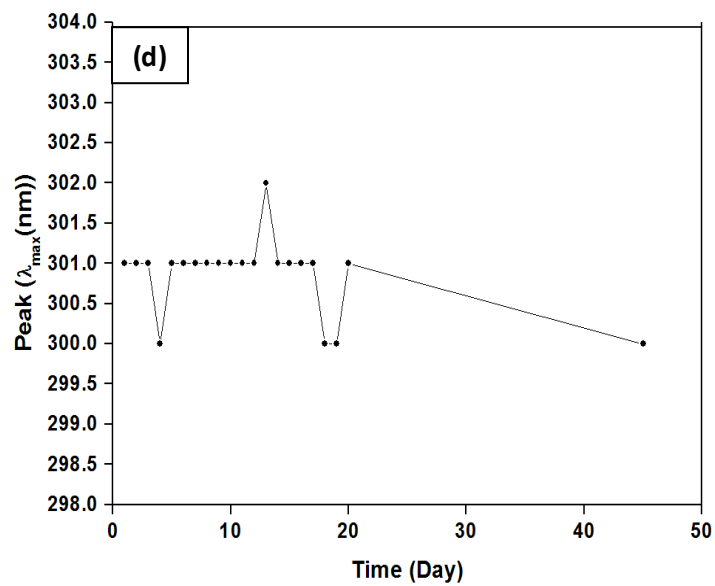
Photostability is resistant to change under the influence of radiant energy, especially light. It represents the stability of nanoparticles towards photochemical change. Moreover, it is the ability to remain in the same composition with the same size and shape, not degrading chemically without alteration of arrangement. If the capping agent is not protecting the nanoparticles well and in the case of aggregation, then they are regarded as less stable and as a function of time, particles of higher size do form. The nanoparticles had been tested for stability as a function of time and graphs had been plotted (Fig. 4.20 (a-h)).

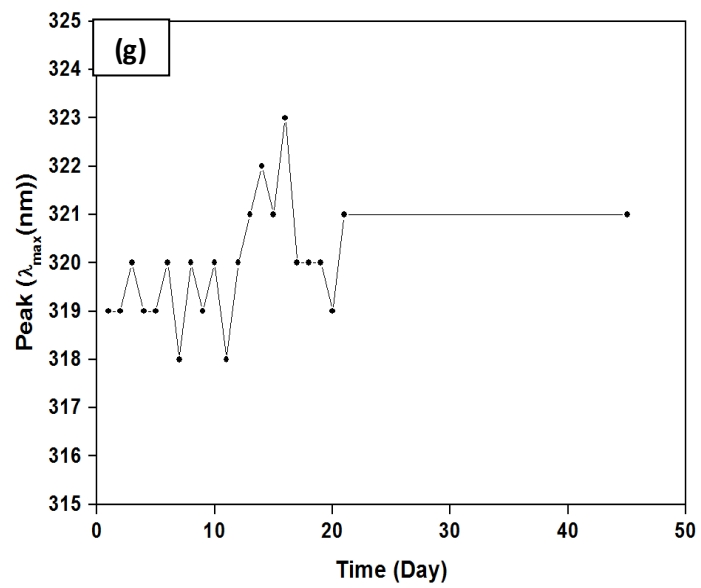
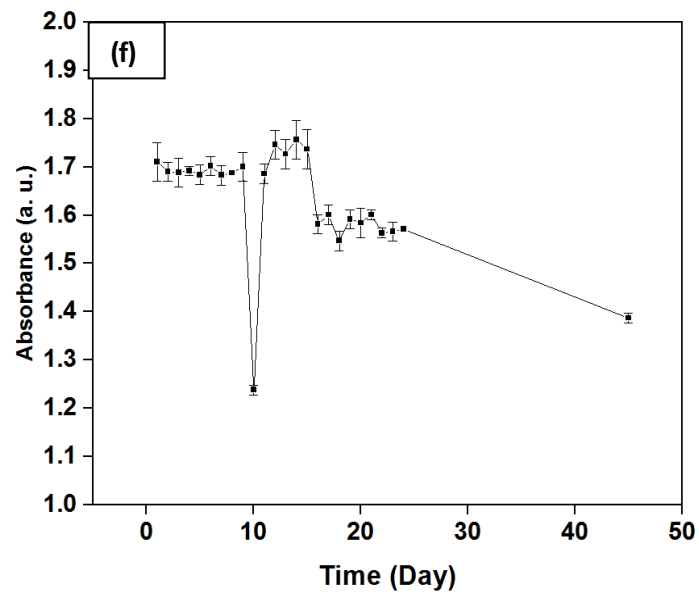
In Fig. 4.20 (a), the initial absorbance intensity was 1.22. The intensity got increasing from 11<sup>th</sup> day to 16<sup>th</sup> day. Thereafter, the intensity reduced and came down to 1.11 on the 45<sup>th</sup> day. In Fig. 4.20 (b), the intensity attained the highest value on the 13<sup>th</sup> day and thereafter, it decreased slowly up to 20<sup>th</sup> day. Then, it became steady from the 24<sup>th</sup> day up to the 45<sup>th</sup> day. In Fig. 4.20 (c), at room temperature, the solution was stable at a maximum peak of 309 nm up to 12 days, thereafter the peak increased up to 312 nm and on the 45<sup>th</sup> day, it blueshifted to 307 nm. Immediately after synthesis, the maximum absorbance was obtained at 304 nm. Peak value varied between 306–312 nm. Overall, the nanoparticles were stable in the wavelength range of 306 – 312 nm. In Fig. 4.20 (d), at 17 °C, the solution was very stable most of the time with its peak at 301 nm.











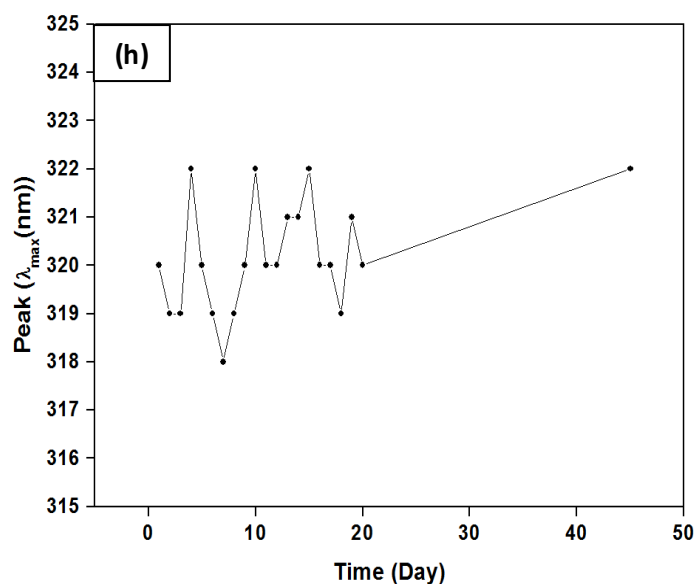


**Fig. 4.20 Photostability curve of nanoparticles (a) intensity of absorbance with respect to time in 2 mM salt concentration (at room temperature) (b) intensity of absorbance with respect to time in 2 mM salt concentration (at 17 °C) (c) wavelength maxima with respect to time in 2 mM salt concentration (at room temperature) (d) wavelength maxima with respect to time in 2 mM salt concentration (at 17 °C) (e) intensity of absorbance with respect to time in 10 mM salt concentration (at room temperature) (f) intensity of absorbance with respect to time in 10 mM salt concentration (at 17 °C) (g) wavelength maxima with respect to time in 10 mM salt concentration (at room temperature) (h) wavelength maxima with respect to time in 10 mM salt concentration (at 17 °C).**

In Fig. 4.20 (e), from day 1 to 13, the intensity continued to be in the range of 1.7. It takes a low on the 16<sup>th</sup> day to attain a value of 1.56. On 45<sup>th</sup> day, the value is 1.6. The decrease in absorbance is due to surface oxidation of nanoparticles by air (Yin et al. 2002). In Fig. 4.20 (f), the initial absorbance is 1.7, it alternates between 1.6 and 1.7, with 1.2 attaining on the 10<sup>th</sup> day. After day 18, intensity ranges in 1.5, with attaining 1.38 on day 45 . The

changes in the absorbance are attributed to a larger excess of free cobalt ions available in solution to form more  $\text{Co}_3\text{O}_4$  nanoparticles, which in turn will be translated in an increase in absorbance (Pinto et al. 2010). In Fig. 4.20 (g), at room temperature, the solution was stable, the peak often alternates between 319 and 321 nm. In Fig. 4.20 (h), the solution was stable most of the time exhibiting the peak at 320 nm, with 45<sup>th</sup> day exhibiting a peak at 322 nm. In biologically synthesized ZnS nanoparticles, a drastic decline in absorbance was observed from 0.95 to 0.6 and they are stable for only 15 days (Uddandarao and Balakrishnan 2017). Solutions kept at room temperature without shielding from light at room temperature undergo color change within 2 weeks (Pinto et al. 2010).

#### **4.19 VIABILITY TEST**

The isolates were found viable and tolerant to prolonged exposure to metal salt at 2 mM, 4 mM, 6 mM, 8 mM, and 10 mM concentrations as fungal mycelium still appeared on PDA plates (Fig. 4.21).



**Fig. 4.21 Viable fungal mycelium after exposure to salt solution**

#### **4.20 EXPLORING THE MECHANISM BEHIND BIOSYNTHESIS OF $\text{Co}_3\text{O}_4$ NANOPARTICLES THROUGH ENDOPHYTIC FUNGUS**

LC spectrum of  $\text{Co}_3\text{O}_4$  nanoparticles sample of various retention times has been depicted in Fig. 4.22. The upper part of the image shows the LC profile in ESI positive ion mode and the lower part of the image displays the profile in ESI negative ion mode. Since the negative mode is filled with background noises, positive ion mode is considered for further analysis. The retention times attained by LC are 2.12 min, 2.33 min, 3 min, 3.44 min, 4.9 min, 6.3 min, 14.46 min, and 15.96 min. Peak obtained at retention time 6.3 min indicates the presence of residual glutathione units (GSH). Peaks obtained at retention times 14.46 min and 15.96 min indicate the presence of two types of phytochelatins respectively ( $\text{PC}_2$  and  $\text{PC}_3$ ) (Damodaran et al. 2013).

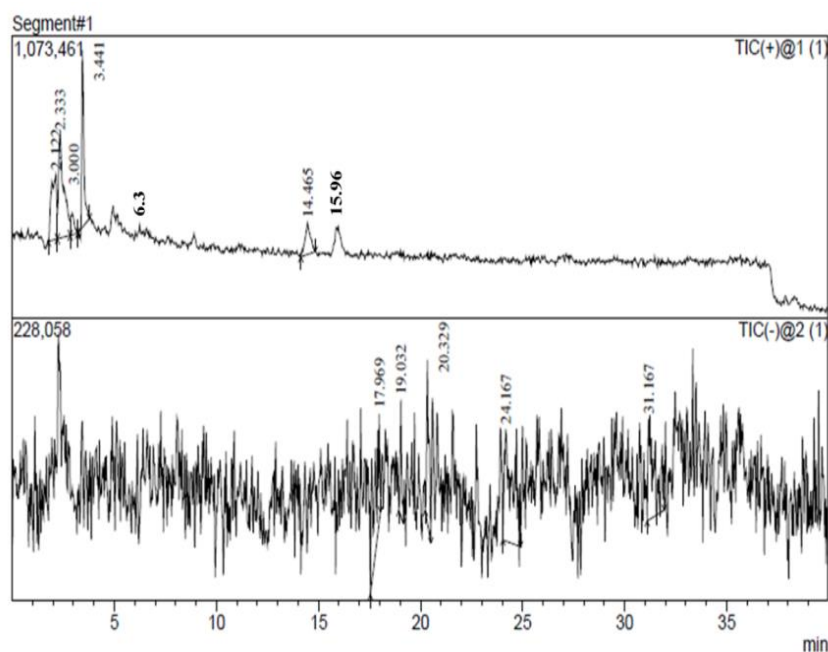


**Fig. 4.22** LC profile of  $\text{Co}_3\text{O}_4$  nanoparticles

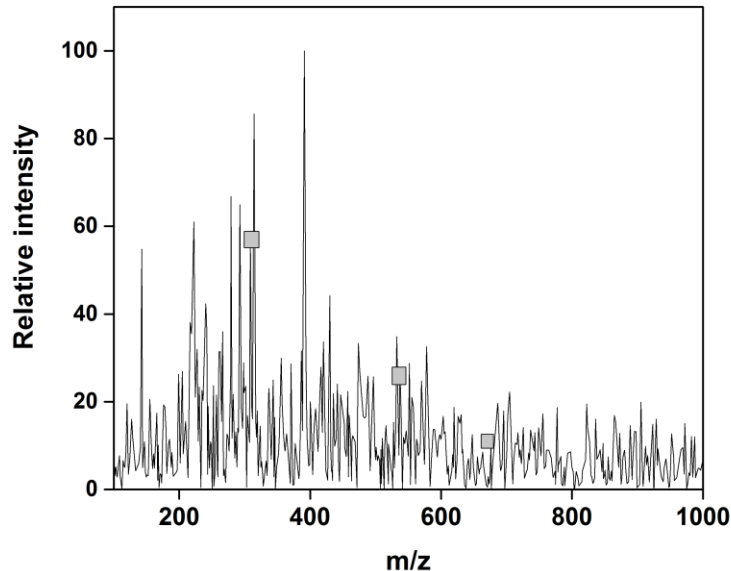


**Fig. 4.23 Mass spectrum of nanoparticles at retention time 3 min, revealing m/z ratio peaks at 308.65, 537.3, and 676.15.**

Fig. 4.23 showed m/z peaks 308.65, 537.3, and 676.15 of GSH, PC<sub>2</sub>, and PC<sub>3</sub> respectively at a retention time of 3 min (Damodaran et al. 2013). Plants react to heavy metal toxicity through the synthesis of PCs. PCs are linear polymers of  $\gamma$ -glutamyl cysteine ( $\gamma$ -GluCys) part of glutathione. Moreover, PCs [ $(\gamma$ -GluCys)<sub>n</sub>-Gly] are cysteine rich peptides synthesized utilizing glutathione (GSH) via phytochelatin synthase (PCS), which is activated upon exposure to metals like Co. PCs bind to toxic cobalt acetylacetonate [Co (acac)<sub>2</sub>] ions and consequently carried to vacuole for Co tolerance (Gill and Tuteja 2011).

#### **4.20.1 Mechanism governing the biosynthesis of Co<sub>3</sub>O<sub>4</sub> nanoparticles by *Aspergillus nidulans***

The mechanism of biosynthesis of nanoparticles by biomolecules involves series of events, like creating metal stress, creation of redox atmosphere, activation of enzyme, tautomerization, phytochelatin synthesis and contribution of phytochelatin synthase,

proteins, cysteine, glutamine, glutathione, phytochelatin, anthraquinones, and naphthoquinones.  $\text{Co}_3\text{O}_4$  nanoparticles have been synthesized through the detoxification mechanism involved in fungi, which has been reported in the present investigation and the same has been depicted in Fig. 4.24.

Extracellular enzymes, naphthoquinones and anthraquinones providing redox atmosphere have been reported in *Fusarium oxysporum* that can act as an electron shuttle in metal reduction (Vahabi et al. 2011). Ahmad et al. (2003) believed in the reduction of ions to nanoparticles through the release of reductases into solution. Nitrate reductase enzyme, which is an iron-sulfur molybdenum flavoprotein, has been involved in electron shuttle enzymatic metal reduction process and the traces of nitrate reductase have been present in *Aspergillus nidulans*, which has been quantified, activity has been checked and NADH dependent enzymes have been an important part of metal oxide biosynthesis (Naveen et al. 2011). Nitrate reductase with electron shuttling compounds and other peptide compounds can be responsible for the reduction of cobalt acetylacetonate ions and subsequent formation of  $\text{Co}_3\text{O}_4$  nanoparticles. Reduction occurs due to electrons from NADH where the NADH-dependent reductase can act as a carrier to form  $\text{NAD}^+$  (Kalishwaralal et al. 2008). Kumar et al. (2007) demonstrated an enzyme route synthesis for the synthesis of silver nanoparticles from  $\text{AgNO}_3$ . The synthesis was performed using NADPH-dependent nitrate reductase and phytochelatin *in vitro*. Usually, nitrate reductase is related to extracellular biosynthesis of nanoparticles using fungus. There is conjugation of electron shuttle with NADH dependent nitrate reductase (Ingle et al. 2008).

Metabolic activity of *Aspergillus nidulans* has led to extracellular precipitation of nanoparticles. The first step is trapping cobalt acetylacetonate ions at the surface of fungal cells and the second step is the reduction of the ions by the enzymes present in the cell. Glutathione acts as the first line of defense in the fungal cell (Mehra and Winge 1991). The primary metal complexation process starts with the synthesis of phytochelatin by phytochelatin synthase (PCS). Metal toxicity prompts the genesis of Reactive Oxygen Species (ROS) from the fungal cell. Quinones undergo radical tautomerization in response to external metal stress (Jha and Prasad 2012).



Metallothionein scavenges free radicals produced during the reactions and helps in detoxification of metals, maintain homeostasis and prevention of toxicity (Carpenè et al. 2007). Further experimentation should be executed to exemplify the complete mechanism participating in the synthesis of  $\text{Co}_3\text{O}_4$  nanoparticles.

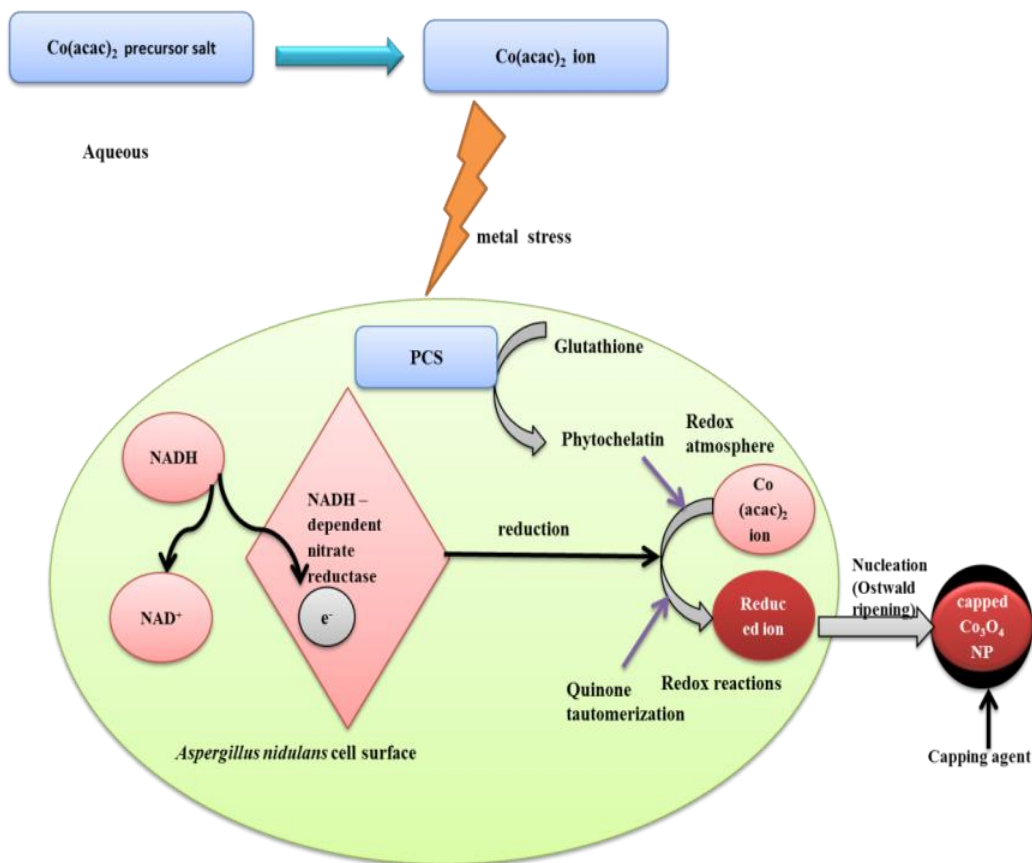


**Fig. 4.24** Probable mechanism for the biosynthesis of  $\text{Co}_3\text{O}_4$  nanoparticles in *Aspergillus nidulans*

#### 4.21 VIBRATING SAMPLE MAGNETOMETRY (VSM) ANALYSIS

The VSM curve of prepared  $\text{Co}_3\text{O}_4$  nanoparticles is shown in Fig. 4.25. The hysteresis curve has been plotted in the range of -15000 G to 15000 G. The curve is almost linear with the field and hence, remanence and coercivity values have not been measured (Koseoglu et al. 2012). There is a linear response of the magnetization with no loop opening (Moro et al. 2013). From the curve, saturation magnetization ( $M_s$ ) is found to be 0.161 emu/g. The magnetic moment has been observed, which indicates that the ions align ordered magnetically to the applied magnetic field (Ramamoorthy and Rajendran 2017). The  $\text{Co}_3\text{O}_4$  nanoparticles exhibit a paramagnetic behavior indicated by an approximately linear curve. This outcome is in concordance with the result proclaimed by Yarestani et al. (2014).

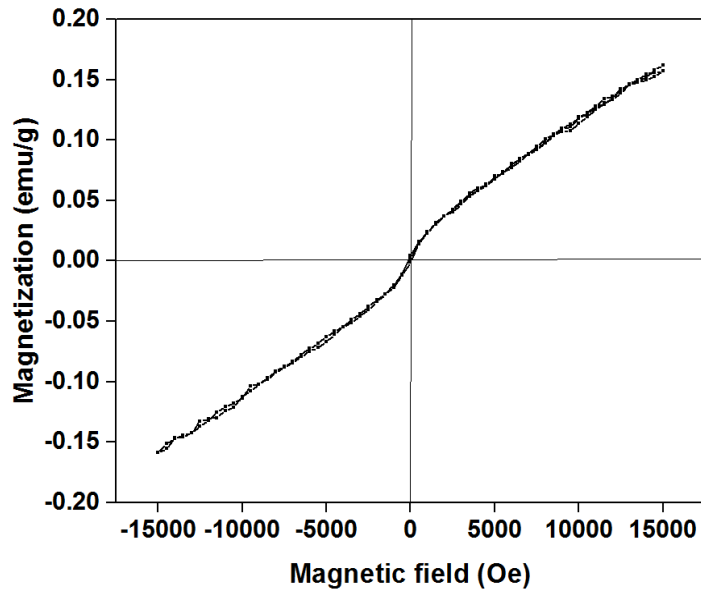
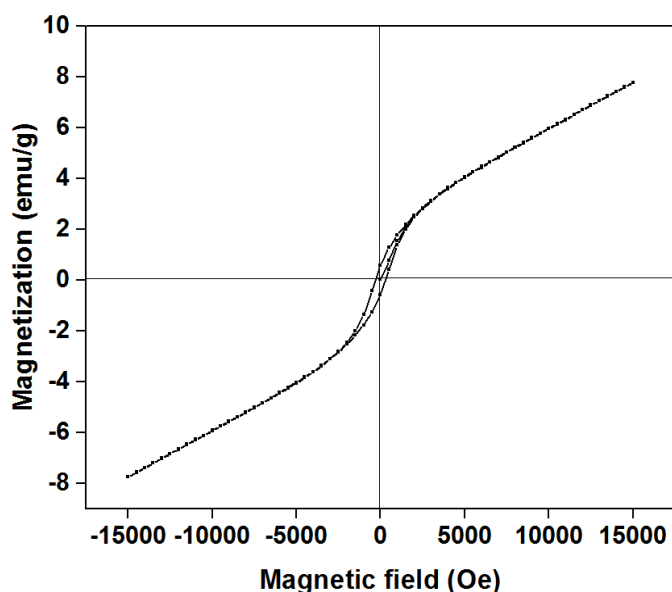


Fig. 4.25 VSM profile of  $\text{Co}_3\text{O}_4$  nanoparticles at room temperature (2 mM concentration)



**Fig. 4.26 VSM profile of  $\text{Co}_3\text{O}_4$  nanoparticles at room temperature (10 mM concentration)**

VSM curve of  $\text{Co}_3\text{O}_4$  nanoparticles (Fig. 4.26) reveals that nanoparticles are weak ferromagnetic at room temperature. There is a narrow hysteresis loop and small coercive force in the narrow hysteresis loop implies a soft magnetic material. Thus, with an increase in the concentration, coercivity force increases and change of paramagnetic to ferromagnetic nature is expected. The curve has been symmetric (Moro et al. 2013). Sharma and Sharma (2016) reported ferromagnetism at a higher temperature of 450 °C. So, the  $\text{Co}_3\text{O}_4$  nanoparticles can be applied in magnetic storage devices (Ramamoorthy and Rajendran 2017). The coercivity ( $H_c$ ), Remanence value ( $M_r$ ) and  $M_s$  are 337.5 Oe, 0.44 emu/g and 7.75 emu/g respectively. Gawali et al. (2014) reported weak ferromagnetic behavior in  $\text{Co}_3\text{O}_4$  nanoparticles, having  $M_s$  of 0.2 emu/g. Ramamoorthy and Rajendran (2017) reported  $M_s$  of 0.09 emu/g and  $H_c$  of 197 Oe in chemically synthesized  $\text{Co}_3\text{O}_4$  nanoparticles. Higher  $M_s$  value obtained is because of a lower surface-to-volume ratio in nanoparticles (Köferstein et al. 2014). Squareness ratio ( $M_r/M_s$ ) is

0.056, which reveals the curve is not square. Weak ferromagnetism can be associated with finite-size effects and excess surface spins (Mansournia and Rakhshan 2016).

#### **4.22 ELECTRICAL CHARACTERIZATION**

In Fig. 4.27, the variation of the dielectric constant of nanoparticles with log frequency has been shown. The dielectric constant was found to increase with an increase in  $\log f$  and remains a constant value before  $\log f$  of 5.5 as dipoles fail to cope up with rapid electric field variations. This may be due to interfacial (Abdelghany et al. 2019) or space charge polarization (Zamiri et al. 2015), which is also due to increased ion jump orientation effect (Prabakaran et al. 2016). There is a dispersion of dielectric constant at higher frequencies and at lower frequencies, it levels off (Masti et al. 2013). The values at the lowest frequency can be explained with Maxwell Wagner model and Koop's theory (Kamran et al. 2019). The higher value of the dielectric constant can also be attributed to smaller particle size (Godara et al. 2014) as Masti et al. (2013) indicates dielectric constant has a proportionality to grain size. The smaller size particles involve a bigger number of particles per unit volume resulting in increasing dipole moment per unit volume and high dielectric constant (Dhaouadi et al. 2012). Dielectric, ionic, bipolar and space charge polarization of the frequencies contribute towards the dielectric constant of materials (Prabaharan et al. 2017).

Variation of dielectric loss with  $\log f$  for cobalt oxide nanoparticles is shown in Fig. 4.28. The dielectric loss was found to decrease with increasing frequency and it is due to space charge polarization. There is an observation of higher energy loss at lower frequency regions due to dielectric polarization, space charge and rotation direction polarization occurring in the low-frequency range (Sagadevan 2015).

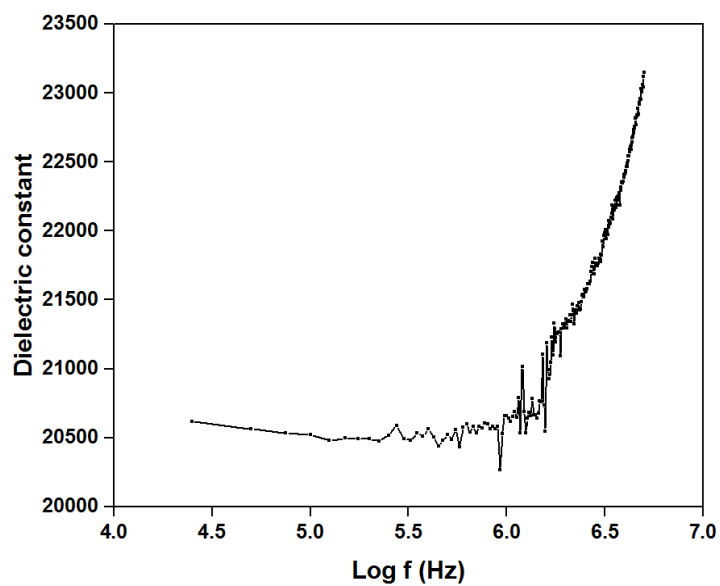


**Fig. 4.27 Dielectric constant of  $\text{Co}_3\text{O}_4$  nanoparticles as a function of log frequency**

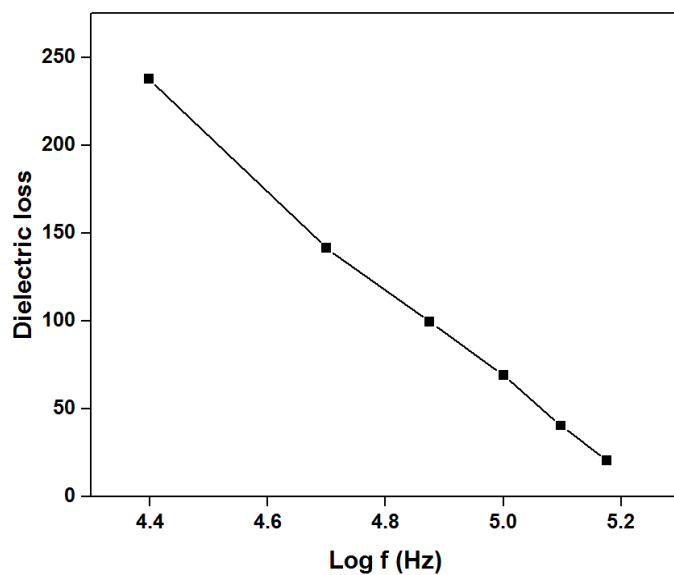


**Fig. 4.28 Dielectric loss of  $\text{Co}_3\text{O}_4$  nanoparticles as a function of log frequency**

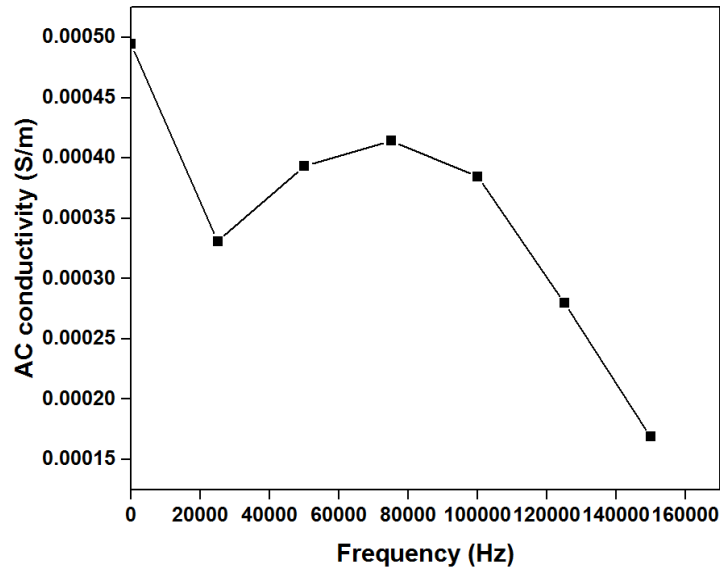


**Fig. 4.29 AC conductivity of  $\text{Co}_3\text{O}_4$  nanoparticles as a function of log frequency**

Fig. 4.29 represents the AC conductivity of  $\text{Co}_3\text{O}_4$  nanoparticles as a function of  $\log f$  to understand the conduction mechanism. AC conductivity keeps increasing with respect to frequency up to 75000, which may be due to thermally activated polaron hopping between different localized states (Das et al. 2014) and due to activity of resistive grain boundaries at lower frequencies (Routray et al. 2018). The increase in ac conductivity is due to the hopping of electrons, which is attributed to lower active grain boundaries in the nanocrystal. The steep increase in conductivity is owing to electron exchange between ions (Velhal et al. 2015). Lower values at higher frequencies are due to the difficulty of molecular realignment in the direction of the applied field (Kumar et al. 2018).

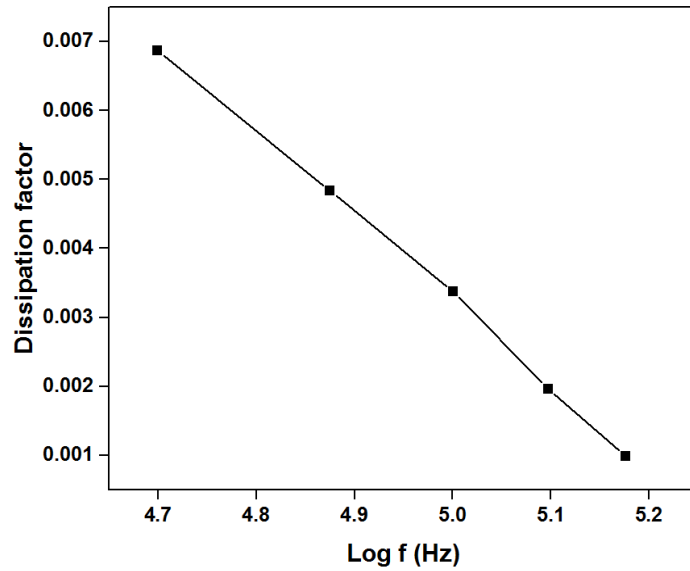


**Fig. 4.30** Loss tangent of  $\text{Co}_3\text{O}_4$  nanoparticles as a function of log frequency

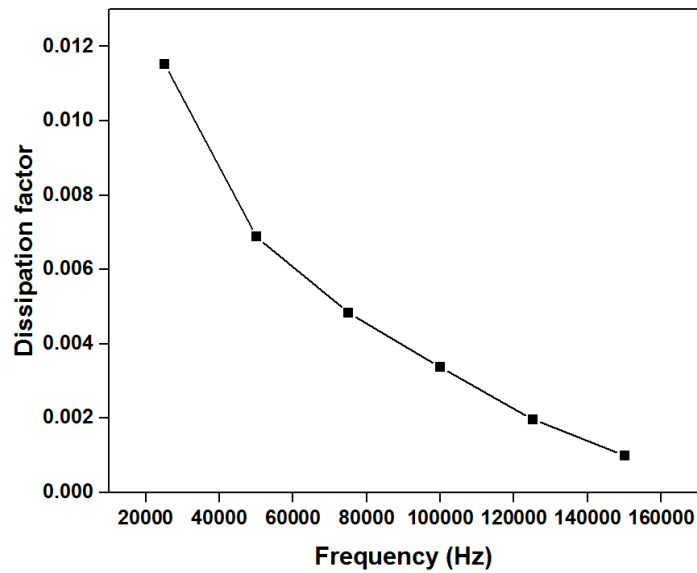


**Fig. 4.31** Loss tangent of  $\text{Co}_3\text{O}_4$  nanoparticles as a function of frequency

Fig. 4.30 indicates the loss tangent of nanoparticles as a function of log frequency. Dissipation factor, the ratio of conductance to stored charge for dielectric material (Ho et al. 2008), slowly drastic decrease in the beginning and beyond 75,000 Hz, it decreases slowly. The initial higher value is due to the semiconducting behavior of nanocomposite as a result of an increase in loss storage ratio. This has been evidenced in the AC conductivity curve too. The dissipation factor is the key to understand the insulator-metal transition (Ho et al. 2008). Loss tangent is in a linear decrease (Fig. 4.31) with respect to log frequency having a value of lesser than one up to 1,50,000 Hz. Decrease in loss tangent value establishes the compound as an insulator and can be used as a dielectric.

#### **4.23 PHOTOTHERMAL CONVERSION**

The intensity of sunlight irradiation has been measured from 9 a.m. to 5 p.m. by placing the lux meter on the terrace. Table 4.2 gives the intensity of sunlight at different times of the day from morning to evening. Since the morning (9 p.m.), the intensity continues to increase steadily and attains peak at noon. It slightly takes a dip to 118,400 lx from 1 p.m. Then it abates steadily from 2 p.m. to 3 p.m. Eventually, there is a drastic decline in intensity leading to a mere 37,000 lx at 5 p.m. Thus, the interval between 12 p.m. and 2 p.m. has been used for further experiments.

In the solar simulator, the maximum temperature reached by nanofluid was 39.3 °C, whereas in natural sunlight, 47.66 °C was the maximum temperature attained. The initial temperature was kept at 31 °C. This temperature rise is greater than some literature and lesser than some of the publications as displayed in Table 4.3.



**Table 4.2 Intensity of sunlight throughout the day**

<b>Time</b>	9 a.m.	10 a.m.	11 a.m.	12 p.m.	1 p.m.	2 p.m.	3 p.m.	4 p.m.	5 p.m.
<b>Intensity of sunlight (lx)</b>	49, 100	75, 700	96, 200	121, 700	118, 400	112, 200	88, 300	64, 400	37, 000

**Table 4.3 Temperature rise achieved for different nanofluids ((He at al. (2013); Hashim et al. (2013); Xuan et al. (2014); Filho et al. (2014); Zhang et al. (2014); Liu et al. (2015); Chen et al. (2015); Khasan et al. (2017); Bhalla and Tyagi (2017); Beicker et al. (2018))**

<b>S. No.</b>	<b>Nanofluid</b>	<b>Temperature increase ( °C)</b>	<b>Source of light used</b>
1	Cu-H <sub>2</sub> O	17.7 in NF, 25.3% greater than water	Sunlight for 23000 s
2	Al <sub>2</sub> O <sub>3</sub>	9 in NF	18 min
3	TiO <sub>2</sub> /Ag	30 in NF, 20 in water	Sunlight for 8 h
4	Ag	10 in NF, 1 in water	Sunlight for 10 h
5	Au	13 in NF, 8 in water	Simulator (106329 – 131645 lx), 5 min
6	Graphene	25 in NF	Simulator (290000 lx), 1200 s

7	Ag	18 in NF, 16 in water	Simulator 57000 lx, 60 min
8	Au	10 in NF	Simulator for 900 s
9	Fe <sub>3</sub> O <sub>4</sub> @ SiO <sub>2</sub>	14 in NF, 10 in water	Simulator for 60 min
10	Co <sub>3</sub> O <sub>4</sub>	23.3 in NF, 14.1 in water	Halogen lamp (5,83,00,000 lx), 120 s
11	Gold, MWCNT	33.1 for Au, 43.5 for MWCNT	Sunlight for 3 h
12	Biosynthesized Co <sub>3</sub> O <sub>4</sub> (this work)	16.66 in NF, 12 in water	Sunlight for 90 min

From Table 4.3, it has been known that various nanofluids have been known to have attained a different amount of temperature rise with MWCNT getting a maximum rise (43.5 °C increase). The difference in rising may be due to variant light sources used and exposure time. In general, the temperature varies in the sample depending on the intensity of solar radiation and it attains maximum value at some time, beyond which, there is no increase in temperature due to no absorption as nanofluid passes beyond the peak absorption capacity. An increase in receiver height constitutes greater absorptive capacity, which will escalate the receiver efficiency (Liu et al. 2015).

**Table 4.4 Temperature of the fluid within the beaker (under natural sunlight)**

S. No.	System	Mean T °C at 5400 s	T °C at 0 s	ΔT °C± Standard deviation
1	Surface absorption system	43	31	12
2	Nanofluid absorption system	47.66	31	16.66±0.47

**Table 4.5 Temperature of the fluid within the beaker (under solar simulator)**

S. No.	System	Mean T °C at 5400 s	T °C at 0 s	$\Delta T$ °C $\pm$ Standard deviation
1	Surface absorption system	39	31	8
2	Nanofluid absorption system	39.3	31	8.3 $\pm$ 0.47

From Table 4.4, it has been understood that the difference in a temperature rise of  $\text{Co}_3\text{O}_4$  nanofluids and water, in this case, is 4.66 °C. The difference is 5.4 °C, in the case of Bhalla et al. (2018), where blended nanoparticles ( $\text{Al}_2\text{O}_3 + \text{Co}_3\text{O}_4$ ) were used. From Table 4.5, it has been understood that during the use of the solar simulator, the temperature rise is the same in the case of both water and  $\text{Co}_3\text{O}_4$  nanofluid as the intensity of LED is 27,000 lx only and it is not able to elevate the temperature to a greater level.

The Photothermal conversion efficiency of water has been calculated (from Eq. (3.5)) as 0.639% and that of  $\text{Co}_3\text{O}_4$  nanofluid has been estimated to be 1.262%. The enhancement in photothermal conversion efficiency (from Eq. (3.6)) has been tallied as 97.4%. Zhang et al. (2014) reported enhancement of efficiency of 20% for gold nanoparticles, at the same time, Xuan et al. (2014) recorded enhancement in the efficiency of 3.4% for  $\text{TiO}_2$  and 25.6% for Ag.

SAR of  $\text{Co}_3\text{O}_4$  nanofluid has been computed (from Eq. (3.7)) to be 23 W/g. Wu et al. (2010) had disclosed SAR of Fe-doped calcium sulfide nanoparticles to be 45 W/g, whilst Zhang et al. (2014) proclaimed SAR of Au nanofluid to be 1000 W/g. In the same year, Filho et al. (2014) communicated SAR of 600 W/g. In the subsequent year, Chen et al. (2015) revealed SAR of Ag nanofluids to be 827 W/g. Finally, Goya et al. (2018) recited the SAR of  $\text{Fe}_3\text{O}_4$  nanoparticles to be 130 W/g. The lower value of SAR value in the study can be related to the lower temperature rise difference between water and nanofluid. Further, exposure time is an important factor, as optimum exposure time refers

to the capacity to store increased thermal energy for a limited amount of hours of sunlight (Andrej and Wang 2012).

VSAR of  $\text{Co}_3\text{O}_4$  nanofluid is found (from Eq. (3.8)) to be  $140.53 \text{ W/cm}^3$ , which is lesser than both gold and MWCNT nanofluids ( $1 \text{ kW/cm}^3$ ) (Beicker et al. 2018).

SER of  $\text{Co}_3\text{O}_4$  nanofluid (from Eq. (3.9)) is 1.38, which is higher than gold nanofluids (1.1) and nearer to MWCNT samples (1.4) (Beicker et al. 2018).

$E_{\text{total}}$  of  $\text{Co}_3\text{O}_4$  nanofluid (from Eq. (3.10)) is calculated to be 514.1 kJ and that of water is estimated as 12.58 kJ.

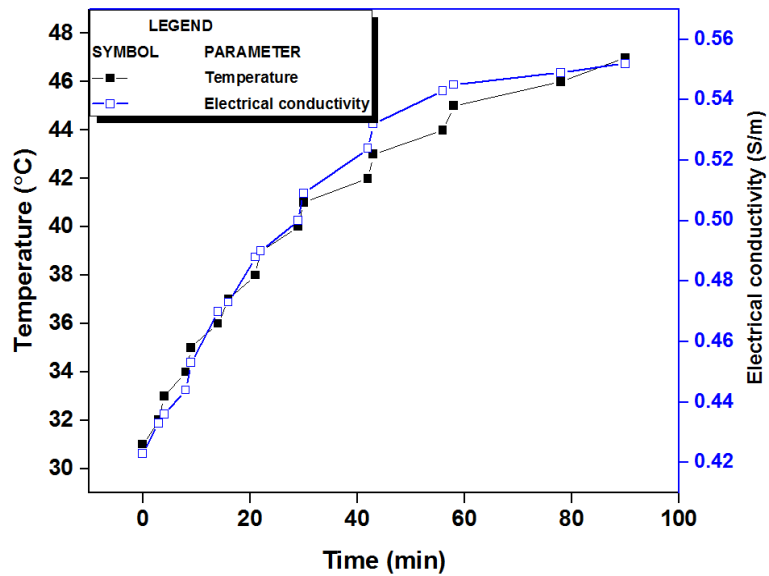


**Fig. 4.32 Transient temperature and electrical conductivity profile of  $\text{Co}_3\text{O}_4$  nanofluids synthesized by 10 mM precursor concentration with respect to time**

Fig. 4.32 displays the temperature and electrical conductivity of nanofluid over time (90 min). Temperature and electrical conductivity increase rapidly from an initial time to 40 min. Beyond 40 min, the rate of increase is less.

**Table 4.6 Value of electrical conductivity obtained in Co<sub>3</sub>O<sub>4</sub> nanofluids synthesized by different precursor concentrations**

S. No.	Nanofluid concentration (mM)	Electrical conductivity (S/m)	Enhancement in electrical conductivity between adjacent concentration %
1	5	0.208	-
2	10	0.316	34.17
3	15	0.368	14.13
4	20	0.430	14.41
5	30	0.497	13.48

**Table 4.7 Value of electrical conductivity obtained in Co<sub>3</sub>O<sub>4</sub> nanofluids before and after keeping in sunlight for 1 h**

S. No.	Nanofluid concentration (mM)	Initial electrical conductivity (S/m)	Final electrical conductivity (S/m)	Enhancement in electrical conductivity %
1	5	0.208	0.241	13.69
2	10	0.316	0.373	15.28
3	15	0.368	0.437	15.78
4	20	0.430	0.516	16.66

5	30	0.497	0.568	12.5
---	----	-------	-------	------

Values of electrical conductivity have been checked for nanofluids and the values have been presented in Table 4.6. A linear increase in electrical conductivity with the increase in the concentration of nanoparticles was found for 15, 20 and 30 mM concentration. This gradual increase in the conductivity may be due to the increase in the number of plasmonic nanoparticles in the base fluid (Nurdin and Satriananda 2017), which facilitate the conductivity. The highest value has been obtained for 30 mM concentration, proving the increase in concentration has led to an increase in electrical conductivity (Azimi and Taheri 2015). Table 4.7 displays values of electrical conductivity before and after keeping in sunlight for 1 h. Except for 5 and 30 mM concentration, the values increase by at least 15% steadily for all other concentrations.

#### **4.24 FEASIBILITY STUDY OF ENERGY STORAGE FOR AN ELECTRICAL APPLICATION**

Figure 4.33 displays voltage drop obtained for different loads in nanofluids synthesized by 10 mM precursor concentration. When the miniature screw base light bulb and DC motor were used as loads, the voltage output has immediately become zero, indicating they require a huge consumption of power, which is not feasible. Without the application of load, the voltage obtained in the solution increases from 0.8V. When red LED bulb and 1 M $\Omega$  resistor have been chosen as load, voltage drop is observed to be in the range 0.1 V, whereas for 380 k $\Omega$  and 1 M $\Omega$  resistors the drop was found to be in the range 0.3 and 0.4 V respectively. Further, for 220 k $\Omega$  resistor, the drop was observed from 0.2 V. Current obtained in the presence of load is less than 5  $\mu$ A. The lower voltage and current values in the solution have been attributed to lower energy confinement in nanofluid.

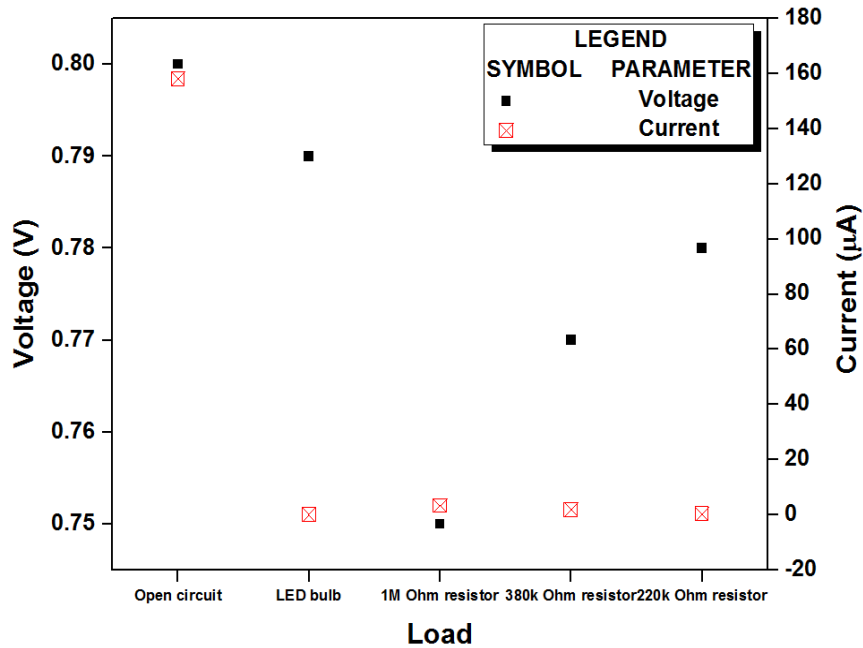


**Figure 4.33 Values of voltage and current obtained in nanofluids synthesized by 10 mM precursor concentration with different loads**

**Table 4.8 Values of voltage obtained in nanofluids synthesized by precursor concentrations (10 mM) after keeping in sunlight for 1 h**

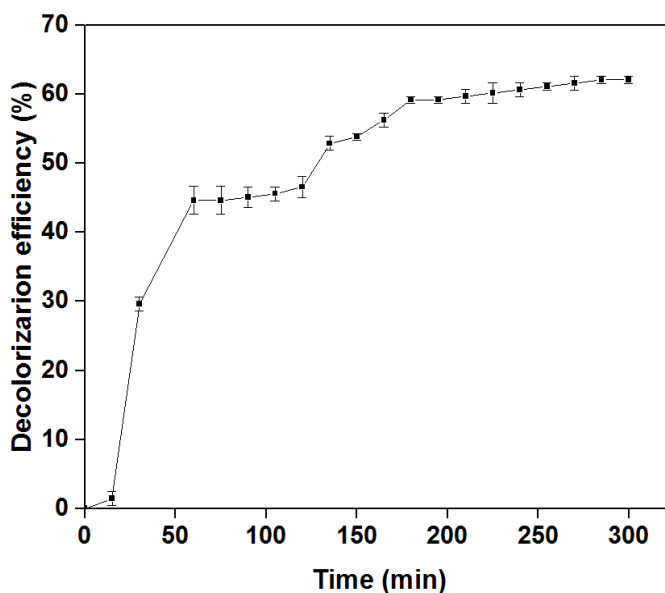
S. No.	Load	V <sub>initial</sub> (V)	V <sub>final</sub> (V)	I <sub>initial</sub> (µA)	I <sub>final</sub> (µA)
1	Without load	0.8	0.92	158	163.2
2	220 kΩ resistor	0.78	0.78	1.8	1.8

Table 4.8 provides voltage and current values of nanofluid without load and with 220 kΩ resistor kept at sunlight for 1 h. There is an increase of 0.12 V and 0.5 µA without a load

in the solution. In the case of 220 k $\Omega$  resistor, no increase was observed for both voltage and current.

## 4.25 DYE DECOLORIZATION

### 4.25.1 Effect of time



**Fig. 4.34 Decolorization efficiency of dye with respect to time**  
(Dye conc. = 20 mg/L, nanoparticle dosage = 150 mg/L, pH = 7)

Fig. 4.34 illustrates the plot of decolorization efficiency with regard to time respectively. The rate of decolorization increases with time. As a greater number of nanoparticles bind to dye with an increase in contact time, there is a significant decrease in dye concentration after 270 min of UV light irradiation after which the removal efficiency becomes almost constant. An increase in treatment span hints at more time accessible for the reaction of dye decolorization (Kale and Kane 2016). Besides, it



increases electron-hole formation, preventing electron-hole recombination, which leads to higher production of hydroxyl radicals (Sari et al. 2017). Maximum decolorization was observed to be 62% at 270 min. This might be due to the unavailability of active sites on nanoparticles for adsorption of the dye or due to insufficient nanoparticles for the dye to get adsorbed (El-Gamal et al. 2015). Since the increase in decolorization efficiency is negligible after 270 min, this value is taken as the optimum time to carry out further experiments. The dye decolorization by  $\text{Co}_3\text{O}_4$  nanoparticle was authenticated by a decrease in absorbance and visually detected by a slow change in the color of the dye solution to colorless (Deshmukh et al. 2018).

#### **4.25.2 Effect of pH**

The pH of the solution can have a great influence on the adsorption of dyes on the nanoparticle surface and thus is a crucial factor in photocatalysis (Thu et al. 2016). The effect of pH of the dye on the removal of dye in terms of decolorization efficiency has been presented in Fig. 4.35. pH regulates surface characteristics, the charge of organic molecules and the size of nanoparticles, thereby influencing the adsorption of RB220 molecules on the surface of nanoparticles (Azeez et al. 2018). From the figure, it is evident that the decolorization efficiency increased with the increase in pH and reached 74% at pH 9. The removal efficiency was better in the alkaline pH when compared to the acidic pH. The electrostatic interaction is higher between dye molecules and surface of nanoparticles at pH 9, paving the way to the highest degree of oxidation, leading to an increase in photocatalytic decolorization of dye molecules (Alshabanat and Al-Anazy 2018). The isoelectric point (IEP) of  $\text{Co}_3\text{O}_4$  semiconductors is relatively high at around 8 (Kittaka and Morimoto 1980; Elhag et al. 2015). Thus, the surface of nanoparticles has a positive charge in an acidic environment and negative charge in an alkaline medium. At lower pH below the IEP,  $\text{H}^+$  ions contend efficaciously with RB220 cations, causing a reduction in decolorization efficiency. Further, a low pH affiliated with a positively charged surface, cannot lend the hydroxyl group, which is a requisite for hydroxyl radical formation. At higher pH above IEF, nanoparticle's surface becomes negatively charged,

which augments the adsorption of positively charged RB220 cations. However, the decolorization of RB220 molecules is hindered while the pH value is high (pH >9), because the hydroxyl ions contend with RB220 molecules in adsorption on nanoparticles' surface (Shamsipur and Rajabi 2014). Further increase in pH may enhance the electron-hole recombination rate, decreasing the photocatalytic activity (Mohamed et al. 2012).

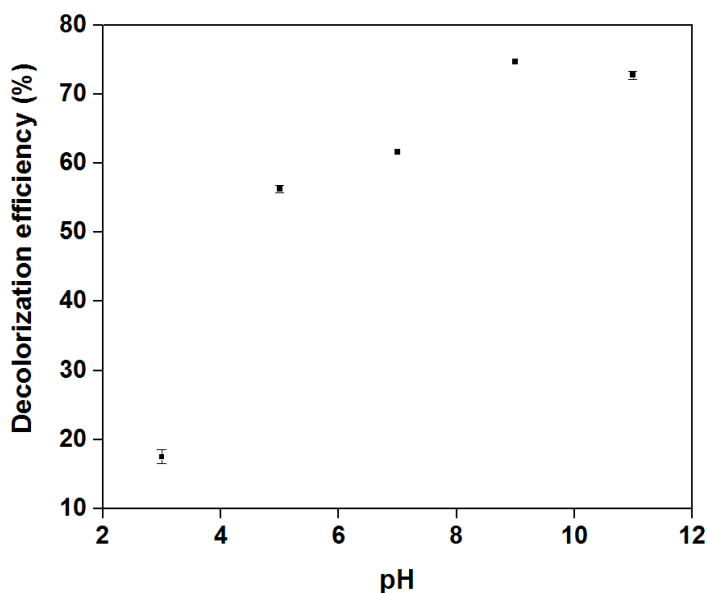


**Fig. 4.35 Decolorization efficiency of nanoparticles with respect to pH**

**(Dye concentration = 20 mg/L, nanoparticle dosage = 150 mg/L, time = 270 min)**

#### **4.25.3 Effect of dye concentration**

Different dye concentration that can be treated using a fixed concentration of nanoparticle solution was obtained and accordingly, the decolorization efficiency was calculated and depicted in Fig. 4.36. It is noted that decolorization efficiency diminishes with an increase in dye concentration. The maximum removal of dye is 10 mg/L concentration with a concentration of nanoparticles being kept constant at 150 mg/L. The observed decrease in decolorization (%) with increase in dye concentration can be as a result of the following reasons: (i) more dye molecules interacted over nanoparticles'

surface as the initial concentration of RB220 elevated, which reduced the origination of hydroxyl ions at the nanoparticle's surface with the active sites occupied by RB220 molecules (ii) an enhancement in the light absorbed by the RB220 molecules may lead to a decrease in the amount of photons that attain the nanoparticle surface (Shamsipur and Rajabi 2014). The sites on the surface of nanoparticles have saturated with time, leading to competitive adsorption of oxygen on the sites, thereby slowing down the generation of radicals. Another factor is contention for photogenerated holes between adsorbed molecules of water and RB220 dye molecules (Alshabanat and Al-Anazy 2018).

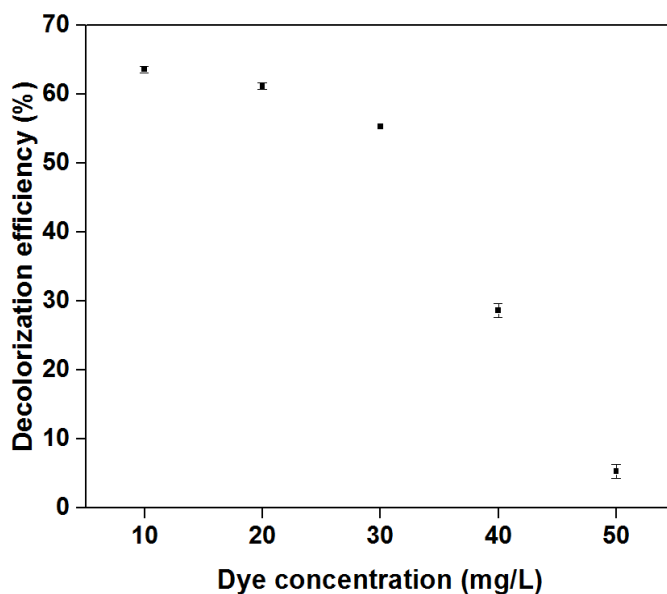


**Fig. 4.36 Decolorization efficiency of nanoparticles with respect to dye concentration (Nanoparticle dosage = 150 mg/L, pH = 9, time = 270 min)**

#### 4.25.4 Effect of $\text{Co}_3\text{O}_4$ nanoparticle dosage

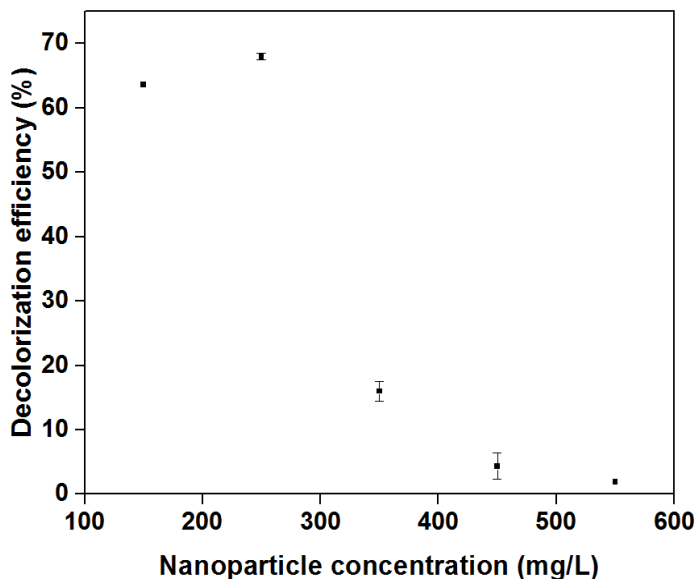


**Fig. 4.37 Decolorization efficiency of nanoparticles with respect to nanoparticles' concentration**  
(Dye concentration = 10 mg/L, pH = 9, time = 270 min)

The change in decolorization of dye with an increase in nanoparticle concentration for a fixed concentration of dye was measured and the results have been summarized in Fig. 4.37. As anticipated, the decolorization of RB220 was found to intensify with a rise in the nanoparticle concentration up to 250 mg/L. Total active surface area and availability for binding heightened with an increase in nanoparticle dose. Enhancing the nanoparticles concentration gave accent to higher number and density, which consecutively let photons to be absorbed and hence, an increase in the adsorption of dye molecules would happen. Further, there is more possibility of a catalyst for attacking chromophores in dye (Kale and Kane 2016). All of these cases have led to an enhancement in the efficiency of decolorization. A further increment in the nanoparticle amount past the optimum dosage decreases the photodegradation by some margin thanks to the overlying of adsorption

sites by virtue of overcrowding and due to a collision with ground state catalyst. The opacity of the suspensions also increases with increased concentration of nanoparticles which in turn increases the light scattering, which resulted in a reduction in the penetration depth of the photons and hence, only a lesser number of nanoparticles were activated (El-Gamal et al. 2015). Also, higher catalyst concentration increases the turbidity of the solution, preventing the path of irradiation to reach sample (Mohamed et al. 2012). Maximum decolorization was about 67%, which was achieved at lower nanoparticle concentration of 250 mg/L. In two cases only, nanoparticles have been used to decolorize RB220 dye, (Mahmoodi et al. 2006; Khanna and Shetty 2014). Mahmoodi et al. (2006) used an immobilized TiO<sub>2</sub> photocatalytic reactor with the addition of H<sub>2</sub>O<sub>2</sub> concentration of 450 mg/L with RB220 concentration 50 mg/L at pH 6 having irradiation time of 90 min, yet decolorization efficiency datum is unavailable. Ag@TiO<sub>2</sub> core-shell nanoparticles were used by Khanna and Shetty (2014), as noble metal Ag is a core and semiconductor dioxide TiO<sub>2</sub> is used as a shell. Decolorization efficiency of RB220 dye was achieved to be 98.9%, when RB220 of 50 mg/L and nanoparticle dosage of 1 g/L at pH 3, were irradiated for 240 min in UV light. Thus, a single nanoparticle in beakers has not been used for RB220 decolorization, indicating this current study is a pioneer one.

#### 4.25.5 COD Analysis

Since the absorbance values in spectrophotometry can't be related to the reduction of COD, it is indispensable to know the imprint of nanoparticles on the COD value of dye solution (Kale and Kane 2016). Residual COD of the sample was calculated in periodic intervals and the COD removal efficiency is plotted against irradiation time as displayed in Fig. 4.38. As time proceeds, COD reduces in the supernatant as more and more dye gets accumulated over the nanoparticle surface (Nezamzadeh-Ejehieh and Shams-Ghahfarokhi 2013). This has led to the inference that nanoparticles have led to the decolorization of dye together with the decrease in the value of COD, indicating the degradation of dye (Kale and Kane 2016).

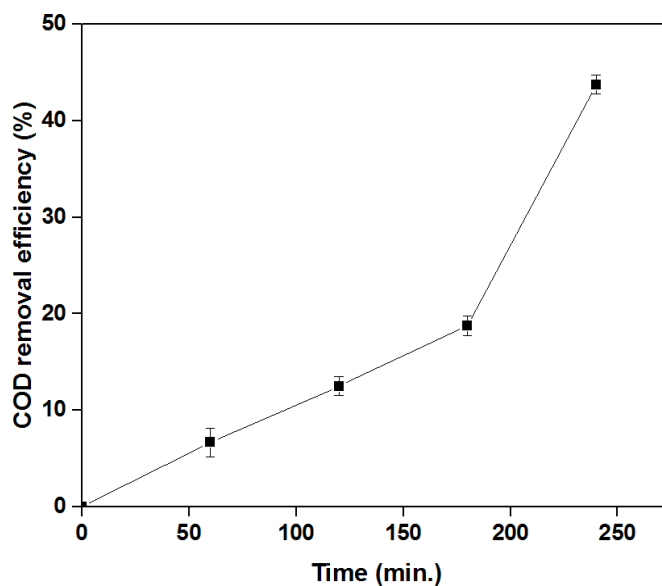


**Fig. 4.38 COD analysis with respect to time**  
**(Dye conc. = 10 mg/L, nanoparticle dosage = 150 mg/L, pH = 9)**

#### 4.25.6 Kinetics

Kinetics curve for pseudo-first-order reaction representing the reaction between nanoparticles and dye was drawn. The integrated rate law of the equation Eq. (4.4) is

$$[A] = [A]_0 e^{-kt} \quad (4.4)$$

The rate constant for the reaction obtained from the slope (Fig. 4.39) is  $0.0029 \text{ s}^{-1}$  and the coefficient of determination ( $R^2$ ) is 0.95.

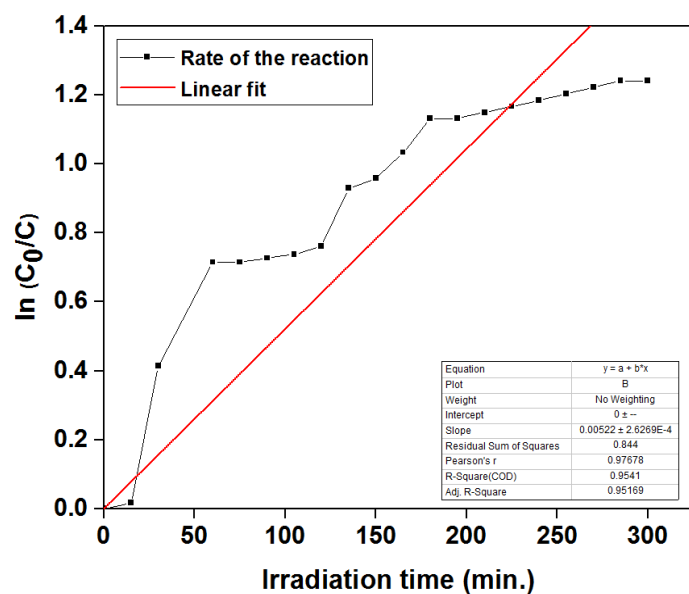


**Fig. 4.39 Pseudo-first-order decay curve**

The reaction kinetics has been noticeable from the color change of the reaction as evident from Fig. 4.40 (a, b). Before the reaction, the solution was deep blue. But after the reaction with nanoparticles, the solution became pale blue due to decolorization.

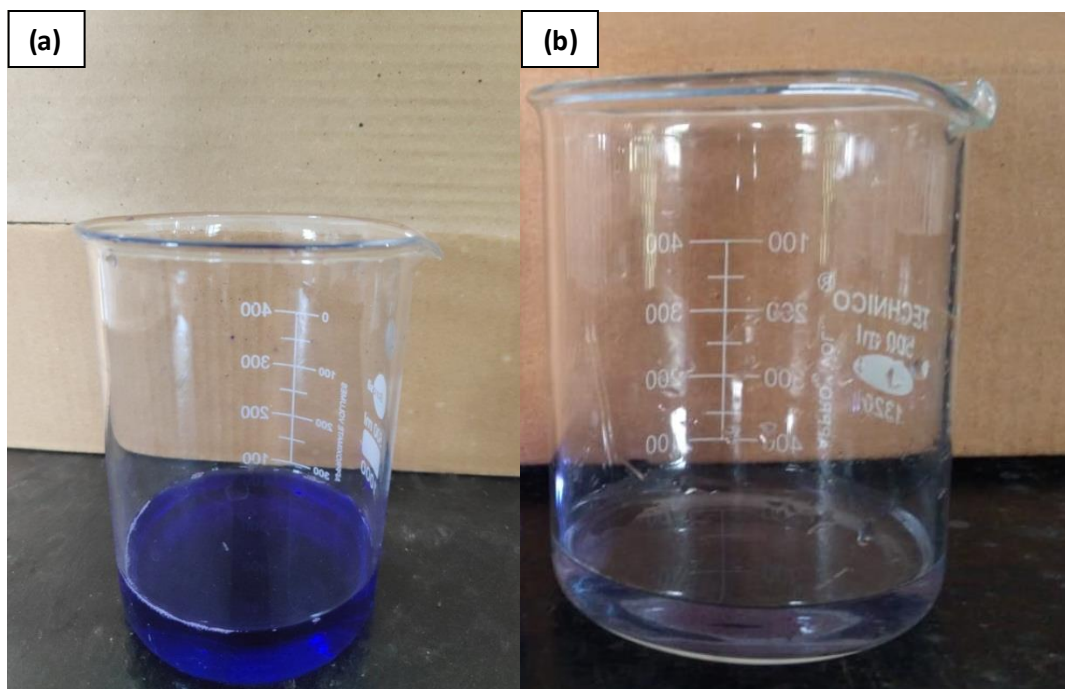


**Fig. 4.40 (a) RB220 dye before the reaction (b) RB220 dye after the reaction**

#### **4.25.7 Mechanism of RB220 decolorization**

Photocatalytic dye degradation banks on the transfer of electrons between donor and acceptor causing an electron relay system (Nakkala et al. 2018). The decrease in the absorbance is related to the electron relay effect (Joshi et al. 2018). When  $\text{Co}_3\text{O}_4$  nanoparticles are irradiated and bombarded against photons from the light source with energy ( $h\nu$ ) energy  $\geq$  its bandgap (3.4 eV) (Vijayanandan and Balakrishnan 2018), the electrons get excited and move to the conduction band from valence band, leaving out a hole in the valence band. These electrons react with oxygen atoms to give superoxide radical anion  $\text{O}_2^-$  and holes that undergo oxidation to react with water to give hydroxyl ions and eventually hydroxyl radicals. These reactions together subsequently yield highly oxidant species like hydroperoxyl radicals, thereby yielding peroxide. Thus, the peroxide radicals attack and break down the bonds of the azo group in the dye and produce lower molecular weight compounds like formate, acetate, glyoxylate and oxalate (Mahmoodi et al. 2006). Lastly, the intermediate compounds have been further mineralized into  $\text{CO}_2$



and  $\text{H}_2\text{O}$ , leading to the decolorization of the dye (Norzaee et al. 2017). The blue color of the dye dimmed and turned into colorless during the process (Fairuzi et al. 2018). This phenomenon is attributed to the Surface Plasmon Resonance effect (charge density oscillation propagating at the interface), in which excited surface electrons react with dissolved molecules, producing hydroxyl molecules (Selvam and Sivakumar 2015; Kumari et al. 2016). The above mechanism of decolorization of the dye RB220 has been depicted in Fig. 4.41.

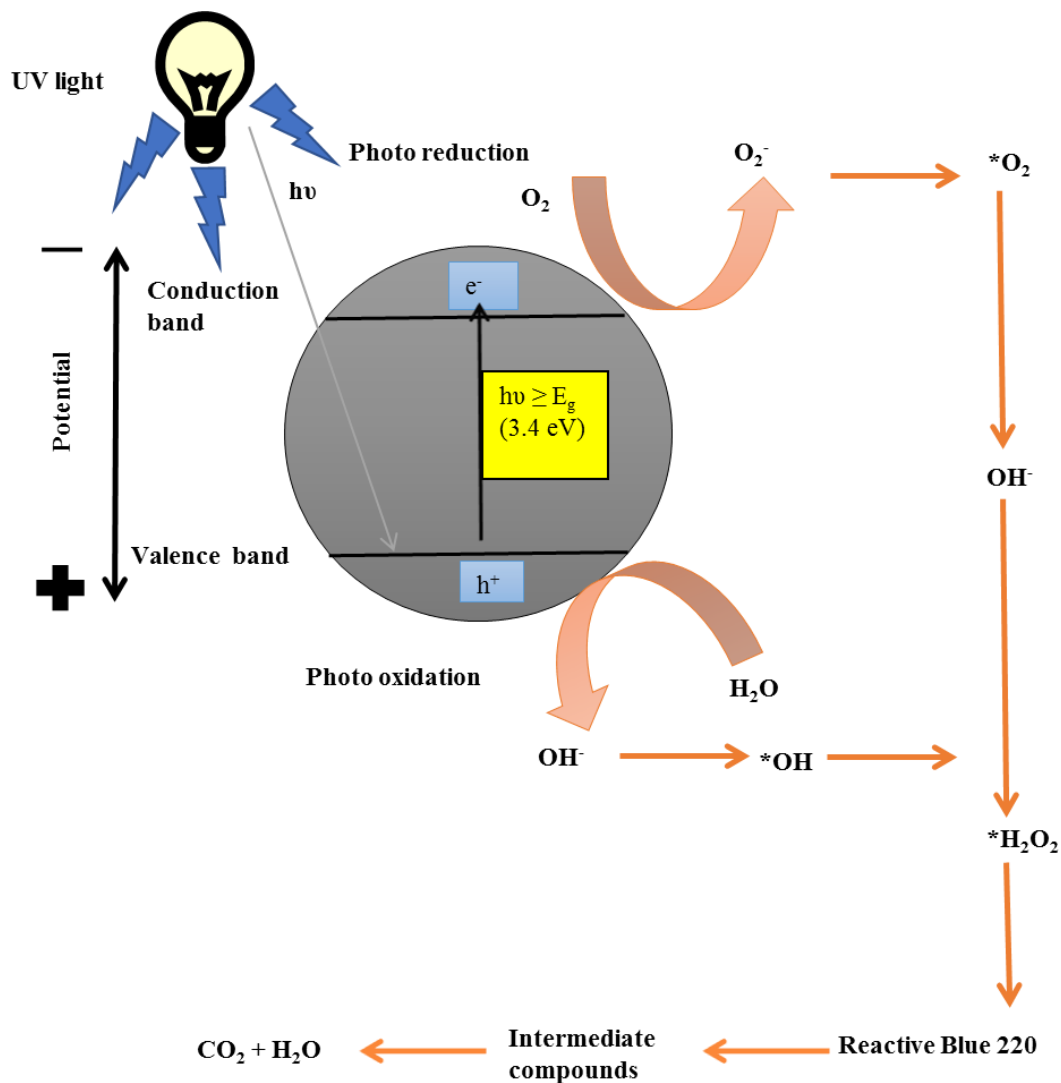


**Fig. 4.41 Mechanism of RB220 decolorization**

#### 4.25.8 Cost analysis of the method followed in the study for biological synthesis of $\text{Co}_3\text{O}_4$ nanoparticles

1 unit of electricity costs Rs. 7

For 100 ml of preparation of nanofluid,

20 ml PDA – 0.78 g – Rs. 3.64

100 ml PDB – 2.4 g – Rs. 11.34

For autoclave =  $3000 \text{ W} * (1/2) \text{ h} = 1.5 \text{ units} = \text{Rs. } 10.50$

For UV light =  $450 \text{ W} * (1/2) \text{ h} = 0.22 \text{ units} = \text{Rs. } 1.54$

8 days power for shaker =  $500 \text{ W} * 24 \text{ h} * 8 \text{ d} = 96 \text{ units} = \text{Rs. } 672$

Total cost involved =  $\text{Rs. } 3.64 + \text{Rs. } 11.34 + \text{Rs. } 10.50 + \text{Rs. } 1.54 + \text{Rs. } 672 = \text{Rs. } 699$

Hence, for synthesizing 88 mg of  $\text{Co}_3\text{O}_4$  nanoparticles by biological method, around Rs. 700 is needed.

## CHAPTER 5

### CONCLUSION

Endophytes have been used mainly in agriculture and medical fields for various applications like plant defense mechanism, phytoremediation, sustainable agriculture, synthesis of bioactive metabolites, antimicrobial activity, anticancer drugs, etc. As endophytic fungi are largely used for enhancing crop resistance and synthesizing drugs, their utility in the greener way of nanoparticle synthesis is relatively new.  $\text{Co}_3\text{O}_4$  nanoparticles are often used in catalysis, electrochemical devices, sensing, batteries and supercapacitors. In this study,  $\text{Co}_3\text{O}_4$  nanoparticles have been synthesized using greener chemistry via endophytic fungus and utilized them for energy applications like photothermal energy conversion and photocatalysis. Some of the significant findings of the study have been given in the upcoming subsection 5.1.

#### 5.1 SIGNIFICANT FINDINGS

- ❖ Four fungi had been isolated from *Nothapodytes foetida* and tolerance study was performed in cobalt acetylacetonate salt solution to choose a suitable candidate for the synthesis of  $\text{Co}_3\text{O}_4$  nanoparticles. Fungus 4 exhibited the highest tolerance for 1000 ppm concentration in cobalt acetylacetonate salt.
- ❖ The Fungus 4 was identified as *Aspergillus nidulans* using morphological analysis and 23S rRNA sequencing technique.
- ❖ Fluorescent, metallic oxide nanoparticles having a narrow absorbance peak at 315 nm in spinel phase with crystallite size of 7.53 nm and a luminescence emission peak at 417 nm was synthesized.
- ❖ The average size distribution estimated by the DLS technique was found to be 30 nm. The zeta potential of nanoparticles was determined as -10.8 mV indicating the negatively charged surface of nanoparticles.

- ❖ SEM microscopy showed biosynthesized nanoparticles were spheres having good connectivity, dispersibility, and homogeneity between them. Through TEM microscopy, the average particle size was estimated to be 34 nm.
- ❖ Photostability studies ensure the nanoparticles are stable for at least up to 45 days.
- ❖ Phytochelatins were identified to be the significant stress factors in biosynthesis of  $\text{Co}_3\text{O}_4$  nanoparticles through LC-MS and a realistic mechanism for the biosynthesis of the same has been outlined.
- ❖ 250 ml of nanofluid was able to absorb solar irradiation indicated by the elevation in the temperature up to 47 °C within 90 min of exposure time. The SAR value estimated through photo-thermal studies was found to be 23 W/g. The study also revealed that the surface temperature of nanofluid was 4 °C greater than that of water on exposure to solar irradiation.
- ❖ 74% decolorization efficiency of 20 mg/L of RB220 dye was achieved using 150 mg/L of nanoparticle at an alkaline pH of 9.

## SUMMARY

Endophytic fungus *Aspergillus nidulans* isolated from the medicinal plant *Nothapodytes foetida* was identified to be potential candidate for the synthesis of  $\text{Co}_3\text{O}_4$  nanoparticles by conducting tolerance studies towards cobalt acetylacetonate solution.  $\text{Co}_3\text{O}_4$  nanoparticles were biosynthesized successfully by *Aspergillus nidulans* using 10 mM precursor salt concentration and their physical, chemical, optical and electrochemical properties have been studied. Biosynthesized  $\text{Co}_3\text{O}_4$  nanoparticles have been evaluated for photothermal conversion efficiency to be used for solar energy storage and found to have appreciable photothermal energy conversion potential when compared to that of chemically synthesized nanoparticles. In this way, a nanofluid-based absorption system can provide a substitute for traditional solar collectors for the confinement of solar energy in volumetric solar thermal receivers. Photocatalytic decolorization of  $\text{Co}_3\text{O}_4$  nanoparticle system over RB220 dye component is considerably good, yielding decolorization efficiency of 74%. The variation in pH, concentration of dye and nanoparticle dosage has

a strong impact on the efficiency of decolorization. Based on the study, a photocatalytic mechanism has also been proposed.

## **5.2 SCOPE FOR FUTURE WORK**

- ❖ The biochemical pathway for the synthesis of cobalt oxide nanoparticles can be studied with an in-depth analysis of the metabolites / bioactive molecules involved in the synthesis.
- ❖ Scale-up studies can be conducted in the bioreactor for large scale production of nanoparticles based on their applications.
- ❖ Since products obtained from endophytes usually exhibit excellent antimicrobial activity, they could be studied further to determine the active antimicrobial compound which would be used for manufacturing broad-spectrum antibiotics in biopharmaceutical industries.
- ❖ The previous studies by researchers in the lab indicate isolation of more than 170 fungal species from the same plant, *Nothapodytes foetida*. In the present study, only 4 fungal species have been screened for cobalt tolerance studies and hence there is a good probability to identify the best fungus among the 170 species that can have a still higher tolerance to cobalt salts and yield nanoparticles with better properties for various real-time electrical applications.

## REFERENCES

Abbasi, A., Golesefidi, M.A., Beigi, M.M., Sadri, N. and Abroudi, M. (2018). “Facile fabrication of  $\text{Co}_3\text{O}_4$  nanostructures as an effective photocatalyst for degradation and removal of organic contaminants.” *J. Nanostruct.*, 8(1), 89-96.

Abdelghany, A. M., Oraby, A. H., & Farea, M. O. (2019). Influence of green synthesized gold nanoparticles on the structural, optical, electrical and dielectric properties of (PVP/SA) blend. *Physica B: Condensed Matter*, 560, 162-173.

Agilandeswari, K., and Rubankumar, A. (2014). “Synthesis, characterization, optical, and magnetic properties of  $\text{Co}_3\text{O}_4$  nanoparticles by quick precipitation.” *Synthesis and Reactivity in Inorganic, Metal-Organic, and Nano-Metal Chemistry*, 46(4), 502-506.

Ahmad, A., Mukherjee, P., Senapati, S., Mandal, D., Khan, M.I., Kumar, R., and Sastry, M. (2003). “Extracellular biosynthesis of silver nanoparticles using the fungus *Fusarium oxysporum*.” *Colloids Surf. B Biointerfaces*, 28, 313-358.

Ahmed, J., Ahmad, T.V., Ramanujachary, K.E., Lofland, S. and Ganguli, A. K. (2008). “Development of a micro emulsion-based process for synthesis of cobalt (Co) and cobalt oxide ( $\text{Co}_3\text{O}_4$ ) nanoparticles from submicrometer rods of cobalt oxalate.” *J. Colloid Interface Sci.*, 321(2), 434-441.

Allen, M., Willits, D., Young, M. and Douglas, T. (2003). “Constrained synthesis of Cobalt Oxide Nanomaterials in the 12-Subunit Protein Cage from *Listeria innocua*.” *Inorg. Chem.*, 42(20), 6300-6305.

Alshabanat, M.N. and Al-Anazy, M.M. (2018). “An experimental study of

photocatalytic degradation of polymer using polymer nanocomposite films.” *J. Chem.*, Article 9651850.

Anahid, S., Yaghmaei, S. and Ghobadinejad, Z. (2011). “Heavy metal tolerance of fungi.” *Sci. Iran. Trans. C*, 18(3), 502-508.

Anandalakshmi, K., Venugobal, J. and Ramasamy, V. (2016). “Characterization of silver nanoparticles by green synthesis method using *Petalium murex* leaf extract and their antibacterial activity.” *Appl Nanosci.*, 6(3), 399-408.

Andrej and Wang (2012). “Optimization of nanofluid volumetric receivers for solar thermal energy conversion.” *Sol. Energy*, 86(1), 253-265.

Athar, T., Hakeem, A., Topnani, N. and Hashmi, A. (2012). “Wet synthesis of monodisperse Cobalt Oxide Nanoparticles.” *ISRN Mater. Sci.*, Article 691032.

Athawale, A.A., Majumdar, M., Singh, H. and Navinkiran, K. (2010). “Synthesis of cobalt oxide nanoparticles/fibres in alcoholic medium using  $\gamma$ -ray.” *Defence. Sci. J.*, 60(5), 507-513.

Azeez, F., Al-Hetlani, E., Arafa, M., Abdelmonem, Y., Nazeer, A. A., Amin, M. O. and Madkour, M. (2018). “The effect of surface charge on photocatalytic degradation of methylene blue dye using chargeable titania nanoparticles.” *Sci. Rep.*, 8(1), 7104.

Azimi, H.R. and Taheri, R. (2015). “Electrical conductivity of CuO nanofluids.” *Int. J. Nano Dimens.*, 6(1), 77-81.

Babick, F., Gropp, S., Katzel, U. and Vorbau, M. (2012). “Dynamic light scattering of dispersed fumed silica aggregates.” *Powder Technol.*, 217, 39-45.

Barreca, D., Gasparotto, A., Lebedev, O.I., Maccato, C., Pozza, A., Tondello, E., Turner, S. and Tendeloo, G. (2010). "Controlled vapor-phase synthesis of cobalt oxide nanomaterials with tuned composition and spatial organization." *Cryst. Eng. Comm.*, 12, 2185-2197.

Baskar, G., Chandhuru, J., Fahad, K.S., Praveen, A.S., Bharathi, R., Fyna, S. (2015). "Mycological synthesis and characterization of silver nanoparticles by *Aspergillus* species." *J. Chem. Pharm. Res.*, 7(7), 300-306.

Bazgir, S. and Farhadi, S. (2017). "Microwave-assisted rapid synthesis of  $\text{Co}_3\text{O}_4$  nanorods from  $\text{CoC}_2\text{O}_4 \cdot 2\text{H}_2\text{O}$  nanorods and its application in photocatalytic degradation of methylene blue under visible light irradiation." *Int. J. Nano. Dimens.*, 8(4), 284-297.

Beicker, C.L.L., Amjad, M., Filho, E.P.B. and Wen, D. (2018). "Experimental study of photothermal conversion using gold/water and MWCNT/water nanofluids." *Sol. Energy Mater. Sol. Cells*, 188, 51-65.

Bhalla, V. and Tyagi, H. (2017). "Solar energy harvesting by cobalt oxide nanoparticles, nanofluids absorption based system." *Sust. Energ. Technol. Assess.* 24, 45-54.

Bhalla, V., Khullar, V. and Tyagi, H. (2018). "Experimental investigation of photo-thermal analysis of blended nanoparticles ( $\text{Al}_2\text{O}_3/\text{Co}_3\text{O}_4$ ) for direct absorption solar thermal collector." *Renew. Energ.*, 123, 616-626.



Bhatt, A.S., Bhat, D.K., Tai, C. and Santosh, M.S. (2011). "Microwave-assisted synthesis and magnetic studies of cobalt oxide nanoparticles." *Mater. Chem. Phys.*, 125(3), 347-350.

Bibi, I., Nazar, N., Iqbal, M., Kamal, S., Nawaz, H., Nouren, S., Safa, Y., Jilani, K., Sultan, M., Ata, S., Rehman, F. and Abbas, M. (2017). "Green synthesis of cobalt-oxide nanoparticle: characterization and photocatalytic activity." *Adv. Powder Technol.* 28(9), 2035-2043.

Bibi, I., Nazar, N., Iqbal, M., Kamal, S., Nawaz, H., Nouren, S., Safa, Y., Jilani, K., Sultan, M., Ata, S., Rehman, F., Abbas, M. (2017). "Green and eco-friendly synthesis of cobalt-oxide nanoparticle: characterization and photo-catalytic activity." *Adv. Powder Technol.*, 28, 2035-2043.

Blumenstein, A., Vienken, K., Tasler, R., Purschwitz, J., Veith, D., Frankenberg-Dinkel, N. and Fischer, R. (2005). "The *Aspergillus nidulans* phytochrome FphA represses sexual development in red light." *Curr. Biol.*, 15(20), 1833-1838.

Carpenè, E., Andreani, G. and Isani, G. (2007). "Metallothionein functions and structural characteristics." *J. Trace Elem. Med. Biol.*, 21(S1), 35-39.

Chen, M., He, Y., Zhu, J. and Kim, D.R. (2016). "Enhancement of photo-thermal conversion using gold nanofluids with different particle sizes." *Energy Convers. Manag.*, 112, 21-30.

Chen, M., He, Y., Zhu, J., Shuai, Y., Jiang, B. and Huang, Y. (2015). "An experimental investigation on sunlight absorption characteristics of silver nanofluids." *Sol. Energy*, 115, 85-94.

Chen, Y., Zhang, Y. and Fu, S. (2007). "Synthesis and characterization of  $\text{Co}_3\text{O}_4$  hollow spheres." *Mat. Lett.*, 61, 701-705.

Chieruzzi, M., Cerritelli, G.F., Miliozzi, A., Kenny, J.M. and Torre, L. (2017). "Heat capacity of nanofluids for solar energy storage produced by dispersing oxide nanoparticles in nitrate salt mixture directly at high temperature." *Sol. Energy Mater. Sol. Cells*, 167, 60-69.

Chin, G., Yin, B., Zeng, G., Niu, Q., Yan, M., Chen, A., Du, J., Huang, J. and Zhang, Q. (2014). "Facile green extracellular biosynthesis of CdS quantum dots by white rot fungus *Phanerochaete chrysosporium*." *Colloids Surf B: Biointerfaces.*, 117, 199-205.

Cove, D.J. (1965). "The induction and repression of nitrate reductase in the fungus *Aspergillus nidulans*." *Biochimica Et Biophysica Acta.*, 113(1), 51-56.

Damodaran, D., Balakrishnan, R.M. and Shetty, V.K. (2013). "The uptake mechanism of Cd(II), Cr(VI), Cu(II), Pb(II) and Zn(II) by mycelia and fruiting bodies of *Galerina vittiformis*." *Biomed. Res. Int.*, Article 149120, <http://dx.doi.org/10.1155/2013/149120>.

Das, S. (2015). Synthesis, characterization and dielectric properties of nanocrystalline nickel. *Indian Journal of Pure & Applied Physics (IJPAP)*, 52(6), 386-390.

Deshmukh, K.K., Hase, G.J., Gaje, T.R., Phatangare, N.D., Shilpa, G. and Ashwini, V. (2018). "Titanium oxide nanoparticles and degradation of dye by nanoparticles." *Int. J. Mater. Sci.*, 13(1), 23-30.

DeSimone, J.M. (2002). "Practical approaches to green solvents." *Science*, 297(5582), 799-803.

Dhaouadi, H., Ghodbane, O., Hosni, F. and Touati, F. (2012). "Mn<sub>3</sub>O<sub>4</sub> nanoparticles: Synthesis, Characterization and Dielectric Properties." *Int. Sch. Res. Notices Spectrosc.*, Article 706398.

Dhas, C.R., Venkatesh, R., Jothivenkatachalam, K., Nithya, A., Benjamin, B. S., Raj, A.M.E., Jeyadheepan, K. and Sanjeeviraja, C. (2015). "Visible light driven photocatalytic degradation of rhodamine B and direct red using cobalt oxide nanoparticles." *Ceram. Int.*, 41(8), 9301-9313.

Dhineshababu, N.R., Rajendran, V., Nithyavathy, N. and Vetumperumal, R. (2016). "Study of structural and optical properties of cupric oxide nanoparticles." *Appl. Nanosci.*, 6(6), 933-939.

Diallo, A., Beye, A.C., Doyle, T.B., Park, E. and Maaza, M., (2015). "Green synthesis of Co<sub>3</sub>O<sub>4</sub> nanoparticles via *Aspalathus linearis*: physical properties." *Green Chem. Lett. Rev.*, 8(3-4), 30-36.

Drasovean, R. and Condurache-Bota, S. (2009). "Structural characterization and optical properties of Co<sub>3</sub>O<sub>4</sub> and CoO films." *J. Optoelectron. Adv. M.*, 11(12), 2141-2144.

El-Gamal, S.M.A., Amin, M.S. and Ahmed, M.A. (2015). "Removal of methyl orange and bromophenol blue dyes from aqueous solution using Sorel's cement nanoparticles." *J. Environ. Chem. Eng.*, 3(3), 1702-1712.

Elhag, S., Ibutoto, Z.H., Nour, O. and Willander, M. (2015). "Synthesis of Co<sub>3</sub>O<sub>4</sub>

cotton-like nanostructures for cholesterol biosensor.” *Materials (Basel)*, 8(1), 149-161.

Fairuzi, A.A., Bonnia, N.N., Akhir, R.M., Abrani, M.A. and Akil, H.M. (2018). “Degradation of methylene blue using silver nanoparticles synthesized from *Imperata cylindrica* aqueous extract.” *IOP Conf. Ser. Earth Environ. Sci.*, 105(1), Article 012018.

Faizal, M., Saidur, R., Mekhilef, S. and Alim, M.A. (2013). “Energy, economic and environmental analysis of metal oxides nanofluid for flat-plate solar collector.” *Energy Convers. Manag.*, 76, 162–168.

Farhadi, S., Javanmard, M. and Nadri, G. (2016). “Characterization of cobalt oxide nanoparticles prepared by the thermal decomposition.” *Acta. Chim. Slov.*, 63(2), 335-343.

Farhadi, S., Pourzare, K. and Sadeghinejad, S. (2013). “Simple preparation of ferromagnetic  $\text{Co}_3\text{O}_4$  nanoparticles by thermal dissociation of the  $[\text{CoII}(\text{NH}_3)_6](\text{NO}_3)_2$  complex at low temperature.” *J. Nanostructure Chem.*, 3(1), 16.

Farhadi, S., Safabakhsh, J. and Zaringhadam, P. (2013). “Synthesis, characterization and investigation of optical and magnetic properties of cobalt oxide ( $\text{Co}_3\text{O}_4$ ) nanoparticles.” *J. Nanostructure Chem.*, 3(1), 69.

Farhadi, S., Sepahdar, A. and Jahanara, K. (2013). “Spinel-Type Cobalt Oxide ( $\text{Co}_3\text{O}_4$ ) Nanoparticles from the mer-Co  $(\text{NH}_3)_3(\text{NO}_2)_3$  Complex: Preparation, Characterization and Study of Optical and Magnetic Properties.” *J. Nanostruct.*, 3(2), 199-207.

Fathima, B.S. and Balakrishnan, R.M. (2014). "Biosynthesis and optimization of silver nanoparticles by endophytic fungus *Fusarium solani*." *Mater. Lett.*, 132, 428-431.

Fernandez-Osorio, A., Vazquez-Olmos, A., Sato-Berru, R. and Escudero, R. (2009). "Hydrothermal synthesis of  $\text{Co}_3\text{O}_4$  nanooctahedra and their magnetic properties." *Rev. Adv. Mater. Sci.*, 22, 60-66.

Filho, E.P.B., Mendoza, O.S.H., Beicker, C.L.L., Menezes, A. and Wen, D. (2014). "Experimental investigation of a silver nanoparticle-based direct absorption solar thermal system." *Energy Convers. Manag.*, 84, 261-267.

Forootanfar, H., Moezzi, A., Aghaie-Khozani, M., Mahmoudjanlou, Y., Ameri, A., Niknejad, F. and Faramarzi, M.A. (2012). "Synthetic dye decolorization by three sources of fungal laccase." *J. Environ. Health Sci. Eng.*, 9(1), 27.

Gaikwad, S. and Bhosale, A. (2012). "Green synthesis of silver nanoparticles using *Aspergillus niger* and its efficacy against human pathogens." *Euro. J. Exp. Bio.*, 2(5), 1654-1658.

Gao Y., Chen, S., Cao, D., Wang, G. and Yin, J. (2010). "Electrochemical capacitance of  $\text{Co}_3\text{O}_4$  nanowire arrays supported on nickel foam." *J. Power. Sources.*, 195(6), 1757-1760.

Gawali, S.R., Pandit, S. and Pant, J. (2014). "Magnetic properties of  $\text{Co}_3\text{O}_4$  nanoparticles." *Int. J. Chemtech. Res.* 6(3), 2178-2180.

George, G. and Anandhan, S. (2013). "Structural characterization of nano-crystalline  $\text{Co}_3\text{O}_4$  ultra-fine fibers obtained by sol-gel electrospinning." *J. Sol-gel Sci. Technol.*, 67(2), 256-266.

Ghorbani, H.R., Mehr, F.P. and Poor, A.K. (2015) "Extracellular synthesis of copper nanoparticles using culture supernatants of *Salmonella typhimurium*." *Orient J. Chem.*, 31(1), 527-529.

Gill, S.S. and Tuteja, N. (2011). "Cadmium stress tolerance in crop plants probing the role of sulfur." *Plant Signal Behav.*, 6(2), 215-222.

Grabolle, M., Ziegler, J., Merkulov, A., Nann, T. and Resch-Genger, U. (2008). "Stability and fluorescence quantum yield of CdSe-ZnS quantum dots-influence of the thickness of ZnS shell." *Ann. N. Y. Acad. Sci.*, 1130, 235-241.

Godara, S., Sinha, N., Ray, G. and Kumar, B. (2014). "Combined structural, electrical, magnetic and optical characterization of bismuth ferrite nanoparticles synthesized by auto-combustion route." *J. Asian Ceram. Soc.*, 2(4), 416-421.

Goya, G., Jr. E.L., Arelaro, A.D., Torres, T., Rechenberg, H.R., Rossi, L., Marquina, C. and Ibarra, M.R. (2008). "Magnetic hyperthermia with  $\text{Fe}_3\text{O}_4$  nanoparticles: The influence of particle size on energy absorption." *IEEE Trans. Magn.*, 44(11), 4444-4447.

Grass, R.N. and Stark, W.J. (2006). "Gas phase synthesis of fcc-cobalt nanoparticles." *J. Mater. Chem. A.*, 16(19), 1825-1830.

Gunasekaran, S. and Ponnusamy, S. (2005). "Vibrational spectra and normal coordinate analysis on an organic non-linear optical crystal-3-methoxy-4-hydroxy benzaldehyde." *Ind. J. Pure Appl. Phys.*, 43, 838-843.

Gupta, R.K., Sinha A.K., Sekhar, B.N.R., Srivastava, A.K., Singh, G. and Deb, S.K. (2011). "Synthesis and characterization of various phases of cobalt oxide nanoparticles using inorganic precursor." *Appl. Phys. A.*, 103(1), 13-19.

Haider, M.J. and Mehdi, M.S. (2014). Study of morphology and zeta potential analyser for the silver nanoparticles. *Int. J. Sci. Eng. Res.*, 5(7), 381-387.

Han, D., Meng, Z., Wu, D., Zhang, C. and Zhu, H. (2011). "Thermal properties of carbon black aqueous nanofluids for solar absorption." *Nanoscale Res. Lett.*, 6(1), 457.

Hashim, A.D., Rashid, F. and Fayyadh, I.K. (2013). "Preparation of nanofluid ( $\text{Al}_2\text{O}_3$ -water) for energy storage." *IOSR- J. Appl. Chem.*, 5(3), 48-49.

He, Q., Wang, S., Zeng, S. and Zheng, Z. (2013). "Experimental investigation on photothermal properties of nanofluids for direct absorption solar thermal energy systems." *Energy Convers. Manag.*, 73, 150-157.

Hewakuruppu, Y.L., Taylor, R.A., Tyagi, H., Khullar, V., Otanicar, T., Coulombe, S. and Hordy, N. (2015). "Limits of selectivity of direct volumetric solar absorption." *Sol. Energy*, 114, 206-216.

Ho, C.H., Liu, C.D., Hiesh, C.H., Hiesh, K.H. and Lee, S.N. (2008). "High dielectric constant polyaniline/poly(acrylic acid) composites prepared by in situ polymerization." *Synthetic Metals*, 158, 630-637.

Hordy, N., Rabilloud, D., Meunier, J., Coulombe, S., (2014). "High temperature and long-term stability of carbon nanotube nanofluids for direct absorption solar thermal collectors." *Sol. Energy*, 105, 82-90.

Ingale, A.G. and Chaudhari, A.N. (2013) "Biogenic synthesis of nanoparticles and potential applications: An eco-friendly Approach." *J. Nanomed. Nanotechnol.*, 4(165), 1-7.

Ingle, A., Gade, A., Pierrat, S., Sönnichsen, C. and Rai, M. (2008). "Mycosynthesis of silver nanoparticles using the fungus *Fusarium acuminatum* and its activity against some human pathogenic bacteria." *Curr. Nanosci.*, 4(2), 141-144.

Ishida, K., Cipriano, T.F., Rocha, G.M., Weissmuller, G., Gomes, F., Miranda, K. and Rozental, S. (2014). "Silver nanoparticle production by the fungus *Fusarium oxysporum*: nanoparticle characterisation and analysis of antifungal activity against pathogenic yeasts." *Mem. Int. Oswaldo. Cruz.*, 109(2), 220-228.

Jacob, J.M., Balakrishnan, R.M. and Kumar, U.B. (2014). "Biosynthesis of lead selenide quantum rods in marine *Aspergillus terreus*." *Mater. Lett.*, 124, 279-281.

Jain, N., Bhargava, A., Majumdar, S., Tarafdar, A.C. and Panwar, J. (2010). "Extracellular biosynthesis and characterization of silver nanoparticles using *Aspergillus flavus* NJP08: a mechanism perspective." *Nanoscale.*, 3, 635-641.

Jha, A.K. and Prasad, K. (2012). "Biological synthesis of cobalt ferrite nanoparticles." *Nanotechnol. Dev.*, 2(e9), 46-51.



Ji, G., Gong, Z., Zhu, W., Zheng, M., Liao, S., Shen, K., Liu, J. and Cao, J. (2009). "Simply synthesis of Co<sub>3</sub>O<sub>4</sub> nanowire arrays using a solvent-free method." *J. Alloys Compd.*, 476(1-2), 579-583.

Joshi, S., Kulkarni, D. and Khandekar, P. (1982). "Structural, magnetic and electrical study of CoMnAlO<sub>4</sub>." *Bull. Mater. Sci.*, 4(4), 455-459.

Joshi, S.J., Geetha, S.J., Al-Mamari, S. and Al-Azkawi, A. (2018). "Green synthesis of silver nanoparticles using pomegranate peel extracts and its application in photocatalytic degradation of methylene blue." *Nat. Pharm. Prod.*, 13(3), e67846.

Kadam, V.V., Ettiyappan, J.P. and Balakrishnan, R.M. (2019). "Mechanistic insight into the endophytic fungus mediated synthesis of protein capped ZnO nanoparticles." *Mater. Sci. Eng.: B*, 243, 214-221.

Kale, R.D. and Kane, P.B. (2016). "Color removal using nanoparticles." *Text. Cloth. Sustain.*, 2(4) <https://doi.org/10.1186/s40689-016-0015-4>.

Kalishwaralal, K., Babu, R.S., Venkataraman, D., Bilal, M. and Gurunathan, S. (2008). "Biosynthesis of silver nanocrystals by *Bacillus licheniformis*." *Colloids Surf. B Biointerfaces*, 65, 150-153.

Kalishwaralal, K., Deepak, V., Ramkumarpandian, S., Nellaiah, H. and Sangiliyandi, G. (2008). "Extracellular biosynthesis of silver nanoparticles by the culture supernatant of *Bacillus licheniformis*." *Mater. Lett.*, 62(29), 4411-4413.

Kameya, Y. and Hannamura, K. (2011). "Enhancement of solar radiation absorption using nanoparticle suspension." *Sol. Energy*, 85, 299-307.

Kamran, M., Shoukat, W., Nadeem, K., Hussain, S. S., Zeb, F., & Hussain, S. (2019). Magnetic and dielectric properties of NiCr<sub>x</sub>Fe<sub>2-x</sub>O<sub>4</sub> nanoparticles. *Materials Research Express*, 6(7), 076106.

Kandalkar, S.G., Gunjekar, J.L., Lokhande, C.D. and Joo, S. (2009). "Synthesis of cobalt oxide interconnected flacks and nano-worms structures using low temperature chemical bath deposition." *J. Alloys Compd.*, 478, 594-598.

Karthikeyan, V., Ragnathan, R., Johney, J. and Kabesh, K. (2019). "Green synthesis of silver nanoparticles and application in dye decolorization by *Pleurotus ostreatus* (MH591763)." *J. Biosci. Biotechnol.*, 8(1), 80-86.

Kayani, Z.N., Saleemi, F. and Batool, F. (2015). "Effect of calcination temperature on the properties of ZnO nanoparticles." *Appl. Phys. A.*, 119, 713-720.

Khalil, N.M. (2013). "Biogenic silver nanoparticles by *Aspergillus terreus* as a powerful nanoweapon against *Aspergillus fumigatus*." *Afr. J. Microbiol. Res.*, 7(50), 5645-5651.

Khalil, N.M., Ovais, M., Ullah, M., Ali, M., Shinwari, Z.K. and Maaza, M. (2017). Physical properties, biological applications and biocompatibility studies on biosynthesized single-phase cobalt oxide nanoparticles (Co<sub>3</sub>O<sub>4</sub>) via *Sageretia thea* (Osbeck). *Arab. J. Chem.*, <http://dx.doi.org/10.1016/j.arabjc.2017.07.004>.

Khanna, A. and Shetty, V. (2014). "Solar light induced photocatalytic degradation of Reactive Blue 220 (RB-220) dye with highly efficient Ag@TiO<sub>2</sub> core-shell nanoparticles: A comparison with UV photocatalysis." *Sol. Energy*, 99, 67-76.

Khashan, S., Dagher, S., Omari, S.A., Tit, N., Elnajjar, E., Mathew, B. and Hilal-Alnaqbi, A. (2017). "Photo-thermal characteristics of water-based Fe<sub>3</sub>O<sub>4</sub>@SiO<sub>2</sub> nanofluid for solar-thermal applications." *Mater. Res. Express.*, 4(5), 055701.

Khullar, V. and Tyagi, H. (2012). "A study on environmental impact of nanofluid-based concentrating solar water heating system." *Int. J. Environ. Stud.*, 69(2), 220-232.

Khullar, V., Tyagi, H., Hordy, N., Otanicar, T.P., Hewakuruppu, Y., Modi, P., and Taylor, R.A. (2014). "Harvesting solar thermal energy through nanofluid-based volumetric absorption systems." *Int. J. Heat Mass Transf.*, 77, 377–384.

Khullar, V., Tyagi, H., Phelan, P.E., Otanicar, T.P., Singh, H. and Taylor, R.A. (2012). "Solar energy harvesting using nanofluids-based concentrating solar collector." *J. Nanotechnol. Eng. Med.*, 3(3), 1-9.

Kimura, Y., Kurimoto, T., Sugii, Y.I.H., Toshimitsu, A., Matsuda, T., Imai, H., Yamada, H. and Konodo, T. (2014). "Novel biocompatible Cobalt Oxide Nanoparticles for Use in Dual Photoacoustic and Magnetic Resonance Imaging." *JSM Biotechnol. Bioeng.*, 2(2), 1043-1047.

Kitching, M., Ramani, M. and Marsili, E. (2015). "Fungal synthesis of gold nanoparticles: mechanism and scale up." *Microb. Biotechnol.*, 8(6), 904-17.

Kittaka, S. and Morimoto, T. (1980). "Isoelectric point of metal oxides and binary metal oxides having spinel structure." *J. Colloid Interface Sci.*, 75(2), 398-403.

Kodge, A., Kalyani, S. and Lagashetty, A. (2011). "Microwave preparation, characterisation and studies of nanosized cobalt oxide" *Int J. Ind. Sci. Technol.*, 3(8), 6381-90.

Köferstein, R., Walther, T., Hesse, D. and Ebbinghaus, S.G. (2014). "Crystallite-growth, phase transition, magnetic properties and sintering behavior of nano-CuFe<sub>2</sub>O<sub>4</sub> powders prepared by a combustion-like process." *J. Solid State Chem.*, 213, 57-64.

Koli, P.B., Kapadnis, K.H., Deshpande, U.G. and Patil, M.R. (2018). "Fabrication and characterization of pure and modified Co<sub>3</sub>O<sub>4</sub> nanocatalyst and their application for photocatalytic degradation of eosine blue dye: a comparative study." *J. Nanostructure Chem.*, 8(4), 453-463.

Koseoglu, Y., Kurtulus, F., Kockar, H., Guler, H., Karaagac, O., Kazan, S. and Aktas, B. (2012). "Magnetic characterizations of cobalt oxide nanoparticles." *J. Supercond. Nov. Magn.*, 25(8), 2783-2787.

Koumoto, K. and Yanagida, H. (1981). "Electrical conduction in Pure and Li-substituted Co<sub>3</sub>O<sub>4</sub>." *J. Am. Ceram. Soc.*, 64(11), 156-157.

Krishnan, R.S., Sankaranarayanan, V.N. and Krishnan, K. (1973). "Raman and infrared spectra of aminoacids." *J. Ind. Inst. Sci.*, 55(2), 66-116.

Kulkarni, P., Rathod, V., Hiremath, J., Ninganagouda, S., Singh, D., Singh, A. K. and Krishnaveni, R. (2014). "Biosynthesis and characterization of silver nanoparticles from *Aspergillus flavus* and its antibacterial activity against methicillin resistant *Staphylococcus aureus* (MRSA)." *Int. J. Eng. Res. Technol.*, 3(6), 1826-1833.

Kumar, D.S., Naidu, K.C.B., Rafi, M.M., Nazeer, K.P., Begam, A.A. and Kumar, G.

R. (2018). Structural and dielectric properties of superparamagnetic iron oxide nanoparticles (SPIONs) stabilized by sugar solutions. *Materials Science-Poland*.

Kumar, H., Sangwan, P. and Manisha (2014). "Synthesis and characterization of cobalt oxide nanoparticles by sol-gel method", *Advances in applied physical and chemical Sciences - a sustainable approach*, G.C. Mishra, B.B. Singh, eds., Excellent Publishing House, New Delhi, 99-104.

Kumar, S.A., Abyaneh, M.K., Gosavi, S.W., Kulkarni, S.K., Pasricha, R., Ahmad, A. and Khan, M.I. (2007). Nitrate reductase-mediated synthesis of silver nanoparticles from AgNO<sub>3</sub>. *Biotechnol. Lett.*, 29, 435-445.

Kumar, U., Shete, A., Harle, A.S., Kasyutich, O., Schwarzacher, W., Pundle, A. and Poddar, P. (2008). "Extracellular bacterial synthesis of protein-functionalized ferromagnetic Co<sub>3</sub>O<sub>4</sub> nanocrystals and imaging of self-organization of bacterial cells under stress after exposure to metal ions." *Chem. Mater.*, 20(4), 1484-1491.

Kumari, R. M., Thapa, N., Gupta, N., Kumar, A. and Nimesh, S. (2016). "Antibacterial and photocatalytic degradation efficacy of silver nanoparticles biosynthesized using *Cordia dichotoma* leaf extract." *Adv. Nat. Sci.: Nanosci. Nanotechnol.*, 7(4), Article 045009.

Kushwaha, R., Garg, S., Bajpai, S. and Giri, A.S. (2018). "Degradation of nile blue sulphate dye onto iron oxide nanoparticles: Kinetic study, identification of reaction intermediates and proposed mechanism pathways." *Asia. Pac. J. Chem. Eng.*, 13(3), e2200.

Ladjewardi, S.M., Asnaghi, A., Izadkhast, P.S. and Kashani, A.H. (2013). "Applicability of graphite nanofluids in direct solar energy absorption." *Sol. Energy*, 94, 327-334.

Latha, K.P., Prema, C. and Sundar, S.M. (2018). "Synthesis and characterization of cobalt oxide nanoparticles." *J. Nanosci. Tech.*, 4(5), 475-477.

Lenert, A. and Wang, E.N. (2012). "Optimization of nanofluid volumetric receivers for solar thermal energy conversion." *Sol. Energy*, 86(1), 253-265.

Li, T., Yang, S., Huang, L., Gu, B. and Du, Y. (2004). "A novel process from cobalt nanowire to  $\text{Co}_3\text{O}_4$  nanotube." *Nanotechnol.*, 15(11), 1479.

Lichušina, S., Chodosovskaja, A., Selskis, A., Leinartas, K., Miecinskas, P. and Juzeliunas, E. (2008). "Pseudocapacitive behaviour of cobalt oxide films on nano-fibre and magnetron-sputtered substrates." *Chemija*, 19(3-4), 7-15.

Lima-Tenório, M.K., Ferreira, C.S., Rebelo, Q.H.F., Souza, R.F.B.d., Passos, R.R. and Pineda, E.A.G. (2018). "Pseudocapacitance properties of  $\text{Co}_3\text{O}_4$  nanoparticles synthesized using a modified sol-gel method." *Mater. Res.*, 21(2).

Liu, J., Ye, Z., Zhang, L., Fang, X. and Zhang, Z. (2015). "A combined numerical and experimental study on grapheme/ionic liquid nanofluids based direct absorption solar collector." *Sol. Energy Mater. Sol. Cells*, 136, 177-186.

Liu, P., Hao, Q., Xia, X., Lu, L., Lei, W. and Wang, X. (2015). "3D Hierarchical Mesoporous Flowerlike Cobalt Oxide Nanomaterials: Controllable Synthesis and Electrochemical Properties." *J. Phys. Chem. C*, 119(16), 8537-8546.

Liu, X., Qiu, G. and Li, X. (2005). "Shape controlled synthesis and properties of uniform spinel oxide nanocubes." *Nanotechnol.*, 16(12), 3035.

Loo, Y.Y., Chieng, B.W., Nishibuchi, M. and Radu, S. (2012). "Synthesis of silver nanoparticles by using teal leaf extract from *Camellia Sinensis*". *Int J. Nanomedicine*, 7, 4263-4267.

Luisetto, I., Pepe, F. and Bemporad, E. (2008). "Preparation and characterization of nano cobalt oxide." *J. Nanopart. Res.*, 10(1), 59-67.

Mahmoodi, N.M., Arami, M., Limaee, N.Y. and Tabrizi, N.S. (2006). "Kinetics of heterogeneous photocatalytic degradation of reactive dyes in an immobilized TiO<sub>2</sub> photocatalytic reactor." *J. Colloid Interface Sci.*, 295(1), 159-164.

Makhlouf, M.T., Abu-Zied, B.M. and Mansoure, T.H. (2013). "Direct fabrication of Cobalt Oxide Nanoparticles Employing Sucrose as a Combustion Fuel." *J. Nanopart. Res.*, 384350, 7.

Mani, U., Dhanasingh, S., Arunachalam, R., Paul, E., Shanmugam, P., Rose, C. and Mandal, A.B. (2013). "A simple and green method for the synthesis of silver nanoparticles using *Ricinus Communis* leaf extract." *Prog. Nanotech. Nanomat.*, 2(1), 21-25.

Manigandan, R., Giribabu, K., Suresh, R., Vijayalakshmi, L., Stephen, A. and Narayanan, V. (2013). "Cobalt oxide nanoparticles: characterization and its electrocatalytic activity towards nitrobenzene." *Chem. Sci. Trans.*, 2(S1), S47-S50.

Manimekalai, R., Thirivikraman, K. and Sinduja, C.R. (2012). "Synthesis of Cobalt Oxide Nano Particles from Hydrazine Metal Carboxylate Complexes." *Int. J. Adv. Chem. Sci. Appl.*, 4(2), 97-102.

Manimozhi, R., Kumar, D.R. and Prakash, A.P.G. (2018). "Enhanced solar light driven photocatalytic degradation of organic dye using solution combustion synthesized CeO<sub>2</sub>-ZnO nanocomposites." *J. Electron. Mater.*, 47 (11), 6716-6721.

Mansournia, M. and Rakhshan, N. (2016). "Amine ligand-based hydrothermal synthesis of Co<sub>3</sub>O<sub>4</sub> nanoparticles, characterization and magnetic study." *J. Mol. Struct.* 1125, 714-720.

Manteghi, F. and Peyvandipour, M. (2013). "Oxalate-assisted synthesis of nano cobalt oxide." The 17<sup>th</sup> International Electronic Conference on Synthetic Organic Chemistry, November 2013, Spain.

Manzoor, U., Islam, M., Tabassam, L. and Rahman, S.U. (2009). "Quantum confinement effect in ZnO nanoparticles synthesized by co-precipitation method." *Physica E.*, 41(9), 1669-1672.

Masti, S.A., Sharma, A.K. and Vasambekar, P.N. (2013). "Behavior of dielectric constant and dielectric loss tangent in Cd<sup>2+</sup> and Cr<sup>3+</sup> substituted magnesium ferrites." *Adv. Appl. Sci. Res.*, 4(4), 335-339.

Mathew, J. and Shetty, N. (2017). "Treatment of wastewater using synthesised photocatalyst cobalt oxide Co<sub>3</sub>O<sub>4</sub>." *Int. J. Civil Eng. Technol.*, 8(4), 1840-1844.

Mehra, R.K. and Winge, D.R. (1991). "Metal ion resistance in fungi: Molecular mechanisms and their regulated expression." *J. Cell Biochem.* 45(1), 30-40.



Mohamed, R.M., Mkhaliid, I.A., Baeissa, E.S. and Al-Rayyani, M.A. (2012). “Photocatalytic degradation of methylene blue by Fe/ZnO/SiO<sub>2</sub> nanoparticles under visiblelight.” *J. Nanotechnol.*, Article 329082.

Moon, S.A., Salunke, B.K., Saha, P., Deshmukh, A.R. and Kim, B.S. (2018). “Comparison of dye degradation potential of biosynthesized copper oxide, manganese oxide and silver nanoparticles using *Kalopanax pictus* plant extract.” *Korean J. Chem. Eng.*, 35(3), 702-708.

Moro, F., Tang, S.V.Y., Tuna, F. and Lester, E. (2013). “Magnetic properties of cobalt oxide nanoparticles synthesised by a continuous hydrothermal method.” *J. Magn. Magn. Mater.*, 348, 1-7.

Musavi, S.F. and Balakrishnan, R.M. (2013). “Biodiversity, antimicrobial potential and phylogenetic placement of an endophytic *Fusarium oxysporum* NFX 06 isolated from *Nothapodytes foetida*.” *J. Mycol.*, Article ID 172056, 1-10.

Nakkala, J.R., Mata, R., Raja, K., Chandra, V.K. and Sadras, S.R. (2018). “Green synthesized silver nanoparticles: Catalytic dye degradation, *in vitro* anticancer activity and *in vivo* toxicity in rats.” *Mater. Sci. Eng. C*, 91, 372-381.

Namdeo, A.G. and Sharma, A. (2012). “HPLC analysis of camptothecin content in various parts of *Nothapodytes foetida* collected on different periods.” *Asian Pac. J. Trop. Biomed.*, 2(5), 389-393.

Nassar, M.Y. and Ahmed, I.S. (2012). “Template-free hydrothermal derived cobalt oxide nanopowders: Synthesis, characterization and removal of organic dyes.” *Mater. Res. Bull.*, 47(9), 2638-2645.

Nassar, M.Y., Aly, H.M., Abdelrahman, E.A. and Moustafa, M.E. (2017). "Synthesis, characterization and biological activity of some novel Schiff bases and their Co(II) and Ni(II) complexes: A new route for Co<sub>3</sub>O<sub>4</sub> and NiO nanoparticles for photocatalytic degradation of methylene blue dye." *J. Mol. Struct.*, 1143, 462-471.

Naveen, K.S.H., Rao K.V.B., Kumar, G., Karthic and Narasimha, G. (2011). "Biosynthesis and characterization of silver nanoparticles by *Aspergillus nidulans*." *Biotechnol.*, 5(4), 237-241.

Nel, A.E., Madler, L., Velegol, D., Xia, T., Hoek, E.M.V., Somasundaran, P., Klaessig, F., Castranova, V. and Thompson, M. (2009). "Understanding biophysicochemical interactions at the nano-bio interface." *Nat. Mat.*, 8(7), 543-557.

Nezamzadeh-Ejhieh, A. and Shams-Ghahfarokhi, Z. (2013). "Photodegradation of methyl green by nickel-dimethylglyoxime/ZSM-5 zeolite as a heterogeneous catalyst." *J. Chem.*, Article 104093, 1-11.

Niebisch, C.H., Malinowski, A.K., Schadeck, R., Mitchell, D.A., Kava-Cordeiro, V. and Paba, J. (2010). "Decolorization and biodegradation of reactive blue 220 textile dye by *Lentinus crinitus* extracellular extract." *J. Hazard Mater.*, 180(1-3), 316-322.

Ninganagouda, S., Rathod, V., Jyoti, H., Singh, D., Prema, K. and Haq, M.L. (2013). "Extracellular biosynthesis of silver nanoparticles using *Aspergillus flavus* and their antimicrobial activity against gram negative MDR strains." *Int. J. Pharm. Bio. Sci.*, 4(2), 222-229.

Norzaee, S., Djahed, B., Khaksefidi, R. and Mostafapour, F.K. (2017). "Photocatalytic degradation of aniline in water using CuO nanoparticles." *J. Water*

*Supply Res. T*, 66(3), 178-185.

Nurdin, I. and Satriananda (2017). "Investigation on electrical conductivity enhancement of water based maghemite ( $\gamma$ -Fe<sub>2</sub>O<sub>3</sub>) nanofluids." *Int. J. Mater. Sci. Eng.*, 6(1), 32-36.

Papis, E., Rossi, F., Raspanti, M., Donne, I.D., Colombo, G., Milzani, A., Bernardini, G., Gornati, R., (2009). "Engineered cobalt oxide nanoparticles readily enter cells." *Toxicol. Lett.*, 189, 253-259.

Parang, Z., Keshavarz, A., Farahi, S., Elahi, S.M., Ghoranneviss, M. and Parhoodeh, S. (2012). "Fluorescence emission spectra of silver and silver/cobalt nanoparticles." *Sci. Iran.*, 19, 943-947.

Patil, V., Joshi, P., Chougule, M. and Sen, S. (2012). "Synthesis and characterization of Co<sub>3</sub>O<sub>4</sub> thin film." *Soft Nanosci. Lett.*, 2, 1-7.

Pinto, V.V., Ferreira, M.J., Silva, R., Santos, H.A., Silva, F. and Pereira, C.M. (2010). "Long term effect on the stability of silver nanoparticles in aqueous medium: Effect of the synthesis and storage conditions." *Colloids Surf. A: Physicochem. Eng. Asp.*, 364(1-3), 19-25.

Prabaharan, D. D. M., Sadaiyandi, K., Mahendran, M., & Sagadevan, S. (2017). Precipitation method and characterization of cobalt oxide nanoparticles. *Applied Physics A*, 123(4), 264.

Prabaharan, D.D.M., Sadaiyandi, K., Mahendran, K. and Sagadevan, S. (2016). "Structural, optical, morphological and dielectric properties of cerium oxide nanoparticles." *Mater. Res.*, 19(2), 478-482.

Pritchard, J., Morris, L., Walsh, D., Sadasivan, S., Menard, H., Bellabarba, R. M., Weller, M.T. and Tooze, R.T. (2018). "Synthesis of well-defined, surfactant-free  $\text{Co}_3\text{O}_4$  nanoparticles: The impact of size and manganese promotion on  $\text{Co}_3\text{O}_4$  reduction and water oxidation activity." *Catal. Lett.*, 148, 235-245.

Prusinkiewicz, M.A., Farazkhorasani, F., Dynes, J.J., Wang, J., Gough, K.M. and Kaminskyj, S.G.W. (2012). "Proof-of-principle for SERS imaging of *Aspergillus nidulans* hyphae using *in vivo* synthesis of gold nanoparticles." *Analyst.*, 137, 4934-4942.

Rahimi-Nasrabadi, M., Naderi, H.R., Karimi, M.S., Ahmadi, F., and Pourmortazavi, S.M. (2017) "Cobalt carbonate and cobalt oxide nanoparticles synthesis, characterization and supercapacitive evaluation." *J. Mater. Sci.: Mater. Electron.*, 28, 1877-1888.

Rajeswari, P., Samuel, P., Vijayakumar, J., Selvarathinam, T., Sudarmani, D. N.P., Amirtharaj, K. and Deenthayalan, R. (2017). "Green synthesis of silver nanoparticles by *Aspergillus* consortium and evaluating its anticancer activity against human breast adenocarcinoma cell line (MCF7)." *Pharm. Biol. Eval.*, 4(1), 28-36.

Ramamoorthy, C. and Rajendran, V. (2017). "Effect of surfactant assisted  $\text{Co}_3\text{O}_4$  nanoparticles and its structural, optical, magnetic and electrochemical properties." *Optik*, 145, 330-335.

Raman, V., Suresh, S., Savarimuthu, P.A., Raman, T., Tsatsakis, A.M., Golokhvast, K.S. and Vadivel, V.K. (2016). "Synthesis of  $\text{Co}_3\text{O}_4$  nanoparticles with block and sphere morphology, and investigation into the influence of morphology on biological toxicity." *Exp. Ther. Med.*, 11(2), 553-560.

Rashad, M., Rusing, M., Berth, G., Lischka, K. and Pawliss, A. (2013). "CuO and Co<sub>3</sub>O<sub>4</sub> nanoparticles: synthesis, characterization and raman spectroscopy." *J. Nanomat.*, 82(8), Article 714853, doi: 10.1155/2013/714853.

Ravindra, B.K. and Rajasab, A.H. (2014). "A comparative study on biosynthesis of silver nanoparticles using four different fungal species." *Int. J. Pharm. Pharm. Sci.*, 6(1), 372-376.

Routray, K. L., Sahoo, B., & Behera, D. (2018). Structural, dielectric and magnetic properties of nano-sized CoFe<sub>2</sub>O<sub>4</sub> employing various synthesis techniques for high frequency and magneto recording devices: a comparative analysis. *Materials Research Express*, 5(8), 085016.

Saeed, M., Akram, N., Haq, A.U., Naqvi, S.A.R., Usman, M., Abbas, M.A., Abdeel, M. and Nisar, A. (2019). "Green and eco-friendly synthesis of Co<sub>3</sub>O<sub>4</sub> and Ag-Co<sub>3</sub>O<sub>4</sub>: Characterization and photo-catalytic activity." *Green process Synth.*, 8(1), 382-390.

Sagadevan, S. (2015). "Investigations on synthesis, structural, morphological and dielectric properties of manganese oxides nanoparticles." *J. Mat. Sci. Eng.*, 4(3), 1000172.

Said, Z., Sajid, M.H., Saidur, R., Mahdiraji, G.A. and Rahim, N.A. (2015). "Evaluating the optical properties of TiO<sub>2</sub> nanofluid for a direct absorption solar collector." *Numerical Heat Transfer, Part A*, 67, 1010-1027.

Salavati-Niasari, M., Khansari, A. and Davar, F. (2009). "Synthesis and characterization of cobalt oxide nanoparticles by thermal treatment process." *Inorg. Chim. Acta*, 362(14), 4937-4942.

Salavati-Niasari, M., Khansari, A. and Davar, F. (2009). "Synthesis and characterization of  $\text{Co}_3\text{O}_4$  nanorods by thermal decomposition of cobalt oxalate." *J. Phys. Chem. Solids*, 70(5), 847-852.

Saleh, S.M. (2018). "Metal oxide nanomaterials as photo-catalyst for dye degradation." *Res. Dev. Mater. Sci.*, 9 (2), 1-8.

Sanghi, R. and Verma, P. (2010). "pH dependant fungal proteins in the green synthesis of gold nanoparticles." *Adv. Mat. Lett.*, 1(3), 193-199.

Saravanan, M. (2010). "Biosynthesis and in vitro studies of silver bionanoparticles synthesized from *Aspergillus flavus* and its antimicrobial activity against multi drug resistant clinical isolates." *World. Acad. Sci. Eng. Technol.*, 4(8), 590-593.

Sari, M.I., Agustina, T.E., Melwita, E. and Aprianti, T. (2017). "Color and COD degradation in photocatalytic process of procion red by using  $\text{TiO}_2$  catalyst under solar irradiation." *AIP Conf. Proc.*, 1903(1), Article 040017.

Seabra, A.B. and Duran, N. (2015). "Nanotoxicology of metal oxide nanoparticles." *Metals.*, 5(2), 934-975.

Selvam, G.K. and Sivakumar, K. (2015). "Phycosynthesis of silver nanoparticles and photocatalytic degradation of methyl orange dye using silver (Ag) nanoparticles synthesized from *Hypnea musciformis* (Wulfen) J. V. Lamouroux." *Appl. Nanosci.*, 5(5), 617-622.

Shadrokh, S., Farahmandjou, M. and Firozabadi, T.P. (2016). "Fabrication and characterization of nanoporous Co oxide ( $\text{Co}_3\text{O}_4$ ) prepared by simple Sol-gel synthesis." *Phys. Chem. Res.*, 4(2), 153-160.

Shamsipur, M. and Rajabi, H.R. (2014). "Study of photocatalytic activity of ZnS quantum dots as efficient nanoparticles for removal of methyl violet: effect of ferric ion doping." *Spectrochimica Acta A Mol. Biomol. Spectrosc.*, 122, 260-267.

Sharma, M., Jain, T., Singh, S. and Pandey, O.P. (2012). "Photocatalytic degradation of organic dyes under UV-visible light using capped ZnS nanoparticles." *Sol. Energy*, 86(1), 626-633.

Sharma, P. and Sharma, A. (2016). "Structural & magnetic properties of cobalt oxide nanoparticles at different annealing temperatures." *Int. J. Mater. Sci. and Eng.*, 4(4), 208-214.

Sharma, S., Ahmad, N., Prakash, A., Singh, V.N., Ghosh, A.K. and Mehta, B. R. (2010). "Synthesis of crystalline Ag nanoparticles (AgNPs) from micro organisms." *Mater. Sci. Appl.*, 1(01), 1.

Shim, H., Jin, Y., Seo, S., Lee, S. and Kim, D. (2011). "Highly Reversible Lithium Storage in *Bacillus subtilis*-Directed Porous  $\text{Co}_3\text{O}_4$  nanostructures." *ACS Nano.*, 5(1), 443-449.

Shinde, V.R., Mahadik, S.B., Gujar, T.P. and Lokhande, C.D. (2005). "Supercapacitive cobalt oxide ( $\text{Co}_3\text{O}_4$ ) thin films by spray pyrolysis." *Appl. Surf. Sci.*, 252(20), 7487-7492.

Sinduja, C.R., Kalpanadevi, K. and Manimekalai, R. (2013). "Characterization of Nanostructured Cobalt Oxide Particles Synthesized by Thermal Treatment." *Global. J. Res. Anal.*, 2(7), 11-13.

Singh, M., Vaya, D. and Das, B.K. (2018). "Green synthesis of cobalt oxide nanoparticles by a starch-assisted method." *Nanosci. Nanotechnol. Asia.*, 9(3), 362-370.

Sinko, K., Szabo, G. and Zrinyi, M. (2011). "Liquid-phase synthesis of Cobalt Oxide Nanoparticles." *J. Nanosci. Nanotechnol.*, 11(5), 4127-4135.

Srinivasan, V. and Weidner, J.W. (2002). "Capacitance studies of cobalt oxide films formed via electrochemical precipitation." *J. Power Sources*, 108(1-2), 15-20.

Staneik, A., Woerdenbag, H.J. and Kayser, O. (2008). "Endophytes: exploiting biodiversity for the improvement of natural product-based drug discovery" *J. Plant. Interact.*, 3(2), 75-93.

Subramaniyan, A.L., Priya, S.L. and Ilangovan, R. (2015). "Energy harvesting through optical properties of TiO<sub>2</sub> and C-TiO<sub>2</sub> nanofluid for direct absorption solar collectors." *Int. J. Renew. Energy Res.*, 5(2), 542-547.

Sundaramoorthi, C., Kalaivani, M., Dhivya, M.M., Palanisamy, S., Kalaiselvan, V. and Rajasekaran, A. (2009). "Biosynthesis of silver nanoparticles from *Aspergillus niger* and evaluation of its wound healing activity in experimental rat model." *Int. J. Pharmtech. Res.*, 1(4), 1523-1529.

Taylor R.A., Phelan, P.E., Otanicar, T.P., Adrian, R. and Prasher, R. (2011). "Nanofluid optical property characterization: towards efficient direct absorption solar



collectors.” *Nanoscale Res. Lett.*, 6(1), 225.

Thu, T.N.T., Thi, N.N., Quang, V.T., Hong, K.N., Minh, T.N. & Hoai, N. L. T. (2016). “Synthesis, characterisation and effect of pH on degradation of dyes of copper-doped TiO<sub>2</sub>.” *J. Exp. Nanosci.*, 11(3), 226-238.

Tomar, R.S., Chauhan, P.S. and Shrivastava, V. (2015). “A critical review on nanoparticle synthesis: physicochemical v/s biological approach.” *World J. Pharm. Res.*, 4(1), 595-620.

Tomaszewska, E., Soliwoda, K., Kadziola, K., Tkacz-Szczesna, B., Celichowski, G., Cichomski, M., Szmaja, W. and Grobelny, J. (2013). “Detection limits of DLS and UV-Vis spectroscopy in characterization of polydisperse nanoparticles colloids.” *J. Nanomater.*, Article 313081, 60.

Tyagi, H., Phelan, P. and Prasher, R. (2009). “Predicted efficiency of a low-temperature nanofluid-based direct absorption solar collector.” *J. Sol. Energy Eng.*, 131(4), 041004.

Uddandarao, P. and Balakrishnan, R.M. (2016). “ZnS semiconductor quantum dots production by an endophytic fungus *Aspergillus flavus*.” *Mater. Sci. Eng. B.*, 207, 26-32.

Uddandarao, P., Hingnekar, T.A., Balakrishnan, R.M. and Rene, E.R. (2019). “Solar assisted photocatalytic degradation of organic pollutants in the presence of biogenic fluorescent ZnS nanocolloids.” *Chemosphere*, 234, 287-296.

Ullah, M., Naz, A., Mahmood, T., Siddiq, M. and Bano, M. (2014). "Biochemical synthesis of nickel and cobalt oxide nanoparticles by using biomass waste." *Int J. Enhanc. Res. Sci. Technol. Eng.*, 3(4), 415-422.

Vahabi, K., Mansoori, G.A. and Karimi, S. (2011) "Biosynthesis of silver nanoparticles by fungus *Trichoderma reesei* (a route for large-scale production of AgNPs)." *Insciences J.*, 1(1), 65-79.

Vala A.K. (2014). "Exploration on green synthesis of gold nanoparticles by a marine-derived fungus *Aspergillus sydowii*." *Environ. Prog. Sustain. Energ.*, 34(1), 194-197.

Vanaja, M., Gurusamy, A., Rajeshkumar, S., Paulkumar, K., Chitra, K., Malarkodi, C. and Annadurai, G. (2015). "Fungal assisted intracellular and enzyme-based synthesis of silver nanoparticles and its bactericidal efficiency." *Int. Res. J. Pharma. Biosci.*, 2(3), 8-19.

Vardhana, J., Kathiravan, G., Dhivya, R. and Vidhya, D. (2015). "Biodiversity of fungi from silver ore with reference to the production of silver nanoparticles." *Int. Res. J. Pharm.*, 6(1), 31-33.

Velhal, N.B., Patil, N.D., Shelke, A.R., Deshpande, Puri, V.R. (2015). "Structural, dielectric and magnetic properties of nickel substituted cobalt ferrite nanoparticles: Effect of nickel concentration." *AIP Adv.*, 5(9), 097166.

Venkatachalam, V. and Jayavel, R. (2014). "Synthesis of  $\text{Co}_3\text{O}_4$  electrode material for supercapacitor applications." *Int. J. ChemTech. Res.*, 6(13), 5404-5407.

Vennela, A.B., Mangalaraj, D., Muthukumarasamy, N., Agilan, S. and Hemalatha, K.V. (2019). "Structural and optical properties of  $\text{Co}_3\text{O}_4$  nanoparticles prepared by

sol-gel technique for photocatalytic application.” *Int. J. Electrochem. Sci.*, 14, 3535-3552.

Vidal-Abarca, C., Lavela, P. and Tirado, J.L. (2008). “Cobalt oxide nanoparticles prepared from Reverse Micelles as High-Capacity Electrode Materials for Li-Ion cells.” *Electrochem. Solid-State Lett.*, 111(98), A198-A201.

Vigneshwaran, N., Ashtaputre, N.M., Varadarajan, P.V., Nachane, R.P., Paralikar, K.M. and Balasubramanya, R.H. (2007). “Biological synthesis of silver nanoparticles using the fungus *Aspergillus flavus*.” *Mater. Lett.*, 61(6), 1413-1418.

Vijayanandan, A.S. and Balakrishnan, R.M. (2018). “Biosynthesis of cobalt oxide nanoparticles using endophytic fungus *Aspergillus nidulans*.” *J. Environ. Manage.*, 218, 442-450.

Wadekar, K.F., Nemade, K.R. and Waghuley, S.A. (2017). “Chemical synthesis of cobalt oxide ( $\text{Co}_3\text{O}_4$ ) nanoparticles using co-precipitation method.” *Res. J. Chem. Sci.*, 7(1), 53-55.

Wang, F.W., Jiao, R.H., Cheng, A.B., Tan, S.H. and Song, Y.C. (2007). “Antimicrobial potentials of endophytic fungi residing in *Quercus variabilis* and brefeldin A obtained from *Cladosporium* sp.” *World J. Microbiol. Biotechnol.*, 23(1), 79–83.

Wang, G., Shen, X., Horvat, J., Wang, B. and Liu, H. (2009). “Hydrothermal synthesis and optical, magnetic and supercapacitance properties of nanoporous cobalt oxide nanorods.” *J. Phys. Chem.*, 113(11), 4357-4361.

Wen, W., Wu, J. and Tu, J. (2012). “A novel solution combustion synthesis of cobalt oxide nanoparticles as negative-electrode materials for lithium ion batteries.” *J. Alloys. Compd.*, 513, 592-596.

Wolf, M., Fischer, N. and Claeys, M. (2018). “Surfactant-free synthesis of monodisperse cobalt oxide nanoparticles of tunable size and oxidation state developed by factorial design.” *Mater. Chem. Phys.*, 213, 305-312.

Xu, J., Gao, J., Cao, J., Wang, W. and Chen, Z. (2010). “Preparation and electrochemical capacitance of cobalt oxide (Co<sub>3</sub>O<sub>4</sub>) nanotubes as supercapacitor material.” *Electrochim. Acta.*, 56, 732-736.

Xu, J., Xu, D., Zhu, B., Cheng, B. and Jiang, C. (2018). “Adsorptive removal of an anionic dye congo red by flower-like hierarchical magnesium oxide (MgO)-graphene oxide composite microspheres.” *Appl. Surf. Sci.*, 435, 1136-1142.

Xu, R., Wang, J., Li, Q., Sun, G., Wang, E., Li, S., Gu, J., and Ju, M. (2009). “Porous Cobalt Oxide (Co<sub>3</sub>O<sub>4</sub>) nanorods: Facile syntheses, optical property and application in lithium-ion batteries.” *J. Solid State Chem.*, 182(11), 3177-3182.

Xuan, Y., Duan, H. and Li, Q. (2014). “Enhancement of solar energy absorption using a plasmonic nanofluid based on TiO<sub>2</sub>/Ag composite nanoparticles.” *RSC. Adv.*, 4(31), 16206.

Xuan, Y., Duan, H. and Li, Q. (2014). “Enhancement of solar energy absorption using a plasmonic nanofluid based on TiO<sub>2</sub>/Ag composite nanoparticles.” *RSC. Adv.*, 4(31), 16206-16213.

Yadav, A., Kon, K., Kratosova, G., Dua, N., Ingle, A.W. and Ra, M. (2015). “Fungi as an efficient mycosystem for the synthesis of metal nanoparticles: progress and key aspects of research.” *Biotechnol. Lett.*, 37(11), 2099-2120.

Yang, H., Hu, Y., Zhang, X., and Qiu, G. (2004). “Mechanochemical synthesis of cobalt oxide nanoparticles.” *Mater. Lett.*, 58(3-4), 387-389.

Yang, J., Liu, H., Martens, W.N. and Frost, R.L. (2010). “Synthesis and characterization of Cobalt Hydroxide, Cobalt Oxyhydroxide and Cobalt Oxide Nanodiscs.” *J. Phys. Chem. C.*, 114(1), 111-119.

Yarestani, M., Khalaji, A.D., Rohani, A. and Das, D. (2014).” Hydrothermal synthesis of cobalt oxide nanoparticles: Its optical and magnetic properties.” *J. Sci. I. R. Iran.*, 25(4), 339-343.

Yin, Y., Li Z.-Y., Zhong Z., Gates B., Xia, Y. and Venkateswaran, S. (2002). “Synthesis and characterization of stable aqueous dispersions of silver nanoparticles through the Tollens process.” *J. Mater. Chem.*, 12(3), 522–527.

Yuanchun, Q., Yanbao, Z. and Zhishen, W. (2008). “Preparation of cobalt oxide nanoparticles and cobalt powders by solvothermal process and their characterization.” *Mater. Chem. Phy.*, 110(2-3), 457-462.

Zamiri, R., Ahangar, H.A., Kaushal, A., Zakaria, A., Zamiri, G., Tobaldi, D. and Ferreira, J.M.F. (2015). “Dielectric properties of CeO<sub>2</sub> nanoparticles at different temperatures.” *Plos One*, 10(4), e0122989.

Zhang, H., Chen, H., Du, X. and Wen, D. (2014). “Photothermal conversion characteristics of gold nanoparticle dispersions.” *Sol. Energy*, 100, 141-147.

Zheng, J., Liu, J., Lv, D., Kuang, Q., Jiang, Z., Xie, Z., Huang, R. and Zheng, L. (2010). "A facile synthesis of flower-like  $\text{Co}_3\text{O}_4$  porous spheres for the lithium-ion battery electrode." *J. Solid State Chem.*, 183(3), 600-605.

Zhou, X., Chen, F., Cao, F., Shen, W., Liu, J. and Xu, X. (2016). "Nanostructured hexagonal cobalt oxide plates and their electrochemical properties" *Mat. Lett.*, 180, 175-178.

Zhu, Y., Wang, G., Jiang, H., Chen, L. and Zhang, X. (2015). "One-step ultrasonic synthesis of graphene quantum dots with high quantum yield and their application in sensing alkaline phosphatase." *Chem. Commun.*, 51, 948-951.

## APPENDIX

### COMPOSITION OF MEDIA

<b>Ingredients</b>	<b>g/L</b>
<b>Potato Dextrose Broth (PDB)</b>	
Potatoes infusion	200.0
Dextrose	20.00
<b>Potato Dextrose Agar (PDA)</b>	
Potatoes infusion	200
Dextrose	20
Agar powder	20

## 23S RNA SEQUENCING

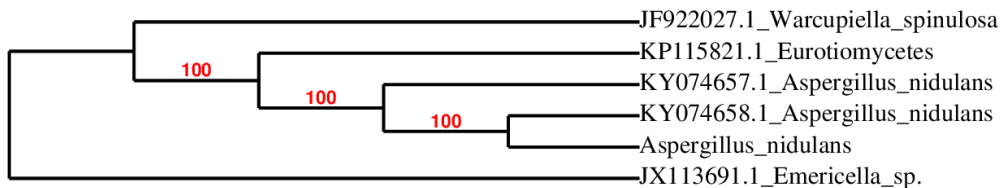
### Comparison of sequence identities of various fungi with isolated fungus *Aspergillus nidulans*

#### Descriptions

Sequences producing significant alignments:

Description	Max score	Total score	Query cover	E value	Ident	Accession
<i>Aspergillus nidulans</i> strain FGSC A4 large subunit ribosomal RNA gene, partial sequence	1829	1829	100%	0.0	100%	<a href="#">KY074658.1</a>
<i>Aspergillus nidulans</i> strain FGSC A4 small subunit ribosomal RNA gene, partial sequence; internal transcribed spacer 1, 5.8S ribosomal RNA gene, and internal transcribed spacer 2, complete sequence; and large subunit ribosomal RNA gene, partial sequence	1829	1829	100%	0.0	100%	<a href="#">KY074657.1</a>
<i>Eurotiomyces</i> DC474 large subunit ribosomal RNA gene, partial sequence	1818	1818	100%	0.0	99%	<a href="#">KP115821.1</a>
<i>Warcuprella spinulosa</i> strain CBS512.65 5.8S ribosomal RNA gene, partial sequence; internal transcribed spacer 2, complete sequence; and 28S ribosomal RNA gene, partial sequence	1818	1818	100%	0.0	99%	<a href="#">JF922027.1</a>
<i>Emericella</i> sp. LZ-2012 28S ribosomal RNA gene, partial sequence	1790	1790	100%	0.0	99%	<a href="#">JX113691.1</a>
<i>Aspergillus</i> sp. FD03 26S ribosomal RNA gene, partial sequence	1786	1786	99%	0.0	99%	<a href="#">KP725296.1</a>
<i>Eurotiomyces</i> sp. genotype 44 large subunit ribosomal RNA gene, partial sequence	1768	1768	100%	0.0	99%	<a href="#">KP115820.1</a>
<i>Aspergillus</i> sp. 3 VH-2016 genomic DNA sequence contains 28S rRNA gene, strain CCF 4682	1762	1762	100%	0.0	99%	<a href="#">LT855552.1</a>
<i>Aspergillus</i> sp. FD01 26S ribosomal RNA gene, partial sequence	1757	1757	100%	0.0	99%	<a href="#">KP725295.1</a>
<i>Aspergillus</i> sp. FD02 26S ribosomal RNA gene, partial sequence	1749	1749	99%	0.0	99%	<a href="#">KP725294.1</a>
<i>Aspergillus croceus</i> genomic DNA sequence contains ITS1, 5.8S rRNA gene, ITS2, 28S rRNA gene, strain CCF 4714	1733	1733	100%	0.0	98%	<a href="#">LN873932.1</a>
<i>Aspergillus sydowii</i> isolate 32R-1-F04 internal transcribed spacer 1, partial sequence; 5.8S ribosomal RNA gene and internal transcribed spacer 2, complete sequence; and large subunit ribosomal RNA gene, partial sequence	1722	1722	99%	0.0	98%	<a href="#">KX958091.1</a>

### Phylogenetic tree of 23S rRNA sequencing





## PUBLICATIONS

- ❖ **Vijayanandan, A.S.** and Balakrishnan, R.M. (2018). “Biosynthesis of cobalt oxide nanoparticles using endophytic fungus *Aspergillus nidulans*.” *J. Environ. Manage.*, 218, 442-450.
- ❖ **Vijayanandan, A.S.** and Balakrishnan, R.M. (2018). “Impact of precursor concentration on biological synthesis of cobalt oxide nanoparticles.” *Data Brief.*, 19, 1941-1947.
- ❖ Valappil, R.S.K., **Vijayanandan, A.S.** and Balakrishnan, R.M. (2019). “Decolorization of Reactive Blue 220 aqueous solution using fungal synthesized  $\text{Co}_3\text{O}_4$  nanoparticles” *J Water. Supply Res. T.*, 68(8), 675-686.
- ❖ **Vijayanandan A.S.**, Valappil R.S.K. and Balakrishnan R.M. (2020). “Evaluation of Photothermal Properties for Absorption of Solar Energy by  $\text{Co}_3\text{O}_4$  Nanofluids Synthesized using Endophytic Fungus *Aspergillus nidulans*.” *Sustain. Energy Technol. Assess.*, 37, 100598.
- ❖ **Vijayanandan, A.S.** and Balakrishnan, R.M. (2019). “Photo, Electrical and Magnetic Properties of Cobalt Oxide Nanoparticles through Biological Mechanism of Endophytic Fungus *Aspergillus nidulans*.” *Appl. Phys. A. Appl. Phys. A.* 126, 234.

## CONFERENCE/SYMPOSIUM PRESENTATIONS

- ❖ Aniket, M., Raghav, .I, Sachin, P., **Ajuy, S.**, Noyel Victoria, S. (2015). “Zinc sulphide as environmental friendly buffer for thin solar cells.” *International conference on Nanotechnology (ICNT 2015)*, February 19-22, Haldia, Kolkata.
- ❖ **Vijayanandan, A.S.**, Balakrishnan, R.M. (2016). “Biosynthesis of cobalt oxide nanoparticles using endophytic fungus.” *5<sup>th</sup> International Conference on Research Frontiers in Chalcogen Science and Technology*, December 19-21, Dona Paula, Goa.
- ❖ **Vijayanandan, A.S.**, Valappil, R.S.K., Balakrishnan, R.M. (2018). “Studies on optical properties of greenly synthesized cobalt oxide nanoparticles.” *Annual Conference on Green Catalysis and Sustainable Energy*, November 15-16, Dubai, U.A.E.
- ❖ **Vijayanandan, A.S.**, Balakrishnan, R.M. (2019). “Photo, Electrical and Magnetic Properties of Cobalt Oxide Nanoparticles through Biological Mechanism of Endophytic Fungus *Aspergillus nidulans*” *National Symposium on Environmental Pollution Prevention and Control: Future Perspectives (EFFCFP-2019)*, August 23-25, NITK Surathkal.

## BIO-DATA

Name Aju Sundar V V  
Registration Number 145054CH14F01  
Course Name Ph.D. in Chemical Engineering  
Name of the Institute National Institute of Technology Karnataka, Surathkal

Address S/O Mr. Vijayanandan V.,  
4/1090 Hussain Colony,  
Sivakasi East,  
Virudhunagar district,,  
Tamil Nadu – 626189.

Date of Birth 25 August 1989  
Phone Number +91 – 9442010760  
Email ID ajsdr08@gmail.com

## QUALIFICATION

S.N.	Degree	Duration	Subject	Institution	CGPA
1	Ph. D.	2014 – 20	Bionanotechnology	National Institute of Technology Karnataka, Surathkal	7
2	M. Tech.	2012 – 14	Biotechnology	PSG College of Technology, Coimbatore	7.3
3	B. Tech.	2007 – 11	Industrial Biotechnology	Government College of Technology,	7.2

				Coimbatore	
4	HSC	2006 – 07	Physics, Chemistry, Maths., Biology	SHNV Matric. Hr. Sec. School, Sivakasi	9.2
5	SSLC	2004 – 05	-----	SHNV Matric Hr. Sec. School, Sivakasi	9.1

## LIST OF PUBLICATIONS

- ❖ **Vijayanandan, A.S.** and Balakrishnan, R.M. (2018). “Biosynthesis of cobalt oxide nanoparticles using endophytic fungus *Aspergillus nidulans*.” *J. Environ. Manage.*, 218, 442-450.
- ❖ **Vijayanandan, A.S.** and Balakrishnan, R.M. (2018). “Impact of precursor concentration on biological synthesis of cobalt oxide nanoparticles.” *Data Brief.*, 19, 1941-1947.
- ❖ Valappil, R.S.K., **Vijayanandan, A.S.** and Balakrishnan, R.M. (2019). “Decolorization of Reactive Blue 220 aqueous solution using fungal synthesized  $\text{Co}_3\text{O}_4$  nanoparticles” *J Water. Supply Res. T.*, 68(8), 675-686.
- ❖ **Vijayanandan A.S.**, Valappil R.S.K. and Balakrishnan R.M. (2020). “Evaluation of Photothermal Properties for Absorption of Solar Energy by  $\text{Co}_3\text{O}_4$  Nanofluids Synthesized using Endophytic Fungus *Aspergillus nidulans*.” *Sustain. Energy Technol. Assess.*, 37, 100598.
- ❖ **Vijayanandan, A.S.** and Balakrishnan, R.M. (2019). “Photo, Electrical and Magnetic Properties of Cobalt Oxide Nanoparticles through Biological Mechanism of Endophytic Fungus *Aspergillus nidulans*.” *Appl. Phys. A. Appl. Phys. A.* 126, 234.